EVALUATION OF THERMAL STRESSES IN PLANAR SOLID OXIDE FUEL CELLS AS A FUNCTION OF THERMO-MECHANICAL PROPERTIES OF COMPONENT MATERIALS

A Thesis

by

MANISHA

Submitted to the Office of Graduate Studies of
Texas A&M University
in partial fulfillment of the requirements for the degree of

MASTERS OF SCIENCE

August 2008

Major Subject: Mechanical Engineering

EVALUATION OF THERMAL STRESSES IN PLANAR SOLID OXIDE FUEL CELLS AS A FUNCTION OF THERMO-MECHANICAL PROPERTIES OF COMPONENT MATERIALS

A Thesis

by

MANISHA

Submitted to the Office of Graduate Studies of
Texas A&M University
in partial fulfillment of the requirements for the degree of

MASTERS OF SCIENCE

Approved by:

Chair of Committee,	Miladin Radovic
Committee Members,	Hong Liang
	Haiyan Wang
Head of Department,	Dennis L. O'Neal

August 2008

Major Subject: Mechanical Engineering

ABSTRACT

Evaluation of Thermal Stresses in Planar Solid Oxide

Fuel Cells as a Function of Thermo-mechanical

Properties of Component Materials. (August 2008)

Manisha, B.En., National Institute of Technology, Jaipur, India

Chair of Advisory Committee: Dr. Miladin Radovic

Fuel cells are the direct energy conversion devices which convert the chemical energy of a fuel to electrical energy with much greater efficiency than conventional devices. Solid Oxide Fuel Cell (SOFC) is one of the various types of available fuel cells; wherein the major components are made of inherently brittle ceramics. Planar SOFC have the advantages of high power density and design flexibility over its counterpart tubular configuration. However, structural integrity, mechanical reliability, and durability are of great concern for commercial applications of these cells. The stress distribution in a cell is a function of geometry of fuel cell, temperature distribution, external mechanical loading and a mismatch of thermo-mechanical properties of the materials in contact. The mismatch of coefficient of thermal expansion and elastic moduli of the materials in direct contact results in the evolution of thermal stresses in the positive electrode/electrolyte/negative electrode (PEN) assembly during manufacturing and operating conditions (repeated start up and shut down steps) as well. It has long been realized and demonstrated that the durability and reliability of SOFCs is not only determined by the degradation in electrochemical performance but also by the ability of its component materials to withstand the thermal stresses.

In the present work, an attempt has been made to evaluate the thermal stresses as a function of thermal and mechanical properties of the component materials assuming contribution from other factors such as thermal gradient, mechanical loading and in-service loading conditions is insignificant. Materials used in the present study include the state of art anode

(Ni-YSZ), electrolyte(YSZ) and cathode materials(LM and LSM) of high temperature SOFC and also the ones being suggested for intermediate temperature SOFC Ni-SCZ as an anode, GDC and SCZ as electrolyte and LSCF as the cathode. Variation of thermo-mechanical properties namely coefficient of thermal expansion, and elastic and shear moduli were studied using thermo-mechanical analyzer and resonant ultrasound spectroscope respectively in 25-900^{o}C temperature range. A non-linear variation in elastic and shear moduli- indicative of the structural changes in the studied temperature range was observed for most of the above mentioned materials. Coefficient of thermal expansion (CTE) was also found to increase non-linearly with temperature and sensitive to the phase transformations occurring in the materials. Above a certain temperature (high temperature region- above 600^{o}C), a significant contribution from chemical expansion of the materials was also observed.

In order to determine thermal stress distribution in the positive electrode, electrolyte, negative electrode (PEN) assembly, CTE and elastic and shear moduli of the component materials were incorporated in finite element analysis at temperature of concern. For the finite element analysis, anode supported configuration of PEN assembly (of 100mm x 100mm) was considered with 1mm thick anode, 10μm electrolyte and 30 μm cathode. The results have indicated that cathode and anode layer adjacent to cathode/electrolyte and electrolyte/anode interface respectively are subjected to tensile stresses at the operating temperature of HT-SOFC (900^{o}C) and IT-SOFC (600^{o}C). However, the magnitude of stresses is much higher in the former case (500MPa tensile stress in cathode layer) when compared with the stress level in IT-SOFC (178MPa tensile stress in cathode layer). These high stresses might have been resulted from the higher CTE of cathode when compared with the adjacent electrolyte. However, it is worth mentioning here that in the present work, we have not considered any contribution from the residual stresses arising from fabrication and the stress relaxation from softening of the glass sealant.

ACKNOWLEDGEMENTS

My committee chair, Dr. Miladin Radovic, is gratefully acknowledged for the constant support and guidance throughout my course of study. Starting from day one at Texas A&M University, his guidance has been a real source of motivation for the graceful completion of my thesis. Committee Members Dr. Hong Liang and Dr. Haiyan Wang are also acknowledged for all their help and moral support. Dr. Sean M. McDeavitt is deeply acknowledged for serving as a substitute for Dr. Wang during the thesis defense. It has been a nice experience to receive the valuable insight and suggestions towards the improvement of my work.

Dr. Nina Orlovskya and her research group from University of Central Florida, Orlando, FL is also thanked for providing us the samples for the study. My sincere most thanks also goes to Dr. Jaime C. Grunlan for providing access to the Thermal Mechanical Analyzer. William Seward from the chemistry machine shop is deeply acknowledged for helping us in building the high temperature set up of the resonance ultrasound spectroscope. My thanks also go to Brian Bachmeyer, Missy Cornett, Johnny Hallford, Sheryl Mallett, James Sajewski, Casey Schumacher and Mike Walker from the Department of Mechanical Engineering for their invaluable help at times. Kevin and Patrick, the members of our research group "Laboratory of high temperature materials" are also thanked for all of their help.

I am indebted to all the faculty members of the Department of Mechanical Engineering who have been a great source of inspiration toward the graceful completion of my graduate studies at Texas A&M University. Thanks go to all of my friends who have been source of motivation and support. Last but not the least; I am indebted to my family back at home who has been a real source of inspiration and motivation throughout my stay.

DEDICATION

To my loving parents and siblings

and

To my Teachers

TABLE OF CONTENTS

Page

LIST OF FIGURES

Page

LIST OF TABLES

Page

1. INTRODUCTION

Fuel cells will undoubtedly find widespread application in the conversion of chemical energy of different fuels (hydrogen, natural gas, diesel, methanol, etc) to electrical energy, as they offer very high energy conversion efficiency at low pollution. Because of their potential to reduce the environmental impact and geopolitical consequences of fossil fuels, fuel cells are being considered as an alternative to combustion engines or other energy conversion devices. They can be used for a wide range of applications such as powering the vehicles, large scale power plants, uninterrupted power supplies, remote power generation, domestic appliances, etc. Other benefits associated with fuel cells are their modular nature, unique scalability in electricity generation applications and zero noise pollution. For above mentioned reasons, it is quite likely that impact of fuel cells upon society will be revolutionary. In the short-term fuel cells allow greatly enhanced conversion efficiencies than that of conventional fuels along with lower CO_2 emission, while in the long-term fuel cells are essential components of any hydrogen or similar clean energy economy[1].

Several technical problems hinder commercialization of fuel cells such as low reliability and durability, limited availability of hydrogen and the low current and power density caused by slow reaction rate. Being electrochemical devices, reliability and durability of fuel cells depend not only on the electrochemical performance, but also on the ability of components of these devices to withstand mechanical stresses that arise during processing and service. Reliability and durability is an important issue in the case of Solid Oxide Fuel Cells (SOFCs) because these operate at high temperatures (800-1000^{o}C) in reducing/oxidizing environment and are made up of inherently brittle but thin ceramic components.

In the case of SOFC, the mechanical reliability and durability is determined by the stress distribution in, and the stochastic distribution of strengths of its components.

This thesis follows the style of *Nature.*

The stress distribution is a complex function of several parameters including geometry of fuel cells, temperature distribution and external mechanical loads. Furthermore, residual stresses are introduced during processing and in-service as a result of mismatch in the thermo-elastic properties and shrinkage during sintering of fuel cell components.

The objective of this work is to determine thermo-mechanical properties of the advanced electrolyte, cathode and anode materials for SOFC and their effect on thermally induced stresses in SOFC stacks. Since a mismatch in Coefficient of Thermal Expansion (CTE) and Elastic moduli between the materials causes the development of detrimental thermal stresses, an attempt has been made to determine these thermo-mechanical properties of materials as a function of temperature using Thermo-Mechanical Analyzer (TMA) and Resonant Ultrasound Spectroscope (RUS). Based on these evaluated properties thermal stresses have been calculated using finite element modeling for the different combination of SOFC components.

1.1. The Basics of Fuel Cell Technology

A Fuel cell is an energy conversion device that produces electricity (and heat) directly from a gaseous fuel by its electrochemical combination with an oxidant[2]. Since fuel cells convert energy from a primary source directly into electricity, without the intermediate conversion to thermal energy, these devices fall into the category of direct–energy conversion devices. Fuel cells are also called ‘batteries with external fuel supplies’.

1.1.1. The Principle of Operation

The direct conversion of chemical into electrical energy is achieved by separating a chemical reaction into two electrochemical reactions that take place inside the two porous electrodes, namely anode and cathode. Fuel is fed to the anode, undergoes an oxidation reaction, and releases electrons to the external circuit. Oxidant that is fed to the cathode, accepts electrons from the external circuit, and undergoes a reduction reaction. The electron flow from the anode to the cathode produces direct-current (DC) electricity. In the case of H_2-O_2 fuel cell, the hydrogen molecules (a fuel) enter a fuel cell at the **anode** where a chemical reaction strips them of their electrons. The hydrogen atoms are now “ionized,” and carry a positive electrical charge

and the electrons provide current to external electrical circuit. Oxygen enters the fuel cell at **cathode,** and combines with the electrons (returning from the electrical circuit). The **electrolyte** plays a key role in the efficient use of a fuel cell. It must permit only the appropriate ions (hydrogen or oxygen) to pass between cathode and anode. Depending on the nature of the electrolyte (whether proton or ion conductor) there would be difference in electrochemical reactions occurring at anode and cathode and in the location of water formation as a by-product of the reaction in the cell.

During operation of a fuel cell (external electrical circuit closed), current is generated. Considering the H_2-O_2 fuel cell with an electrolyte which is ionic conductor, as shown in the Fig. 1-1, the electrochemical reactions would be as following[3]:

$$\text{At Anode: } H_2 + O^{2-} \rightarrow H_2O + 2e^- \quad \text{..... (1.1)}$$

$$\text{At Cathode: } \tfrac{1}{2}O_2 + 2e^- \rightarrow O^{2-} \quad \text{..... (1.2)}$$

$$\text{Total cell reaction: } H_2 + \tfrac{1}{2}O_2 \rightarrow H_2O \quad \text{..... (1.3)}$$

Fuel cell is a galvanic cell, in which free energy of a chemical reaction (also known as chemical energy) is converted to electric energy. Gibbs free energy of the reaction is related to cell voltage via[4]:

$$\Delta G = -nFE \quad \text{..... (1.4)}$$

where n is the number of electrons involved in the reaction, F is the Farady Constant and E is the thermodynamic equilibrium potential (also called as Nernst potential) in the absence of a current flow and is given by:

$$E = E_o + \frac{nF}{RT}\ln\left(\frac{\Pi[\text{Re}\,ac\,\text{tan}\,t..Activity]}{\Pi[\text{Pr}\,oduct..Activity]}\right) \quad \text{..... (1.5)}$$

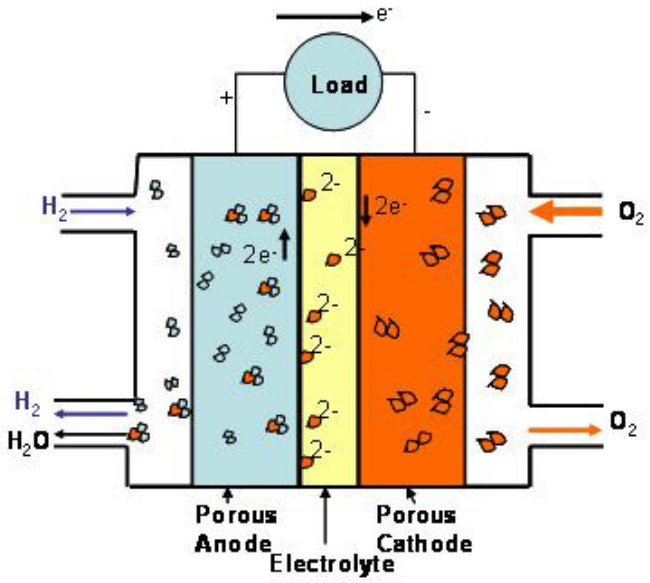

Figure 1-1 Schematic of operation of a fuel cell based on oxide ion conducting electrolyte

Here R is gas constant and T is temperature. Equation (1.5) is known as the *Nernst equation* and provides a relationship between ideal standard potential (E_o) for to overall cell reaction and ideal equilibrium potential (E) at other temperature and partial pressures (in case of gaseous) of the reactants and products of interest. For a typical reaction (equation 1.3) in fuel cell, the equilibrium potential is given by:

$$E = E_o + \frac{RT}{nF} \ln\left(\frac{p_{o_2}^{1/2} * p_{H_2}}{p_{H_2O}} \right) \quad \ldots\ldots (1.6)$$

where p_{O_2}, p_{H_2} and p_{H_2O} are partial pressure of O_2, H_2, and H_2O, respectively. Under the standard conditions of reactant and fuel at temperature of 25°C, the equilibrium Nernst potential E_o for the H_2-O_2 fuel cell is given by[3]:

$$E_o = \frac{\Delta G_o}{nF} = 1.229V \quad \ldots\ldots (1.7)$$

for the free energy change associated with the reaction (equation (1.3)) ΔG_o = -237kJ/mol[3] and number of electrons involved n = 2.

1.1.2. Efficiency of the Fuel Cells

The overall efficiency of a fuel cell is the product of electrochemical efficiency (ε_{elec}) and the heating value efficiency (ε_H). Electrochemical efficiency is a product of thermodynamic efficiency (or thermal or theoretical) efficiency (ε_r^{cell}), voltage efficiency (ε_V), and Faradic or current efficiency (ε_F). The total efficiency of a fuel cell is given by[2]:

$$\varepsilon_{FC} = \varepsilon_{elec} * \varepsilon_H \quad \text{..... (1.8)}$$

$$\varepsilon_{FC} = \varepsilon_r^{cell} * \varepsilon_V * \varepsilon_F * \varepsilon_H \quad \text{..... (1.9)}$$

The **Thermodynamic Efficiency** of a system is determined by the maximum amount of the Gibbs free energy change associated with the chemical reaction that may be totally converted to electrical energy. In case of a fuel cell, thermodynamic efficiency can be calculated from the Gibbs free energy change and the enthalpy change of the fuel cell reaction as follows:

$$\varepsilon_r^{cell} = \frac{W_e}{(-\Delta H)} = \frac{nFE}{(-\Delta H)} = \frac{\Delta G}{\Delta H} = 1 - \frac{T\Delta S}{\Delta H} \quad \text{..... (1.10)}$$

where W_e is the electrical work performed by the cell reaction according to equation (1.3) and ΔS and ΔH are isothermal entropy change and enthalpy change of the reaction respectively.

In fuel cell, each electrochemical reaction is characterized by Nernst potential. However, the observed fuel cell voltage is always lower than the Nernst potential given by equation (1.5). This deviation from equilibrium value is termed as the overpotential, or polarization or over-voltage (η). As current is drawn from a fuel cell, there is further fall in the operating cell

voltage due to various losses such as electrode over-potentials and the electrolyte resistance. Thus, **voltage efficiency** is defined as the ratio of operating cell voltage under load, E_{cell} to equilibrium cell voltage or open circuit voltage E_o and is given as:

$$\varepsilon_V = \frac{E_{cell}}{E_o} = 1 - \frac{\left(|\eta_a| + |\eta_c| + \eta_{\Omega(electrolyte)} + E_{cross}\right)}{E_o} \quad \text{..... ..... (1.11)}$$

Where $\eta_{\Omega(electrolyte)}$ is ohmic overpotential associated with electrolyte, E_{cross} is cross-over potential and $|\eta_a|$ and $|\eta_c|$ are anode and cathode overpotential, respectively. Total polarization $|\eta|$ of an electrode, is the sum of three types of polarization: charge transfer or activation polarization, diffusion or concentration polarization and resistance or ohmic polarization[2] as:

$$\eta = \eta_{act} + \eta_{diff.} + \eta_{\Omega} \quad \text{..... (1.12)}$$

Charge transfer or activation polarization **(η_{act})** is the extra potential necessary to reduce the energy barrier of the rate determining step of the reaction to a value such that the electrode reaction proceeds at a desired rate. In general, the slowest reaction step is the rate determining step. Thus, activation polarization can be reduced by raising the cell temperature, using more effective catalysts, increasing the roughness of the electrodes, reactant concentration, and pressure[5].

Diffusion or Concentration polarization **(η_{diff})** appears when the electrode reaction is hindered by mass transport effects, i.e. when the feeding velocity of the reactant and/or the removing velocity of the reaction product from the electrode are slower than the discharge current. Diffusion polarization is directly related to the mass transport properties of the system.

Resistance or Ohmic polarization **(η_{Ω})** is caused by the resistance to conduction of ions (through the electrolyte) and electrons (through the electrodes and current collectors), and by contact resistance between cell components. This can be reduced by attaining a balance between

increased temperature, by utilizing conducting electrodes, thin electrolyte and appropriate material for the cell interconnect.

Cross over potential **(** E_{cross} **)** is the voltage drop caused by fuel passing through electrolyte and by electron conduction as well. To minimize crossover potential electrolyte should be as dense as possible and should have minimum electronic conductivity.

Summing up the polarization effects, the total polarization is given by:

$$\eta = \eta_a + \eta_c + \eta_{\Omega(electrolyte)} + E_{cross} \quad \text{.....} \quad (1.12)$$

$$\eta = \left[\left(\eta_{act} + \eta_{diff.} + \eta_{\Omega}\right)_a + \left(\eta_{act} + \eta_{diff.} + \eta_{\Omega}\right)_c + \eta_{\Omega_{(electrolyte)}}\right] + E_{cross} \quad \text{.....} \quad (1.13)$$

And observed cell potential is given by [1]:

$$E = E_o - \left(|\eta_a| + |\eta_c| + \eta_{\Omega(electrolyte)} + E_{cross}\right) \text{.....} \quad (1.14)$$

In practice, theoretical (standard) cell potential can never be achieved and difference between standard cell potential and observed lower electrode potential is caused by all four voltage drops.

The **Faradic Efficiency (** ε_F **)** is defined as ratio of observed current I_{obs} to maximum possible current I_{max} [3]. The importance of Faradic efficiency lies in the fact that in practice, parallel electrochemical reactions exist which lead to a lower current than the theoretical current expected from primary electrochemical reaction. It also accounts for the possibility of heterogeneously catalyzed chemical reactions occurring at the electrode surfaces.

$$\varepsilon_F = \frac{I_{obs}}{I_{\max}} = \frac{n_{obs} * F * E_0}{n_{\max} * F * E_0} = \frac{n_{obs}}{n_{\max}} \quad \text{.....} \quad (1.15)$$

where $I_{\max}$ is the theoretical /maximum expected current from the primary electrochemical cell reaction, I_{obs} is the current observed from secondary chemical reaction, and n is the number of electrons involved in the respective reaction.

The **Heating Value Efficiency (ε_H)** is defined as ratio of enthalpy change (heating value) associated with all fuel components that are converted electrochemically (ΔH_r) to enthalpy change of all fuels supplied (ΔH_c), and can be expressed as:

$$\varepsilon_H = \frac{\Delta H_r}{\Delta H_c} \quad \text{..... (1.16)}$$

where ΔH_r is the heating value of electrochemically converted fuel (H_2) and ΔH_c is heating value of all the fuels (CH_4 and CO) being fed to anode. The origin of this efficiency exists in the fact that when using a mixture of the fuels, all the components are not electrochemically converted. This causes an additional amount of reactants to be supplied and thus subsequently heated.

It is worth noting here that efficiency of a fuel cell system can be significantly enhanced by cogeneration of the electricity and heat power. Cogeneration is simultaneous utilization of electricity and by product heat from an energy conversion device. The byproduct heat is utilized to either produce more electricity through gas or steam turbine (also known as bottoming cycle) or to supply hot water, generate steam for industrial process or simply for the space heating. This utilization of the byproduct heat increases overall efficiency of the system and is given by:

$$\varepsilon_{overall} = \frac{E_e + Q}{Q_o} \quad \text{..... (1.17)}$$

where 'Q_o' is the total heat content of supplied fuel and 'E_e'is electrical energy produced and 'Q' is by product heat which can be further utilized.

1.1.3. Fuel Cell Performance

The performance of a given fuel cell is depicted through its characteristic current density vs. voltage plot where current density is current normalized by anode area to obviate dependency of the current produced on the size of electrode. Such a schematic plot is shown in Fig. 1-2[1,6]. It can be observed that the cell potential is always smaller than that of the theoretical potential (presented through the horizontal dotted line) because of various polarization and cross over potential losses. The plot consists of three different voltage regions at different current density levels.

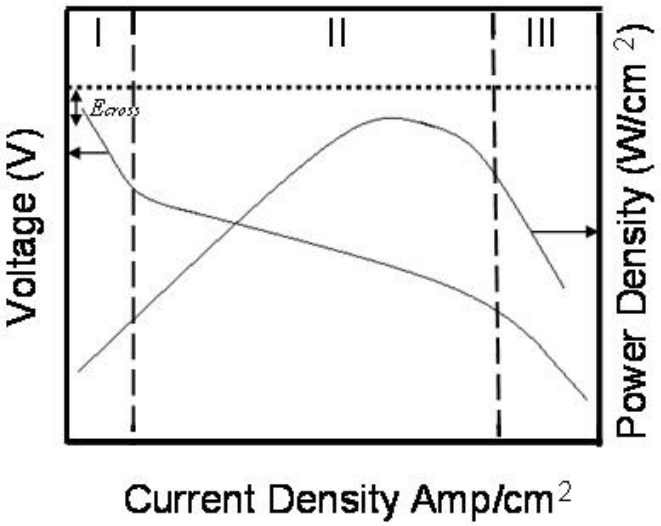

Figure 1-2 The schematic of fuel cell polarization (voltage vs. current density) and superimposed power density curve[1]

At low current densities, region 1 in Fig.1-2, the major contribution to cell voltage losses is from activation polarization, as indicated by sharp drop in cell voltage with increasing current. As the current increases, the resistance polarization or Ohmic loss dominates- region 2 while at high current densities, the cell resistance is controlled by mass transport limitation, resulting in a rapid decrease in cell voltage - region 3. Under ideal conditions (i.e. all the polarization losses are

zero), the expected constant voltage is independent of the current drawn and is equal to theoretical or open circuit voltage defined by equation (1.7).

The power delivered by a fuel cell is given by the product of current and voltage while the power density is given by:

$$P = E * i \quad \ldots\ldots\ldots\

Table 1-1 A comparative study of low temperature fuel cells

	Alkali Fuel Cell	Polymer Electrolyte Membrane Fuel Cell	Direct Methanol Fuel Cell
Anode	Pt-Pd	PTFE-bonded Pt on C	PTFE-bonded Pt on C
Cathode	Pt-Au	PTFE-bonded Pt on C	PTFE-bonded Pt on C
Electrolyte	KOH solution	Sulfonated polymers (Nafion TM)	Sulfonated polymers (Nafion TM)
Interconnect	Ni	Graphite	Graphite
Fuel	H_2	H_2	CH_3OH
Oxidant	O_2	O_2/Air	O_2/Air
Conducting ion	OH-	$(H_2O)_nH^+$	H+
Electrochemical Half cell reactions (anode and cathode)	$H_2 + 2OH^- \rightarrow 2H_2O + 2e^-$	$H_2 \rightarrow 2H^+ + 2e^-$	$\frac{3}{2}O_2 + 6H^+ + 6e^- \rightarrow 3H_2O$
	$\frac{1}{2}O_2 + 2H^+ + 2e^- \rightarrow H_2O$	$\frac{1}{2}O_2 + H_2O + 2e^- \rightarrow 2OH^-$	$CH_3OH + H_2O \rightarrow CO_2 + 6H^+ + 6e^-$
Contaminant Tolerance	No CO/CO_2 and no Sulfur	<50 ppm CO, and no sulfur	
Operating temperature	<100	60-120^{o}C	60-120 ^{o}C
Pressure	1 to 10 atm	1 to 5 atm	
Reforming		External	
Efficiency(without and with cogeneration)		35-50% and 60%	
Maximum Power output	5-150Kw	5- 250 kW	5kW
Application field	Used in space vehicles such as Apollo, Shuttle	Vehicles and mobile applications, and for low power CHP applications	Suitable for portable electronic systems of low power, running for longer times.
Waste Heat Usage		Space heating or water heating	

Table 1-2 comparative study of medium and high temperature fuel cells

	Phosphoric Acid Fuel Cell	**Molten Carbonate Fuel Cell**	**Solid Oxide Fuel Cell**
Anode	PTFE-bonded Pt on C	Ni	Ni/YSZ
Cathode	PTFE-bonded Pt on C	Li-Doped NiO	Sr doped $LaMnO_3$
Electrolyte	Liquid phosphoric acid	Molten carbonate salt ($LiCO_3$-	Yttria Stabilized Zirconia
Interconnect	Glassy Carbon	Stainless Steel clad with Ni	Doped $LaCrO_3$
Fuel	H_2	Hydrocarbons, CO	Hydrocarbons, CO
Oxidant	O_2/Air	CO_2/O_2/Air	O_2/Air
Conducting ion	H^+	CO_3^{2-}	O^{2-}
Electrochemical Half cell reactions (anode and cathode)	$H_2 \rightarrow 2H^+ + 2e^-$	$H_2 + 2CO_3^{2-} \rightarrow H_2O + CO_2 + 2e^-$	$H_2 + O^{2-} \rightarrow H_2O + 2e^-$
	$\frac{1}{2}O_2 + 2H^+ + 2e^- \rightarrow H_2O$	$\frac{1}{2}O_2 + CO_2 + 2e^- \rightarrow CO_3^{2-}$	$\frac{1}{2}O_2 + 2e^- \rightarrow O^{2-}$
Contaminant Tolerance	<1 to 2% CO, <50 ppm	<1ppm Sulfur	<10-100 ppm sulfur
Operating temperature	150-200°C	600-800°C	800-1000°C
Pressure	1 to 8atm	1 to 3 atm	1 atm
Reforming	External	External/Internal	External/internal
Efficiency(without and with cogeneration)	35-50% and 80%	45-60% and 85%	45-60% and 85%
Maximum Power output	50kW-11 MW	100kW- 2MW	220 MW
Application field	Large transportation vehicles	Suitable for medium to large	Small (less than 1kW)to
Waste Heat Usage	Space heating or water heating	Excess heat can produce high pressure steam	Excess heat can be used to heat water produce steam

1.3. The Advantages and Disadvantages of Fuel Cells

The major advantages associated with fuel cells when compared with other energy conversion devices can be summarized as following: [2,11]

i. Fuel cells offer extremely **high chemical to electrical conversion efficiencies** (40-50%) because of absence of Carnot limitation. Further energy gains (additional 20-25%) can be achieved when produced heat is utilized in combined heat and power (CHP) co-generation. Also, since no mechanical conversion is required the losses associated with these steps do not exist in fuel cells. More importantly, **efficiency** of a fuel cell is **independent** of its size.
ii. Certain types of fuel cells (such as the high temperature fuel cells) have **the multi-fuel capability.** These can process (reform) hydrocarbon fuels internally and do not need expensive subsystems to process conventional fuels into simple forms. The fuel cells are capable of using the different fuels as an energy source with **insignificant environmental impact**. The emissions of key pollutants such as NO_x and SO_x from the fuel cells are several orders of magnitude lower than those produced by conventional power generators.
iii. Since there are no moving parts in the operation of fuel cell, they **provide silent electrical power** and thus can be easily located near the point of use such as urban residential area.
iv. Very **low maintenance** is required since fuel cells do not experience wear, tear and corrosion when compared with batteries.
v. It is noteworthy that fuel cells consume fuel and oxidant only when power is drawn from the system. There is **no fuel consumption during the idle periods** of a fuel cell.
vi. Thus **the sitting efficiency and the modularity** of fuel cell is an additional advantage. Since the current delivered by an individual cell is proportional to the geometrical area of the electrode; thus to increase current, electrode may be increased in size or several cells may be connected in parallel or series to yield very high currents at high voltages. This flexibility is most convenient from the design point of view and for weight distribution and space utilization.

Although numerous advantages of fuel cells make them very attractive as energy conversion devices, their commercialization is mostly limited for the following reasons[2]:

i. The **high cost** associated with the fabrication of a fuel cell is the chief among the problems associated with the commercialization. Most of the component pieces for a fuel cell are quite costly. Such as for a PEMFC system, proton exchange membranes, precious metal catalysts (usually platinum), gas diffusion layers, and bipolar plates make up 70 percent of a system's cost. In order to be competitively priced (compared to gasoline-powered vehicles), fuel cell systems must cost $35 per kilowatt. Currently, the projected high-volume production price is $110 per kilowatt[1].
ii. Fuel cell should have **low tolerance to impurities** in the fuel.
iii. Currently, fuel cells have **lower or in some cases unknown reliability and durability** when compared to other energy conversion devices. The components of fuel cell sometimes break down and /crack after very few cycles of operation.
iv. Other issues include the concerns with **safe and reliable delivery of the hydrogen** fuel, infrastructure, and storage and other considerations.

Despite of above mentioned challenges in commercializing fuel cells, the possibility of zero-emissions electricity generation and increased energy security offered by these energy conversion devices have drawn attention of the scientific community around the world to contribute towards the wholesome development of a fuel cell.

2. SOLID OXIDE FUEL CELLS

2.1. Introduction

A solid oxide fuel cell (SOFC) is an all solid state fuel cell with ionic conducting ceramic electrolyte[2]. Alternatively, an SOFC is called a "ceramic fuel cell" because its main constituents are predominantly made of ceramic materials. The direct conversion of chemical energy of the fuel into electrical energy in SOFC is achieved in the similar way as described in section 1.1 The oxidation of the fuel is an exothermic reaction and the heat thus produced is further utilized to maintain the functionality of electrolyte (ionic conductivity is a thermally activated process), to process the fuel, and for space heating and/or for cogeneration. Various reactions occurring in an oxygen ion conductor SOFC employing CO-H_2 as a fuel are shown in the Fig. 2-1.

The present generation of ceramic fuel cells may be classified as those based on the (a) oxygen ion conducting electrolyte and (b) proton conducting electrolyte. The oxygen ion conductor SOFC is the most common and can be considered as *an oxygen concentration cell*. The oxide ions formed at the cathode have to diffuse through a non porous, ionic conductor electrolyte. Because ion conduction is a thermally activated process, the SOFC needs to be operated at high temperatures[12]. The diffused oxide ions then reach to the fuel electrode (Anode), oxidize fuel at the anode/electrolyte interface and/or at the reaction sites where the three phases are in contact (also called the *three phase boundaries (TPB*) and produce water as a by product. The basic elements of a single SOFC are electrolyte, anode and cathode.

In the standard conditions of fuel and oxidant and no losses, a cell can generate voltage of about 1 V. However in practice this output voltage is rarely achieved and fuel cell is typically operated at around 0.6-0.7V at a power output of 250 to 450 mW/cm^2 [,13]. In practical applications, multiple SOFCs are assembled to form a stack – known as SOFC stack and make a serial connection in the electric loop to generate high voltage and power. Interconnects or Bipolar plates are used as the current collector and to connect the cells in series. An interconnect for planar SOFC is either ceramic or metallic depending on the operating temperature.

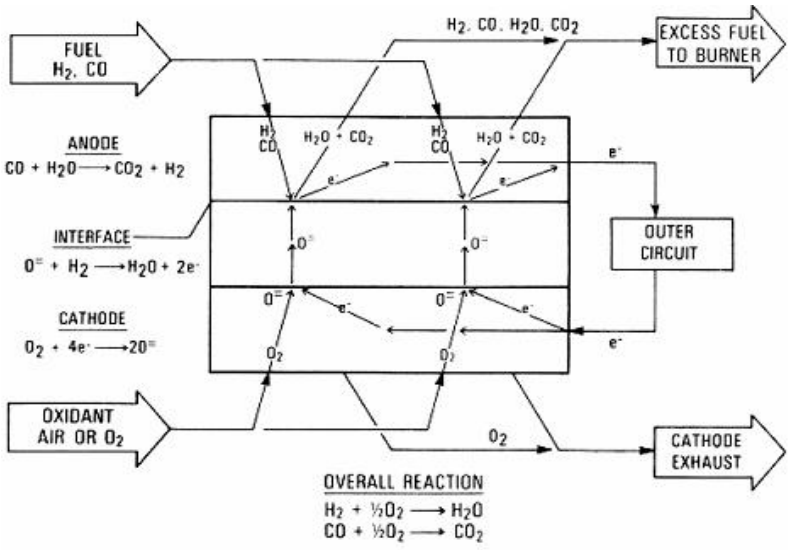

Figure 2-1 The schematic of the operation of an SOFC employing CO-H2 as the fuel[2]

2.2. Historical Development of an SOFC

The principle of fuel cell operation was first reported by Sir William Grove '*father of fuel cell*' in 1839[2]. In 1899, Nernst introduced ZrO_2 with 15wt% Y_2O_3 (Nernst Mass) as one of the first known solid oxygen-ion conductor while Schottkey suggested the use of Nernst mass as fuel cell solid electrolyte in 1935. Following this, Baur and Preis demonstrated the operation of the first ceramic fuel cell in 1937. The initial development work on practical ceramic fuel cells began in the early 1960s. During this period, cell configuration was either in the form of a flat plate design using the electrolyte in the form of a disk, or a segmented- cell-in series design (Bell-and Spigot configuration). The further development included segmented cell-in-series (banded configuration) (1970), sealless tubular SOFC (1980), Monolithic SOFC (1982) leading towards the development of the advanced flat plate (Planar) SOFC. Along with the SOFC design as a whole, advance materials were being developed for the various components. In the early 1970s, Nickel/YSZ, doped In_2O_3, and $CoCr_2O_3$ were used as anode, cathode and interconnect respectively. During the same time period $LaCoO_3$ was also considered as an alternate cathode

material to doped In_2O_3. $CoCr_2O_3$ was later replaced by $LaCrO_3$. In 1980, and $LaMnO_3$ was proposed as cathode material. Fig. 2-2 summarizes the key historical events in the development of the SOFC technology.

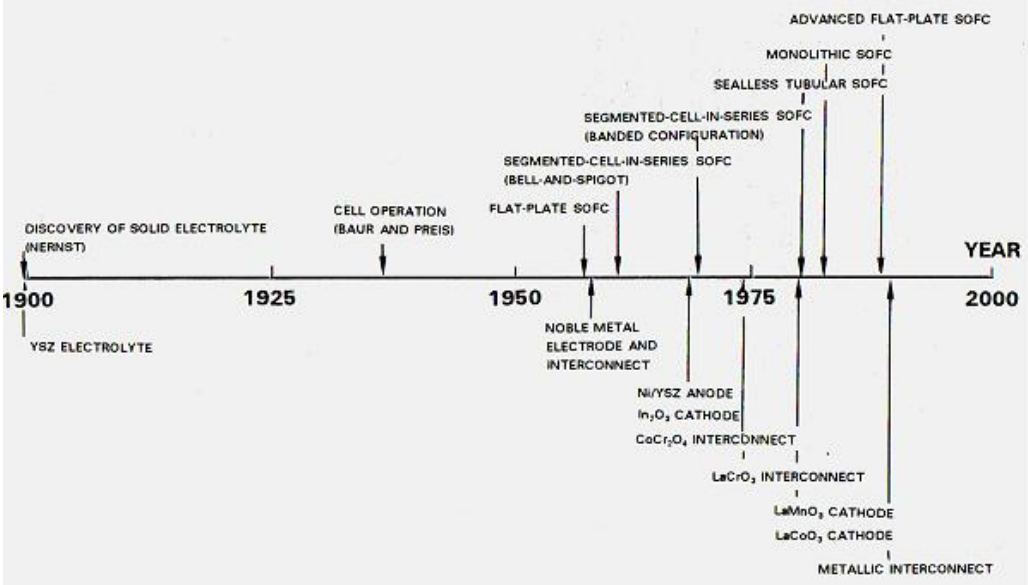

Figure 2-2 The schematic chart of historical events in technology development of an SOFC2

2.3. Configuration of Modern SOFCs

An SOFC cell can be configured into various shapes depending on the specific stack design. However, any design should meet the desired electrical and electrochemical performance along with the thermal management and mechanical/structural integrity to meet the operating requirements of specified power generation applications. Among various SOFC cell configurations, the two mainly adopted designs are planar and tubular configurations as shown in Fig. 2-3 (a) and (b) respectively. In the *planar configuration* the cell components - electrodes, electrolyte and interconnect - are in the planar geometry (circular discs or square plates) which are arranged in the "sandwich" configuration as shown in Fig. 2-3(a). In the *tubular configuration,* the cell components are deposited in the form of thin layer on a cylindrical tube as shown in Fig. 2-3 (b). Tubular designs have the self sealing structure which improves thermal

stability and eliminates the need for good thermal resistant sealants. However, the drawbacks associated with the tubular configuration are low volumetric power density (caused by the small current collector region) and high manufacturing costs. Planar SOFCs are more popular because of the ease of fabrication and high power density.

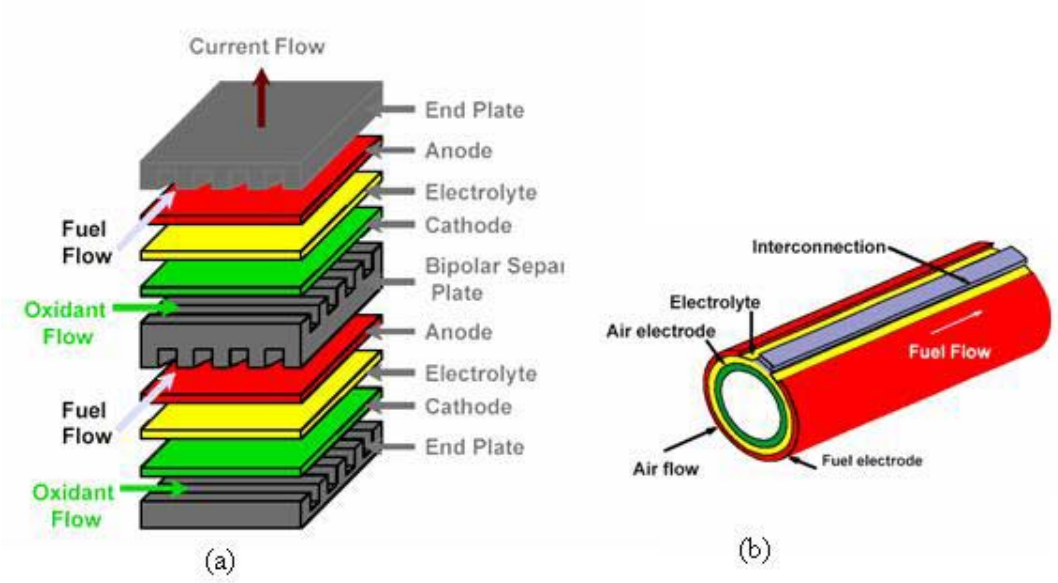

Figure 2-3 (a) Planar configuration and (b) tubular configuration of solid oxide fuel cells [13],[14]

Fuel and oxidant flow in planar SOFC can be arranged in cross flow (as shown in the Fig. 2-3 (a)), co-flow, or counter–flow. The selection of particular flow configuration has significant effects on the temperature and current distribution depending on the precise stack design and thus on the mechanical and structural integrity of the stack Flow-fields (flow channels) are engraved in interconnects to increase uniformity of the gas distribution and to promote heat and mass transport in each cell. Thus defining the flow field for both fuel and oxidant flow is an important aspect in designing planar SOFC. To route the fuel and oxidant from a common supply point and to remove unreacted gases and reaction products from each cell manifold are provided. These can be classified as internal/ external depending on the construction. As the name suggests, external manifolds are constructed separately from the cell or interconnect of the

stack while the internal manifolds are formed and designed as part of the cell or interconnect. Depending on the design, gas manifolds often require sealing to prevent gas leakage or cross over[14].

Fabrication process selected for each planar SOFC cell/stack design depends on the configuration of the cell in the stack. However, the key step in any selected process is the fabrication of dense electrolyte. Based on the fabrication approach for the electrolyte, ceramic fabrication process for planar SOFCs can be classified into two groups - the particulate approach and deposition approach. The particulate approach involves the compaction of ceramic powder into cell components and densification at elevated temperatures. Examples of the particulate approach are *tape casting* and *tape calendaring*. The deposition approach involves the formation of cell components on a support by a chemical or physical process.

For solid oxide fuel cells to survive the mechanical loading associated with residual manufacturing stresses, assembly, thermal mismatches, ion activity gradients, or operational loading, one or more components of the fuel cell stack must provide sufficient mechanical strength. Thus, the configurations in planar SOFC single cells can be classified into two broad categories: self-supporting and external-supporting depending on the type of support. In the self-supporting configuration one of the cell components (often the thickest layer) acts as the cell structural support. Thus single cells can be designated as anode-supported (Fig. 2-4(a)), electrolyte-supported (Fig. 2-4(b)) or cathode-supported based on the component which provides the support. *Anode-supported SOFC*s with thinner electrolytes (maximum thickness up to 20 μm) have received more attention because of their relatively low operation temperature and achievable high current densities. Other advantages associated with reduced temperature SOFCs include a wider choice of materials (especially low cost materials for interconnect), low fabrication cost, longer cell life caused by reduced thermal stresses and thus the improved reliability. However, the lower operation temperature result in slow electrode reaction kinetics (resulting in the high losses with activation polarization) and reduced thermal energy that can be extracted from the hot exhaust stream by a turbine or heat exchanger. Low ionic conductivity of the electrolyte limits the wider use of the electrolyte supported SOFCs at low operating temperatures. Tubular cell configuration shown in Fig. 2-3 (b) is an example of cathode

supported tubular SOFC wherein thin electrolyte and anode covers the cathode, except a little strip where the current collector is placed.

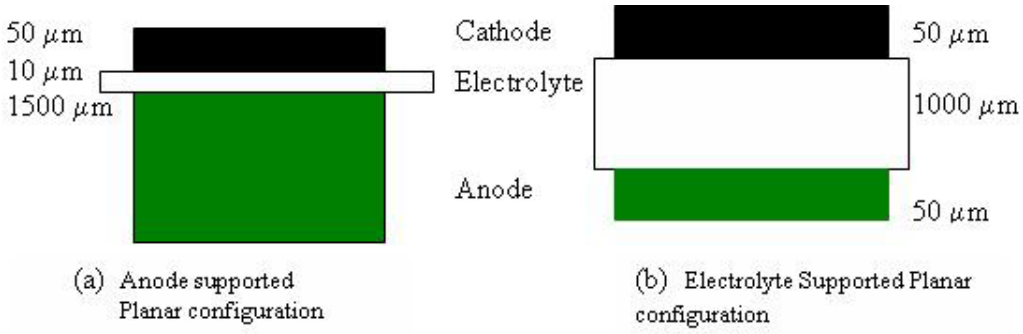

Figure 2-4 Schematic of single cell structure of (a) Anode and (b) Electrolyte supported planar configuration of an SOFC[15]

2.4. Materials for SOFC Components

This subsection deals with the development of state of the art materials for the components of SOFCs. Function and specific requirements of each component has been described followed by the issues associated with the conventional materials. With the increasing attention towards intermediate / low temperature SOFC, many more attempts have been made to develop the materials which may ensure the reliability and thus the viable commercialization. A brief review of recently investigated materials has also been presented.

2.4.1. Electrolyte Materials

The main function of electrolyte is to conduct ions between anode and cathode. Electrolyte carries the ions produced at one electrode to the other electrode to balance charge from the electron flow and to complete the electrical circuit in the fuel cell. The electrolyte also separates the fuel from oxidant thus must be as dense as possible to prevent cross over, stable in both oxidizing and reducing atmosphere and of sufficiently high ionic conductivity and low electronic

conductivity at the cell operating temperatures. The key requirements of SOFC electrolyte are as follows[2,14]:

i. The electrolyte must be **chemically, microstructurally and dimensionally stable** in dual atmosphere (oxidizing atmosphere at cathode side and reducing atmosphere at anode side).
ii. The electrolyte should be **sufficient ionic conductor** in the dual atmosphere but with very low electronic conductivity to minimize the ohmic losses and voltage losses respectively.
iii. The electrolyte should also be **compatible** with other cell components in order to have minimum or no chemical interaction and/or elemental diffusion with other cell components at the fabrication and operating temperatures and environments.
iv. There should be **minimum thermal expansion mismatch between electrolyte and other cell components** in the fabrication and in-service temperature range in order to avoid cracking and delamination. Also, the CTE of electrolyte must not change despite of changes in the oxygen partial pressure of the fuel and oxidant during in-service conditions.

Other requirements include low fabrication cost, processibility, high strength and toughness.

The conventional electrolyte is based on stabilized (cubic) zirconia which is a classic oxygen ion conductor. Cubic zirconia has fluorite structure with face centered cubic arrangement of cations wherein anions occupy all the tetrahedral position. Unoccupied octahedral sites give rise to higher mobility of the oxide ions and vacancies. This high temperature stable fluorite structure of zirconia can be stabilized at lower temperature by doping with divalent and/or trivalent cations such as CaO_2 or Y_2O_3. Dissolution of yttria into the fluorite phase of ZrO_2 can be given by the following defect equation[14] :

$$Y_2O_3 \xrightarrow[ZrO_2]{} 2Y'_{Zr} + V_{\ddot{O}} + 3O_o^x \quad \text{..... (2.1)}$$

This equation suggests that addition of the dopant also assists in increased concentration of oxygen vacancies, and thus ionic conductivity which is rather low in otherwise pure ZrO_2.

It is worth mentioning here that the diffusion of oxide ion vacancies is affected by elastic strain energy which is related to the size mismatch between the host and dopant ions and this reasoning supports the higher solubility of Sc^{+3} (around 11%), when compared with other dopants such as

Dy^{3+} and Gd^{3+} (8mol%) which have higher ionic radii than the host ion Zr^{+4} at 1000°C [15]. Scandia doped zirconia (SDZ) has a higher conductivity and at 780°C its value is comparable to that of YSZ at 1000°C[16]. Thus Scandia doped zirconia is an attractive electrolyte candidate for intermediate to low temperature SOFCs. However, SDZ exhibits aging on long term exposure at high temperatures. It has been reported by Uchida and Yamamoto et. al. that ZrO_2 stabilized with 8mol% Sc_2O_3 experiences a decrease in conductivity from 0.3 S/cm to 0.12 S/cm at 1000°C after 1000h [17,18] while ZrO_2 stabilized with 11mol% Sc_2O_3 has been reported not to exhibit any aging effect at 1000°C even after 6000h. The cubic phase of ZrO_2 doped with 11 mol% Sc_2O_3 can be stabilized by addition of Al_2O_3 or CeO_2. ZrO_2 stabilized with 11 mol% Sc_2O_3 and 1 wt% Al_2O_3 has been suggested to be an attractive electrolyte for the intermediate temperature SOFC because of its high oxide ion conductivity (0.26 S/cm), phase stability and excellent mechanical property (Bending strength 250MPa)[19,20]

Ceria (CeO_2) possesses fluorite structure similar to stabilized zirconia. **Ceria based electrolytes** have been suggested as the potential candidates for intermediate and low temperature SOFCs because of much higher ionic conductivity in the lower temperature regime. However, at lower oxygen partial pressure (under reducing conditions as is experienced at the layer in contact with anode) ceria gets partially reduced which introduces detrimental electronic conductivity in the material which in-turn impairs the efficiency of SOFC. Similar to ZrO_2, Pure CeO_2 has negligible ionic conductivity. Mobile oxygen vacancies and ionic conductivity is introduced by substituting Ce^{+4} with trivalent rare earth ions (Gd^{+3}, Sm^{+3}, and Y^{+3}). Both Samaria doped ceria (SDC) and Gadolinia Doped Ceria (GDC) (with 10-25% dopant) have been shown to exhibit conductivity very similar to YSZ at 1000°C[21]. However, the application of SDC as electrolyte material is limited to temperatures below 600°C caused by its efficiency loss due to high electronic leakage[22].

Other potential electrolytes for low-intermediate temperature SOFC are the **Lanthanum Gallate perovskites based ceramics**. When trivalent lanthanum and gallium are substituted by divalent cations like Sr and Mg, the resulted compound $La_{1-x}Sr_xGa_{1-y}Mg_yO_{3-x/2-y/2}$ (LSGM) has much higher ionic conductivity than that of YSZ and higher stability than that of GDC in the temperature regime 600-800°C. However, fabrication of single phase LSGM electrolyte is rather

difficult, formation of secondary phases such as $La_4Ga_2O_9$ and $SrLaGa_3O_7$ at grain boundaries leads to lowered conductivity[23]. Moreover, limited stability of LSGM has also been attributed to introduction of n-and p-type conductivity at low and high oxygen partial pressures respectively [24]. Another drawback of lanthanum gallate electrolyte is its high reactivity with Ni from anode. However, latter limitation can be prevented by incorporating ceria buffer layers between the electrolyte and anode[25].

2.4.2. Anode Materials

The main function of the SOFC anode is to provide reaction sites for the electrochemical oxidation of the fuel. By definition of its role, the anode should be electro-catalytically active for electrochemical oxidation of the fuel and have good electrical conductivity. Ionic conductivity would allow the spread of oxide ions across the electrolyte/ anode interface while high electronic conductivity would accelerate the flow of electrons into the external circuit. The various requirements of anode materials are[2,14]:

i. The anode must be **chemically, morphologically and dimensionally stable** over the whole temperature range to which it is exposed from fabrication process to in-service conditions (including repeated start up and shut downs) in the reducing environment. *Redox stability* is a further desirable attribute of an anode material to permit brief excursions to high oxygen concentrations (even to air), without irreversible loss of structural coherence and electrochemical functionality.
ii. The anode must **possess high ionic and electronic conductivity** to minimize the ohmic losses and to optimize the electron flow respectively. Also, anode conductivity should not change significantly during cell operation caused by changes in oxygen partial pressure in the fuel environment.
iii. The anode must be both **physically and chemically compatible** with other cell components in the whole temperature range and reducing environment in order to minimize a mismatch of thermomechanical properties and formation of the secondary phases respectively.

iv. A significant mismatch of **thermal expansion** between anode and other cell components would lead to loss of mechanical integrity and thus should be minimized in the fabrication and in-service temperature range. Also, it is required that the coefficient of thermal expansion (CTE) of anode should not get altered during in-service conditions.
v. The anode should have **sufficient porosity** to allow gas transport to the reaction sites. The lower limit on porosity is set by the mass transport consideration while the upper limit is set by the mechanical strength of the component.
vi. **Catalytic properties** of the anode are required for oxidizing the fuel with the oxide ions coming through the electrolyte. However, the catalytic behavior of anode materials should not extend to the promotion of unwanted side reactions which may lead to degraded performance of the cell.

Since anode material has to have a good electronic conductivity, several metallic materials and alloys have been investigated as the SOFC anode materials caused by their stability under reducing atmosphere over a range of temperature. Among other transition metals, Ni has been the material of choice due to its high electrochemical activity for the hydrogen oxidation, acceptable cost, and suitable chemical compatibility. However, pure metal anode had not been accepted because of its significantly higher thermal expansion and the aggregation at higher temperatures. This had led to the development of a **conventional anode material - Ni/YSZ** Cermet[26]. The role of YSZ is to delocalize the electrochemical active zone by dispersing nickel particles, maintain the electro-catalytic action of the metallic phase by inhibiting the coarsening of metallic phase at cell operating temperature, to lower down the CTE of the otherwise metallic anode and to provide ionic conductivity as a complementary to the electronic conductivity of the metal particles[27]. The electrical conductivity of the Ni/YSZ cermet is strongly dependent on nickel content as predicted by the percolation theory, 30 Vol% Nickel has been reported to exhibit the threshold electrical conductivity[28]. In the composite ceramic-metal anode the electrochemical reaction takes place at *triple phase boundaries- TBPs* - the sites where these three phases, namely fuel gas, YSZ and Ni are in contact.

It is now well established that **Ni/YSZ anode has some limitations** as well. After long term operation anode performance gets lowered because of *Ni coarsening or agglomeration* which in-

turn leads to reduction of electrochemical reaction sites (TPBs) and electrical conductivity. Various additives (MgO, TiO_2, Mn_3O_4 and Cr_2O_3–low surface energy oxides) have been suggested to minimize Ni coarsening[29]. In addition, these additives also improve mechanical properties of the anode by assisting in sintering of YSZ and enhance the wettability of Ni particles by acting as anchoring sites at the anode/electrolyte interface. The *fuel specification* has been known as a major limiting factor for the conventional Ni/YSZ anode. Nickel is an excellent electrocatalyst for electrochemical oxidation of hydrogen. However, this activity is impaired when natural gas or methane is directly used as a fuel which leads to *carbon formation.* Formation of carbon in turn causes pore clogging and blocking of the reaction sites on Nickel surface, leading to excessively high activation polarization. If methane or other hydrocarbon is to be used, it has to be first converted to hydrogen via internal or external steam reforming. Depending on the fuel origin such as coal gasification, biomass pyrolysis or fermentation, there may be impurities such as that of H_2S, HCl, ammonia and some organics, for which Ni has very *poor tolerances*. At high temperatures this limit get further reduced[30]. Also, the long service hours cause loss of metallic conductivity resulting from the oxidation of nickel and degrade the anode performance commonly known as *redox instability*. A rise in Oxygen potential above -0.68V, causes the formation of a volatile compound $Ni(OH)_2$ leading to loss of active nickel[31]. Also, Ni particles resulting from reduction of NiO react with the Cr_2O_3 a major constituent of metallic interconnects, yielding Ni-Cr spinels at the anode/ interconnect interface which further results in degraded performance[32].

In order to achieve high conductivity and hence an excellent cell performance along with a low overall shrinkage, novel conceptual microstructure that is composed of coarse YSZ, fine YSZ and NiO has been proposed[33]. A Broader size spectrum of YSZ powders has been shown to have improved packing efficiency thus more stable anode, more electrochemical sites leading to suppressed polarization and hence enhanced electrical conductivity[33,34].

Most research aimed at overcoming the limitations of nickel based anodes have focused on the development of **alternative anode materials** that are catalytically active for the oxidation of more readily available hydrocarbon fuel (e.g. methane) at lower operating temperatures and inactive for cracking reactions that can lead to carbon depositions.

A **ternary component anode** consisting of Cu, CeO_2 and YSZ has been reported to demonstrate encouraging results in terms of direct electrochemical oxidation of a variety of hydrocarbon gases and very low carbon deposition by Park et. al.[35]. Also, Cu containing anodes have been reported to more tolerant towards presence of sulfur[36]. Long term sustainability of $Cu/CeO_2/YSZ$ anode would help in reducing the cost and complexity of SOFC power generation system.

Considering the compatibility to YSZ electrolyte, **Yttria-Titania modified Zirconia (YZT)** has also been suggested as a mixed conducting anode material[37]. YZT has been reported not to promote methane cracking but is less electrochemically active than those of Ceria based anodes. *Mixed ionic-electronic oxides* with perovskite structure have also been considered as potential single phase anode materials. Despite of poor mechanical performance and lattice expansion in reducing atmosphere, **lanthanum chromite** has been considered as an alternative because of its desired chemical and thermal stability. A composite anode approach, having substitution of La with Sr and that of Cr with V has been reported to have materials with n-type conductivity along with the dimensional stability in reducing atmosphere[38]. $La_{0.8}Sr_{0.2}Cr_{0.97}V_{0.03}O_3$ /YSZ, a composite anode, has been shown to exhibit comparable electrochemical performance to that of Ni-YSZ with excellent resistance to carbon deposition [39]. However, methane steam reforming capability of this system has been suggested to improve by incorporation of Ru.

Also, Ceria has been long been known as an excellent catalyst for methane (CH_4) oxidation[40]. Gadolinia doped ceria (GDC) has higher electronic conductivity and structural stability than the undoped ceria as mentioned earlier[41]. Similar to Ni/YSZ anode, **Ni/GDC anodes** have been developed which allow the direct electrochemical oxidation of methane with a suppressed carbon deposition for *intermediate temperature SOFCs* utilizing GDC as the electrolyte[42]. Also, Ni/GDC has been shown to outperform in terms of anodic overpotential when used with H_2 as the fuel[43].

2.4.3. Cathode Materials

The main function of the cathode for an SOFC is to provide reaction sites for electrochemical reduction of oxidant. The cathode should have high electro-catalytic activity towards oxygen reduction and high electrical (ionic and electronic) conductivity, chemical and dimensional stability during fabrication and oxidizing environments at high temperature regime encountered during cell operation. Various requirements of cathode materials are as following[2]:

i. The cathode material must be **chemically, morphologically and dimensionally stable** in the oxidizing environments at high operation temperatures.
ii. The cathode should have enough **electronic conductivity** to support electron flow in the oxidizing environment and **ionic conductivity** to allow the passage of oxide ions towards electrolyte.
iii. Cathode material should be **chemically compatibl**e with the other cell components to avoid the formation of secondary phases at the interface which may lead to the degraded performance of cell.
iv. There should be **minimum thermal expansion mismatch** between cathode and other adjoining cell components in order to avoid cracking and delamination during cell fabrication and in-service conditions.
v. Cathode should have **sufficient porosity** to allow the inward diffusion of oxidant and provide enough triple phase boundaries to provide electrochemical sites for reduction of oxidant. Also, cathode must have sufficient catalytic activity and thus low polarization towards electrochemical reduction of oxidant.

Other requirements include processibility, low fabrication cost and high strength and toughness.

SOFC cathodes are usually p-type semiconductors that can be either electronic or mixed ionic-electronic conductors (MIEC). Most of the cathodes are perovskite types – ABO_3 in which structure A cations (large cations) occupy the corner positions (with coordination number of 12), B cations (smaller cations) occupy the octahedral positions and O^{2-} are at the face centered

positions[14]. As for most perovskites, electrical properties such as ionic conductivity and oxygen exchange rate can be tailored by partially substituting A and B sites.

Lanthanum Manganite $LaMnO_3$, has long been considered as the cathode material because of it high electrical conductivity and catalytic properties towards reduction of oxidant. However, high operation temperature was found to get impaired because of formation of secondary phase $La_2Zr_2O_7$ when used in a cell with YSZ electrolyte[44]. A site (La)-deficient $LaMnO_3$ cathode was suggested to avoid formation of this reaction compound. Substitution of La with lower valence cations such as (Ca^{2+} or Sr^{2+}) results in improved mixed conductivity as well[14] . This has led to the development of the **state of art cathode $La_{1-x}Sr_xMnO_{3-x/2}$ (LSM).** This cathode has compatible CTE and chemical properties with the other SOFC components (electrolyte YSZ). However, in a contradictory study it has been reported by Lau and Singhal, that at high temperatures, inter-diffusion of Mn, La and Sr ions occur into the adjacent electrolyte YSZ[45]. Efforts have been made to minimize the reactions between cathode and electrolyte and one such approach has led to the development of **composite cathodes** by mixing LSM and YSZ powders and laying down a thin layer of this mixture on the electrolyte and then a thicker layer of porous LSM is laid on top of this functional layer to provide the contact with the interconnect[14]. The composite layer provides large three phase boundary area and also improves the mixed ionic – electronic conductivity of the material both of which would reduce polarization. **Strontium doped lanthanum ferrites** ($La_{1-x}Sr_xFeO_3$ - LSF) have also been investigated since they have relatively good match of CTE with YSZ and do not form reaction products[46].

Since 1969, $LaCoO_3$ has been suggested as an effective cathode material because of its high electronic and ionic conductivity[47]. However, its performance was found to deteriorate after a few cycles because of its chemical interaction with YSZ and high CTE $20x10^{6-}K^{1-}$when compared with YSZ[48]. CTE of $LaCoO_3$ has been reported to get lowered by doping with Sr and other alkaline rare earth ions. Resulting **$La_{1-x}Sr_xCoO_3$ (LSC)** based cathodes are typical mixed conductors, however chemical incompatibility (formation of insulating phases $La_2Zr_2O_7$ and $SrZrO_3$ at the interphase) with YSZ electrolyte still imposes restrictions. However, no such reaction products have been found when used with ceria based electrolyte (GDC)[49]. Thus cobaltite based cathodes have been investigated for intermediate to low temperature applications.

Further, to adjust CTE of LSC with Gadolinia doped ceria (GDC) incorporation of Fe has been suggested resulting in **$La_{1-x}Sr_xCo_yFe_{1-y}O_{3-d}$ (LSCF)** cathodes for the intermediate/ low temperature SOFCs[50]. One strategy to improve performance of LSCF cathodes is the fabrication of composite cathodes electrodes with GDC, GDC/Ag or SDC[51,52].

2.4.4. Materials for Interconnect

The roles of interconnects in high temperature SOFCs are electrical connection between cells and gas separation within the cell stack. The fact that the interconnect must be compatible with all of the cell components as well as to be stable in both oxidizing and reducing gas environments places stringent materials requirements on it. These requirements plus the additional constraints of cost and ease of fabrication tend to limit the possible choices to only a few materials. The other typical requirements of interconnects are as following:

i. An interconnect works similar to the electrical wire providing the passage to electron from anode to cathode thus **very high electronic conductivity** with low ionic conductivity are the prime requirements to be met. It should possess good thermal conductivity.
ii. An interconnect must be **chemical stable in both oxidizing and reducing atmospheres** since on one side (in contact with anode) it is exposed to fuel and on the other side (in contact with cathode) it is in contact with the oxidant at higher temperatures.
iii. There should be a good **match of thermal expansion** with cathode and anode between the materials it is in contact with in order to avoid any cracking and delamination during fabrication and in-service conditions.
iv. Interconnect should be **chemically stable** with regard to other cell components such as cathode, anode and electric contact materials to avoid any disruption in the passage of electrons.
v. Also, it should have **low permeability for oxidant and fuel** in order to minimize the direct combination of these two.
vi. It should be of **high mechanical strength**.

Only oxide materials that comply with all these requirements along with the high operation temperature of SOFC are the rare earth chromites while for intermediate/low temperature SOFCs metallic alloys (e.g. Ferritic steels) can be used as well[14]. Lanthanum chromite is a p-type conductor which has the electronic conductivity due to small polaron hopping mechanism from ambient temperature to cell fabrication temperature (~1400^{o}C). The conductivity can further be enhanced by doping with lower valence ions such as (Ca^{+2}, Mg^{+2}, Sr^{+2} etc.) by replacing La^{+3} or Cr^{+3} , which will result in **$(La,Sr,Ca)(Cr, Mg)O_3$**[53]. However, the issues with lanthanum chromites are its large CTE and chemical stability at very low oxygen partial pressure (10-20 bars).

For intermediate and low temperature SOFCs metallic alloys have been suggested because they may overcome some of the limitations imposed by ceramic materials. Various advantages associated with metallic interconnect are low cost of material, complex shaping, ease of fabrication and better electrical and thermal conduction. Chromium based alloy **(Cr-5Fe-1Y_2O_3)** have been suggested because of a good match of CTE with YSZ however, diffusion of Cr to cathode has been reported to degrade the performance[12]. Ferritic steels have been suggested as another interconnect material. However, long term stack tests have been reported to degrade between 2 and 25% after 1000 h of operation[54]. It has also been reported that the thermal expansion of the ferritic steels is not only the function of %Cr but also that of the Si and Al. If added above a certain limit, Al/ Si oxide layers are formed which improve the corrosion resistance but are insulator as well and thus lower down conductivity and degrade the performance of an interconnect[55]. Alkaline-earth free and cobalt containing perovskites have been suggested to be most suitable materials for contact layers between the metallic interconnect and ceramic component of SOFC to minimize corrosion, contact resistance, and permeability of chromium species[14].

3. MATERIALS AND EXPERIMENTAL METHODS

3.1. Materials

In order to assess the magnitude and distribution of thermal stresses in the Positive electrode-Electrolyte-Negative electrode (PEN) assembly of intermediate and high temperature SOFCs, thermo-mechanical properties of various component materials have been studied.

Electrolyte materials used in the present study include yttria stabilized zirconia (YSZ) ((TOSOH Corp., Japan), Scandia (Sc_2O_3) and ceria (CeO_2) doped zirconia – $ScCeZrO_2$ (SCZ) (supplier DKKK, Japan) and Gadolinia (GdO_2) doped ceria ($GdCeO_2$) (Praxair, USA). All examined samples were fabricated in the form of discs. The powders were cold pressed at 20MPa (Uniaxial pressure) and then sintered. Sintering details such as sintering temperature, holding time and heating /cooling rates of thus processed materials are provided in Table 3-1.

Anode materials used in the present study include NiO-YSZ (powder suppliers for NiO was J.T.Baker, Phillipsburg, NJ and for YSZ was TOSOH Corp., Grove City, OH) and NiO-$ScCeZrO_2$ (powder supplier for NiO was Novamet and for $ScCeZrO_2$ was DKKK, Japan). NiO and YSZ/$ScCeZrO_2$ powders were ball milled in ethanol for 48 hrs to ensure good mixing and then cold pressed at 20 MPa Uniaxial pressure and sintered Table 3-1.

Cathode materials under study include Lanthanum Manganite (LM), Strontium (Sr) doped lanthanum manganite (LSM), and Sr and Co doped lanthanum ferrite (LSFC). For these cathodes, solid solution powders (supplied by Praxair) were cold pressed at 20 MPa Uniaxial pressure and sintered Table 3-1.

Table 3-1 Raw material and processing details of the anode, cathode and electrolyte materials used in the present study

Samples as received, with the details of processing conditions and procurement							
SOFC Componen	**Composition**	**Powder details**			**Processing Details**		
		Constituent powder	**Abbreviation**	**Supplier**	**Powder**	**Forming**	**Sintering Details**
Anode	75mol % $Y_{0.08}Zr_{0.92}O_2$, 25mol%	$Y_{0.08}Zr_{0.92}O_2$	YSZ	TOSOH	Ball milling,	tape cast with 30vol% pore	1400°C;2h, 1°C/min
		NiO	NiO	J.T.Baker			
	50wt% of $ScCeZrO_2$*, 50wt% of NiO,	$Sc_{0.1Ce0.01}Zr_{0.86}O_2$*	SCZ	DKKK	Ball milling,	Cold pressing at 20 MPa	1100°C;2h,1°C/min
		NiO	NiO	Novamet			
Electrolyte	20mol%Gd_2O_3,	Gd_2O_3+CeO_2	GDC	Praxair	No	Cold pressing at	1400°C 2h,5°C/min
	$ScCeZrO_2$	$ScCeZrO_2$	SCZ	DKKK	No	Cold pressing at	1550°C,4h,5°C/min
	8mol% Y_2O_3 92mol% ZrO_2	Y_2O_3 and ZrO_2	YSZ	TOSOH, Japan	Ball milling	Cold pressing at 20MPa	1400°C, 2h, 5oC/min
Cathode	$La_{0.6}Sr_{0.4}Fe_{0.8}Co_{0.2}O_3$	$La_{0.6}Sr_{0.4}Fe_{0.8}Co_{0.2}O_3$ (solid solution)	LSCF	Praxair	No	Cold pressing at 20MPa	1150°C/1300°C, 2h,5°C/Min
	$LaMnO_3$	$LaMnO_3$	LM	Praxair	No	Cold pressing at	1150°C/1300°C,2h,
	$(La_{0.7}Sr_{0.3})_{0.98}MnO_3$	$(La_{0.7}Sr_{0.3})_{0.98}MnO_3$ (solid solution)	LSM	Praxair	No	Cold pressing at 20MPa	1150°C/1300°C,2h, 5°C/min

*$ScCeZrO_2$ (DKKK) -10.07mole % Sc_2O_3 + 0.92 mole% HfO_2 + 1.03 mole% CeO_2 + 1.4 mole % TiO_2 + bal. ZrO_2

3.2. Experimental Procedures

3.2.1. Density Measurement

Density of all of the sintered samples was measured by following ASTM Standard C20-00 alcohol immersion method[56]. The procedure involved measurement of dry mass of the sample (W_{Dry}) followed by immersion in 200% proof ethanol in vacuum for 5 minutes to remove entrapped air during processing. After evacuation, the samples immersed in alcohol were kept for 30 minutes at room temperature. Then, temperature of ethanol was measured and corresponding density of the ethanol, $\rho_{Ethanol}$ was determined from standard temperature-density tables. The sample suspension wire was attached to the balance and immersed in the dish with ethanol and samples. The mass of sample suspension wire was recorded as W_{Wire}. Then sample was placed on the wire and the measured mass was recorded as W_{Susp}. This was followed by removing the sample from alcohol and blotting with a damp towel for 60 seconds. After 60 seconds, mass of the sample was measured and recorded as W_{Wet}. Analytical balance with resolution up to 0.0001g was used to measure the weight of the samples. All the measured entities were utilized to evaluate bulk density, % open porosity, and % closed porosity as following:

$$\text{Bulk Density} = W_{Dry} \times \frac{\rho_{Ethanol}}{\left(W_{Wet} - W_{Susp} + W_{Wire}\right)} \quad \text{(3.1)}$$

$$\%\ \text{Open Porosity} = \frac{\left(W_{Wet} - W_{Dry}\right) \times 100}{\left(W_{Wet} - W_{Susp} + W_{Wire}\right)} \quad \text{(3.2)}$$

$$\%\text{Closed Porosity} = \left(\frac{W_{Wire} - W_{Dry} - W_{Susp}}{\rho_{Ethanol}} - \frac{W_{Dry}}{\rho_{Theoritical}}\right) \times \frac{100 \times \rho_{Ethanol}}{W_{Wire} - W_{Wet} - W_{Susp}} \quad \text{(3.3)}$$

3.2.2. Elastic Moduli Measurement Using Resonant Ultrasound Spectroscope

Elastic moduli of the materials used in the present study were determined using Resonance Ultrasound Spectroscope (Quasar International, Albuquerque, NM). RUS is a high-precision

dynamic technique that allows us to determine elastic moduli of the materials by measuring vibrational eigenmodes (natural resonances) spectrum of mechanical resonance for samples of well defined geometry, usually in the shape of parallelepipeds or cylinder[57]. In addition, RUS can be used as nondestructive technique because position and shape of resonance peaks are sensitive to both microscopic and macroscopic properties of an object. This technique can also be used to determine ultrasonic attenuation according to following equation[57-59]:

$$Q^{-1}_{k} = \Delta\omega_{\kappa}/\omega_{ko} \quad \text{.....(3.4)}$$

where ω_{ko} is the frequency associated to with k^{th} eigenmode, and $\Delta\omega_k$ is the full width at half maximum, FWHM, of that mode.

A schematic of the experimental tripod setup used in this study for resonant ultrasound spectroscopy is shown in Fig. 3-1[60]. The sample in the form of disc was supported by three piezoelectric transducers. One transducer (transmitting transducer- marked as Drive in the Fig. 3-1) generates an elastic wave of constant amplitude but of varying frequency (covering a large number of vibrational eigenmodes of the sample). The resonance response of excited sample is detected by the other two transducers (receiving transducers- marked as Channel 1 & 2).

In order to study the variation of elastic moduli as a function of temperature, the commercially available setup for RUS at room temperature was further modified for high temperature. A photograph of high temperature set up for RUS that was designed and custom built for this study is shown in Fig. 3-2. For the high temperature set up the transducers were arranged in a similar way to the room temperature set up (at 120^{o}) except that the large SiC extension rods were used to transit ultrasound waves. This arrangement has facilitated to hold the specimen at the tip of the extension rods at desired temperature in the furnace while keeping the transducers unaffected by high temperature. Also, to avoid any potential damage of PZT transducers induced by high temperature, the additional cooling system for the transducers was facilitated.

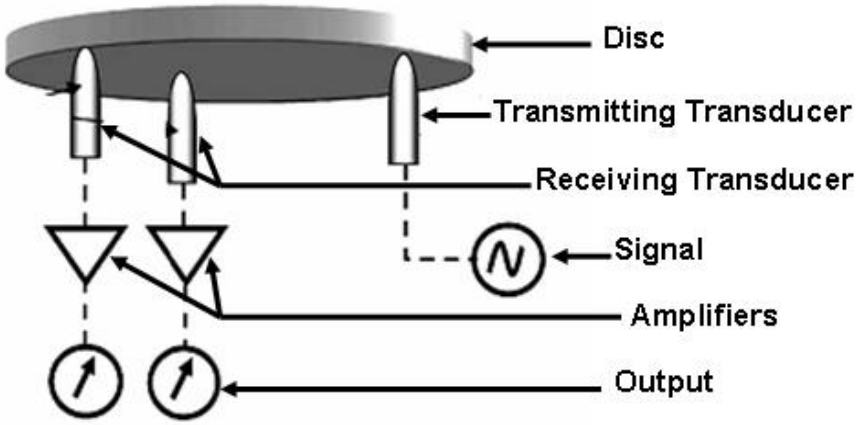

Figure 3-1 Schematic of experimental setup of the tripod for RUS

In order to detect and subtract the noises from the extension rods, the resonance spectrum of the same sample was first taken at room temperature by using both room-temperature and high-temperature set up and compared. This was followed by collection of resonance spectrum at an interval of 100^{o}C up to 900^{o}C. The samples were heated at a ramping rate of 10^{O}C/min. The process controller and the other parts were supplied by Watlow Thermal Solutions, Houston, Texas.

The RUS spectra cannot be deconvoluted directly to deduce the elastic constants. From the known sample dimensions, density, and a set of "guessed" elastic constants - namely C_{11} and C_{44} for isotropic solid, an approximate spectrum is calculated.

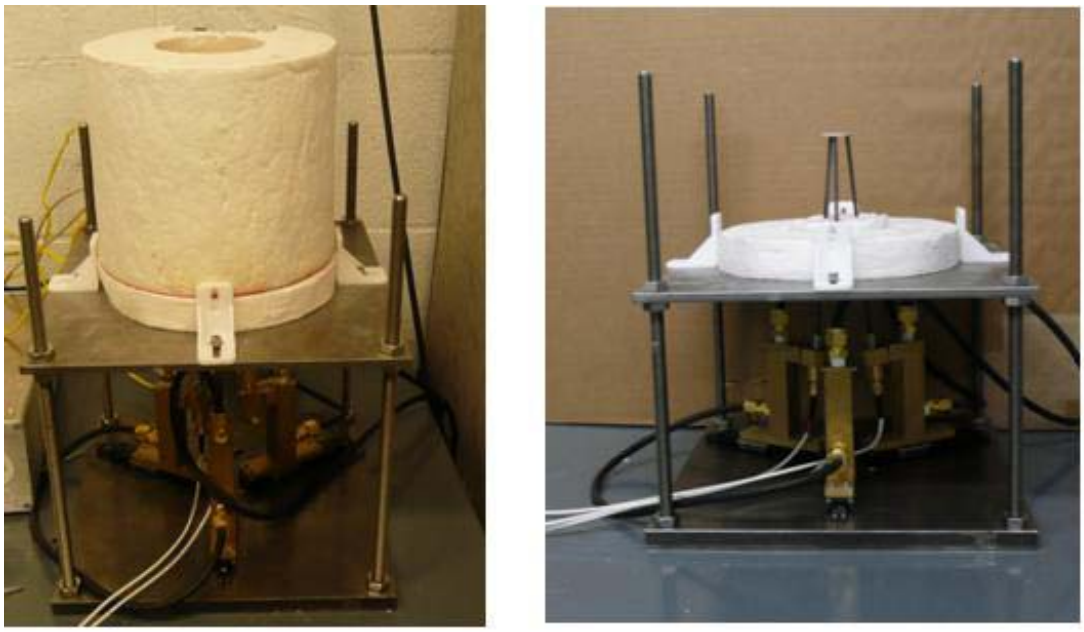

Figure 3-2 (a) Experimental setup of transducers for obtaining the resonant spectrum at high temperature and (b) detailed view of arrangement of transducers and extension rods

A multidimensional algorithm (Quasar International, Albuquerque, NM) that minimizes the root-mean-square (RMS) error between the measured and calculated resonant peaks enables the determination of the elastic constants from a single frequency scan as[58]:

$$\chi = \sqrt{\sum_n w_n \frac{\left(f_{calc} - f_{meas}\right)^2}{f_{meas}^2}} \quad \text{..... (3.5)}$$

where w_n is the weight factor given to the normalized difference between the calculated frequencies f_{calc} and measured frequencies f_{meas}. Here, it has been assumed that the RMS functions χ will have a minimum when the correct set of input parameters is achieved. Thus the numerical part of RUS consists of calculating a large matrix, finding the eigenvalues, and then using the eigenvectors to calculate "corrections" to the set of input parameters so as to iterate toward a match between computed and measured frequencies.

The typical resonance spectrum of $ScCeZrO_2$ electrolyte is shown in Fig. 3-3. A large jump at a particular frequency is observed when frequency of driving transducer corresponds to one of the eigen-frequency (resonance) of the sample. In the plot, 'x' mark corresponds to the calculate frequencies from the input parameters. For every material, a total of 40 resonant frequencies were calculated with a convergence rate of 0.5 and for polynomial order 12. To start with, first 5-10 resonance peaks were fitted with the initial guessed elastic constants and then the elastic constants obtained by fitting these initial peaks were utilized to fit the whole spectrum consisting of 40 peaks. With the aim to minimize the error associated with the difference in measured and the calculated frequencies, attempts were made to minimize the number of missing peaks. If some of the peaks were missing in the measured resonate spectrum the sample is remounted, re-scanned, and re-fitted for the observed spectrum. To obtain the best fitting, weight factor of zero is usually used for the first 2-3 peaks and for the missing peaks during the fitting process. Depending on the density and stiffness of the material, measurements were done in the 0-350 kHz frequency range to cover the first 40 eigenfrequencies. For every material under study more than 2 samples were studied to ensure reproducibility of determined elastic moduli.

Considering materials as the isotropic ones, two free constants namely constants C_{11} and C_{44} were estimated using multidimensional fitting software. Young's modulus, *E*, shear modulus, *G*, and Poisson ratio, ν, for known C_{11} and C_{44} were then calculated using following equations (3.6 – 3.8)

$$C_{44} = \mu = G \quad \text{..... .....} \quad (3.6)$$

$$E = 2\mu(1+\nu) \quad \text{.....} \quad (3.7)$$

$$\nu = \frac{C_{12}}{C_{11} + C_{12}} \quad \text{And } C_{12} = C_{44} \quad \text{.....} \quad (3.8)$$

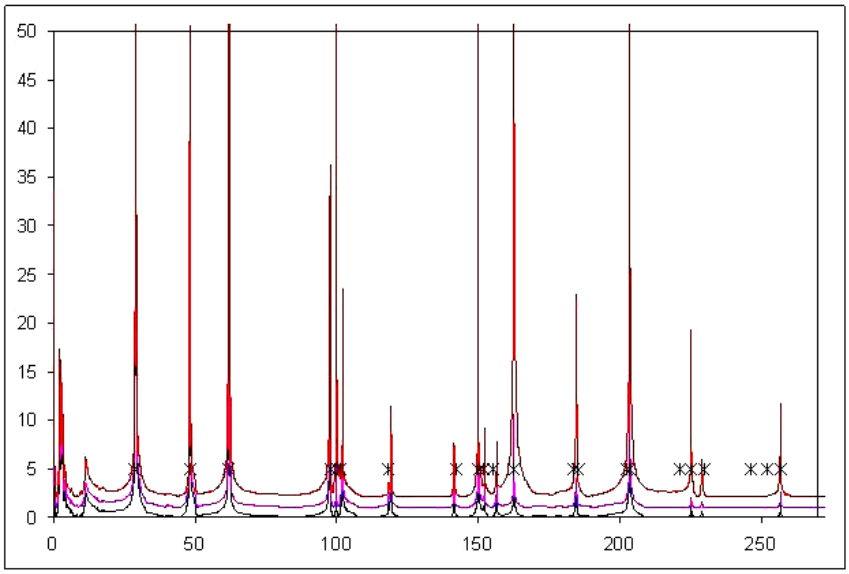

Figure 3-3 Resonance spectrum of an electrolyte (ScCeZrO2)

3.2.3. Measurement of Coefficient of Linear Thermal Expansion: Thermo-Mechanical Analyzer

Coefficients of thermal expansion (CTE) of the examined materials were determined using Q400 series Thermal Mechanical Analyzer, TMA (TA Instruments, IL, USA). TMA instrument is shown in Fig. 3.4(a) while the set up of glass stage and macro expansion probe is shown in Fig. 3.4(b)[61].

Nitrogen at flow rate of 40ml/min was used as purge gas for all materials except for reduced anodes where 4%H_2-96%Ar gas mixture was used. Smooth and parallel surfaces were ensured by getting the samples machined from The M&P Lab (Schenectady, NY) and BOMAS, Inc. (Somerville, MA). To minimize the error associated with the measurement sample thickness was kept larger than 5mm (as recommended by instrument supplier). For thicker samples (cathodes and electrolytes except YSZ) samples were cut into the shape 5x4x8 mm parallelepipeds, while for the thinner samples (anodes), several 5x4x2 mm sized parallelepipeds were stacked to obtain the recommended thickness.

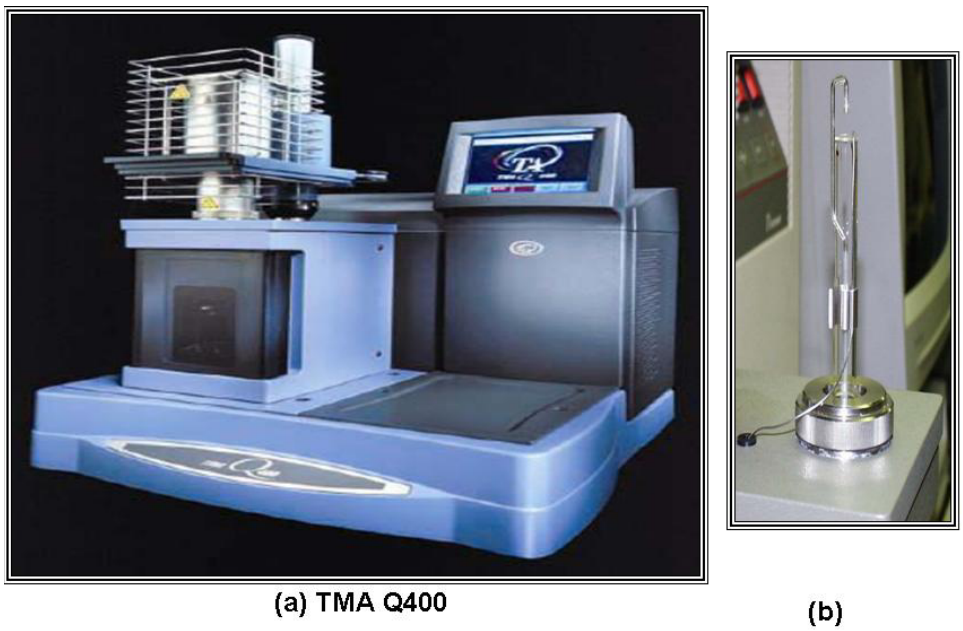

Figure 3-4 (a) The photograph of TMA Q400 (TA Instruments) used in present study and (b) probe-glass stage set up65

Tests were performed in Standard mode in which force was held constant at 0.01 N during the test. At the beginning of the test the force of 0.5N was first applied to ensure the firm contact between the expansion probe and the surface of the sample. The displacement of the probe that corresponds to the expansion of the sample was monitored under a linear temperature ramp during heating and cooling. Each sample was subjected to two consecutive heating-cooling thermal cycles. Each thermal cycle included, heating from room temperature to 900^{o}C with a heating rate of 5^{o}C/min and isothermal holding for 1 hr, followed by cooling till room temperature. Weight of the sample was measured before and after every test to ensure that there was no any change related to the oxidation or reduction of the sample.

Instantaneous thermal expansion at any temperature in ~25-900^{o}C temperature range was calculated from the thermal expansion vs. temperature curve using following equation:

$$\alpha_L = \frac{1}{L_0}\frac{dL}{dT} \quad \text{..... (3.10)}$$

where, L_o is the original length (in this case thickness of the sample), while ΔL and ΔT are changes in length (thermal expansion) and temperature respectively. Instantaneous (differential) coefficient of thermal expansion was calculated from the slope of the tangent on thermal expansion vs. temperature curve at the particular temperature. Thus obtained data points were smoothened by taking an average of 40 data points accounting for $\pm 5^{o}$C at the selected temperature.

3.3. Finite Element Analysis of Thermal Stresses

The results taken from the room temperature and high temperature measurement of elastic moduli and coefficient of thermal expansion of the materials under study were utilized to model the evolution and distribution of thermal stresses at different temperatures. The Planar SOFC considered in the present study was of Anode supported SOFC (100mm x 100mm) wherein the thickness of anode, electrolyte and cathode layers were taken to be 1mm, 10μm and 30μm respectively. For high temperature SOFC YSZ, Ni-YSZ and LSM were taken as the electrolyte, anode and cathode respectively while for intermediate temperature SOFC GDC, Ni-SCZ and LSCF were taken as the electrolyte, anode and cathode respectively. SolidWorks and CosmosWorks 2007 were utilized for the object fabrication and modeling the stresses. Care has been taken to ensure the iso-strain conditions at the interface and to generate a compatible mesh between the components. A mesh of 1.524 mm with aspect ratio 0.07mm was created which resulted in 45,514 elements and 80,982 nodes.

4. RESULTS AND DISCUSSION

This chapter contains the results of density measurements, instantaneous (or differential) coefficients of thermal expansion (CTE) in 25-900^{o}C temperature range measured using thermo-mechanical analyzer and elastic properties, namely Young's (E) and shear modulus (G) determined using resonant ultrasound spectroscope (RUS) in the same temperature range. Details of the examined electrolyte, cathode and anode materials and experimental conditions were described in more details in Chapter 3. This section has been divided in three subsections dealing with electrolyte, anode and cathode materials. In addition, all experimental results have been analyzed and discussed in detail in the respective subsections.

In general, all results of thermo-mechanical analysis are presented on two plots – (a) percent thermal expansion vs. temperature and (b) derived instantaneous coefficient of thermal expansion as a function of temperature. It has to be noted here that we have reported instantaneous CTE measured in N_2 atmosphere at 40ml/min flow rate for all materials except reduced anode in which case 4%H_2-96%Ar gas mixture was used to prevent oxidation of Ni. Oxygen deficient atmosphere might affect results of thermal expansion measurements since oxygen diffuses inward or outward of the oxide material at different oxygen partial pressures. Diffusion of oxygen introduces point defects in oxide ceramics that in turn results in changes in the crystal dimension and is accounted by chemical expansion[62]. In the present study materials were subjected to an increase in temperature from room temperature to 900^{o}C in N_2 or 4%H_2-96%Ar atmosphere (partially reducing atmosphere) thus contribution from both thermal and chemical expansion may have been observed. This combination of thermal and chemical expansion is also termed as thermo-chemical expansion. For fluorite structured oxides, the lattice constant has been reported to obey Vegard's Law which suggests the linear dependency of lattice constant on defect concentration[63,64]. This almost linear relationship has been observed after 600^{o}C temperature in case of all of the three electrolytes under study.

Elastic properties of any material are very sensitive to any structural change in the material and are related to the shape of free energy potential plot. Utilization of highly accurate techniques for determining elastic moduli such as in RUS have allowed us to detect effect of any macro- and

micro structural features and lattice defects which are related to electron-phonon interaction, and/or structural and magnetic phase transitions being occurred in the studied temperature range (25-900^{o}C) on elastic properties[65,66]. Also, while determining the elastic moduli at various temperatures, changes in dimensions were taken in account using average coefficient of thermal expansion at the respective temperature.

4.1 Electrolyte

The result obtained for various electrolyte materials used in the present study namely Yttria Stabilized Zirconia (YSZ), Scandia and Ceria doped Zirconia (SCZ) and Gadolinia doped Ceria (GDC) (see Table 3-1) are shown and discussed in this subsection. YSZ is the state of art electrolyte that is used in high temperature SOFCs (HT-SOFC) while SCZ and GDC are the potential electrolytes for the intermediate temperature SOFCs (IT-SOFC). Higher ionic conductivity at relatively low temperature ensured by SCZ and GDC is the main drive for determining the suitability of these electrolytes for IT-SOFCs.

4.1.1. Density and Porosity Measurement

As mentioned in subsection 2.4.1, dense electrolytes are needed to prevent the fuel and oxidant cross-over. Table 4.1 shows the average values for density and standard deviation obtained from 5 to 9 measurements of different samples from the same batch. Very less (2-5%) porosity especially open porosity usually remains after sintering and can be tolerated. However GDC has been found to have slightly highest porosity.

Table 4-1Density and porosity of examined electrolyte materials

	Theoretical Density , (g/cm^3)	Archimedean Density (gm/cm^3)		Open Porosity		Closed Porosity	
		Avg.	Std. Dev.	Avg.	Std. Dev.	Avg.	Std. Dev.
E1- GDC	7.29	6.82	0.042	3.96	0.496	2.44	0.296
E2- SCZ	5.74	5.62	0.008	0.07	0.053	2.01	0.186
E3- YSZ	5.9	5.9	0.005	0.027	0.045	-0.01	0.084

4.1.2. Thermo-Mechanical Analysis

This subsection deals with the thermo-mechanical analysis of the YSZ, GDC and SCZ electrolyte materials that were used in the present study.

4.1.2.1. State of Art – Yttria Stabilized Zirconia (YSZ)

The results obtained from the thermo-mechanical analysis of YSZ are presented in Fig. 4-1. As can be noted, there was a non linear increase in the sample dimension with increasing temperature, Fig. 4-1 (a) that has further been confirmed by the derived instantaneous CTE as a function of temperature, Fig. 4-1 (b).

The average CTE from two thermal cycles has been found to increase from 8.5 x10^{-6}/^{o}C at room temperature to 12x10^{-6}/^{o}C at 850^{o}C. It is worth noting that the results from 2 heating cycles are in excellent agreement with the reported values[67-70]. However, little higher value observed in the present case may be the consequence of performing the tests in N_2 (partially reducing atmosphere). In a study by Hayashi et al. effect of doping ZrO_2 with Y_2O_3 been studied and the relatively lower CTE for the higher doping concentration has been attributed to the increase in binding energy of the system.[71]. This increased binding energy has been suggested to be the resultant of greater contribution from decrease in Zr-O and Y-O bond length than to the decrease

caused by introduction of oxygen vacancies. However, the increase in CTE at higher temperature is attributed to increased number of oxygen vacancies in the crystal caused by a high temperature and gradient in oxygen partial pressure in the material.

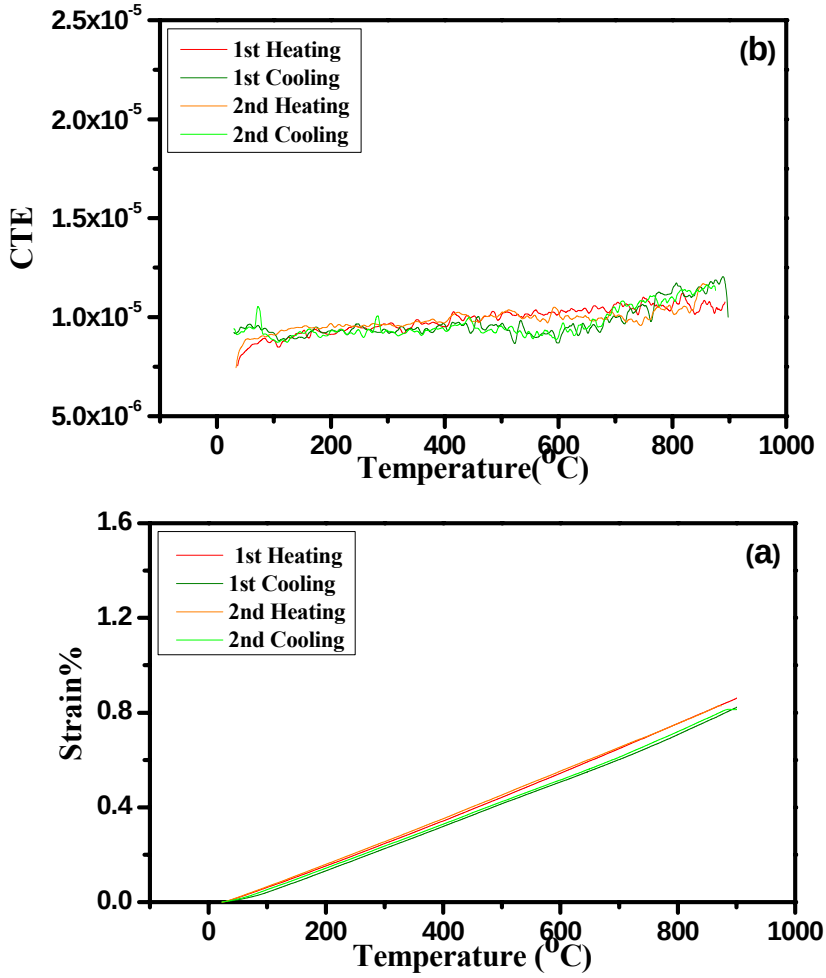

Figure 4-1 (a) Thermal expansion (b) instantaneous CTE vs. temperature plot for YSZ

4.1.2.2. Scandia Ceria Stabilized Zirconia (SCZ)

The results obtained from the Thermo- mechanical analysis of Scandia Ceria Stabilized Zirconia (SCZ) are shown in Fig. 4-2. As it can be noted there was a continuous but non linear increase in the sample dimension with increasing temperature (Fig. 4-2 (a)) that has been further confirmed by the derived CTE vs. temperature plot (Fig. 4-2 (b)).

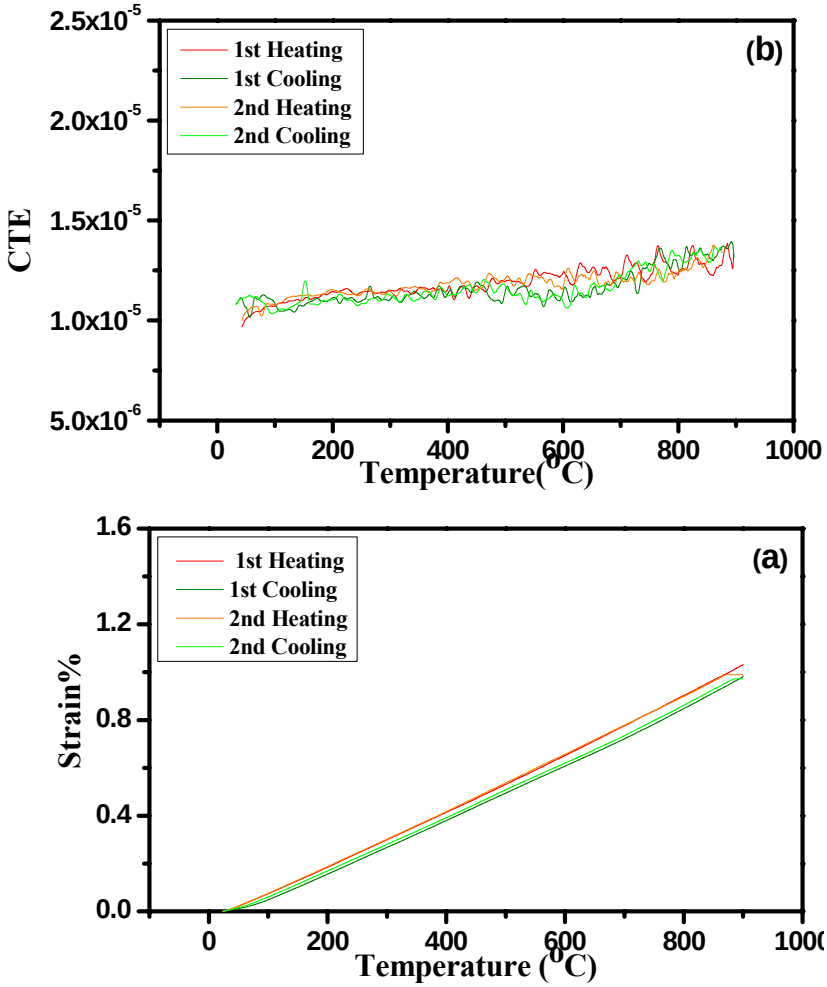

Figure 4-2 a) Thermal expansion and (b) instantaneous CTE vs. temperature plot for SCZ

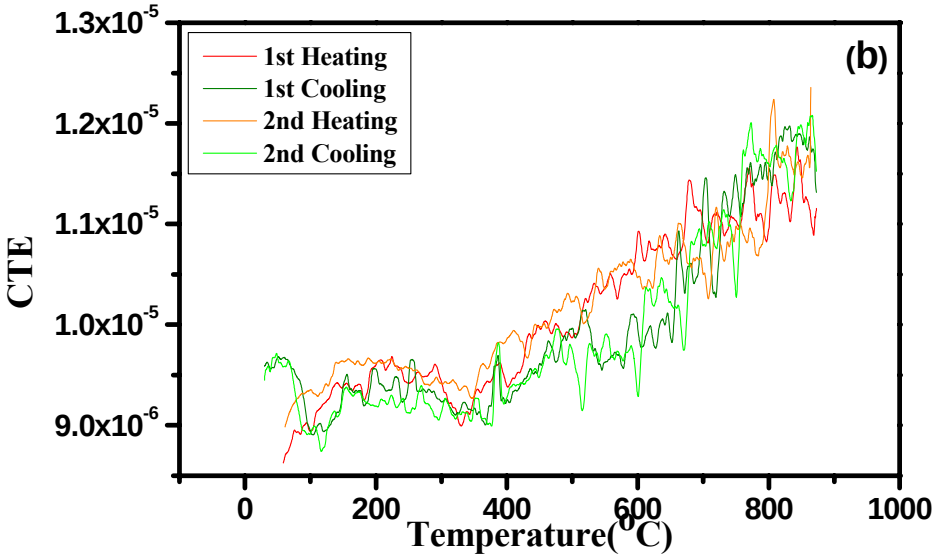

Figure 4-3 Thermal expansion temperature plot for SCZ – magnified view of Fig. 4-2(b)

Fig. 4-3 shows that the CTE is almost independent on temperature up to 350°C ($8.9x10^{-6}$/°C at room temperature to $9.2x10^{-6}$/°C at 350°C) however a sharp increase in CTE from $9.2x10^{-6}$/°C at 350°C to $12x10^{-6}$/°C at 860°C was observed. The material studied in the present work consists of 10.07mole% Sc_2O_3, 1.4 mole%TiO_2, 1.03%CeO_2 and 0.92mole% HfO_2 as well. As it was mentioned in subsection 2.4.1, addition of 10mole% Sc_2O_3 ensures highest ionic conductivity in the Sc_2O_3-ZrO_2 system but it also stabilizes rhombohedral structure at room temperature. In a study by Haering et. al. it has been reported that 10.7mole%Sc_2O_3-ZrO_2 undergoes a martensitic phase transformation at around 550°C from rhombohedral to cubic accounting for 0.15% volume change in the material[72] . However, this phase transition has been suggested to be suppressed by addition of around 2mole% TiO_2. As was mentioned above, the material used in present study was doped with 1.4mole% TiO_2 and this doping might have suppressed the phase transformation, resulting in cubic structure of examined samples even at room temperature.

4.1.2.3. Gadolinia Doped Ceria (GDC)

The result obtained from the Thermo- mechanical analysis of Gadolinia doped Ceria (GDC) is provided in Fig. 4.4. A non linear increase in dimension of the material and thus of the CTE vs.

temperature as well have been observed for the studied temperature range in N_2. CTE has been found to increase from $10x10^{-6}/^oC$ at room temperature to $14x10^{-6}/^oC$ at 900^oC. This result is in well agreement with the reported CTE[73-75]. It is worth noting, that CTE of GDC is higher than that of examined YSZ (Fig. 4-1b) and SCZ (Fig. 4-2b).

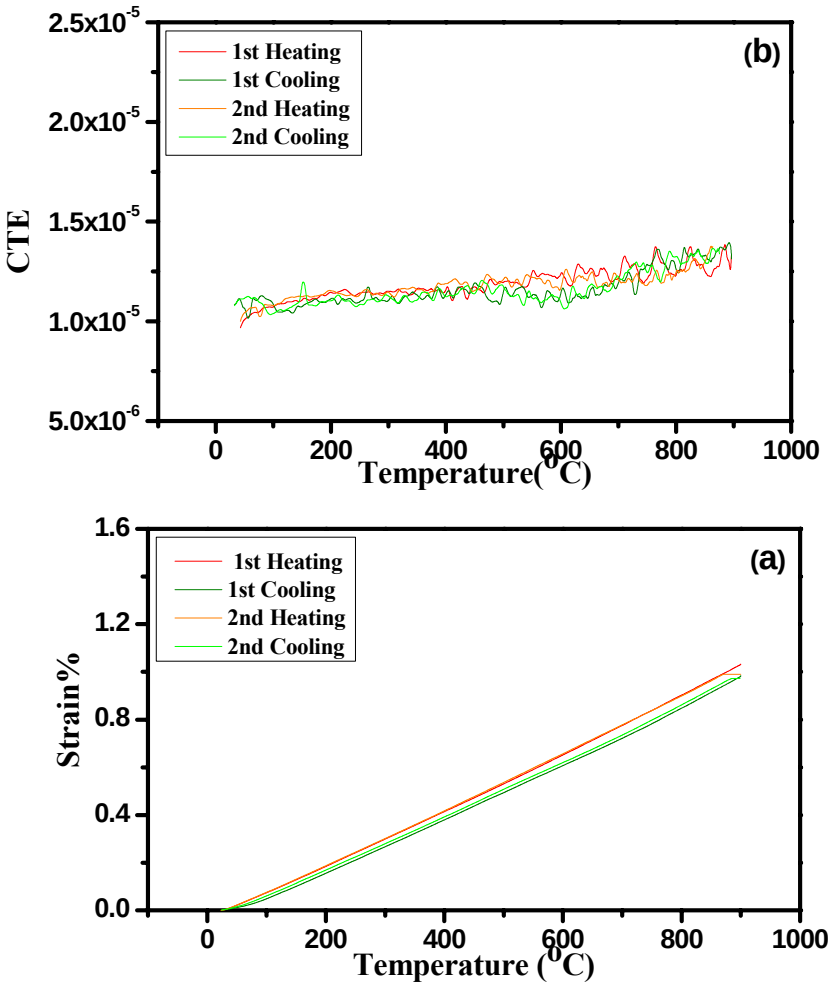

Figure 4-4 (a) Thermal expansion and (b) instantaneous CTE vs. temperature plot for GDC

The CTE observed for $Gd_{0.2}Ce_{0.8}O_2$ is higher than that of the $Gd_{0.1}Ce_{0.9}O_2$ and pure CeO_2[74,75]. This higher CTE is attributed to the decrease in binding energy with increased doping concentration. Higher dopant concentration in the system increases the number of Gd^{+2}-O^{-2}

bonds when compared to un-doped ceria. The lower binding energy of Gd^{+2}-O^{-2} bonds than Ce^{+4}-O^{-2} makes it easier for oxygen to leave the crystal. In a study by Gorelov et al, a second order phase transformation has been reported around 230°C for the similar material[73]. Higher temperature above this order-disorder transition further aggravates the outward flow of oxygen from the crystal. This effect is accompanied by increased concentration of oxide ion vacancies or Ce^{+3} concentrations in the crystal which is reflected in the increased lattice parameter and thus observed CTE above transition temperature (Fig. 4-5).

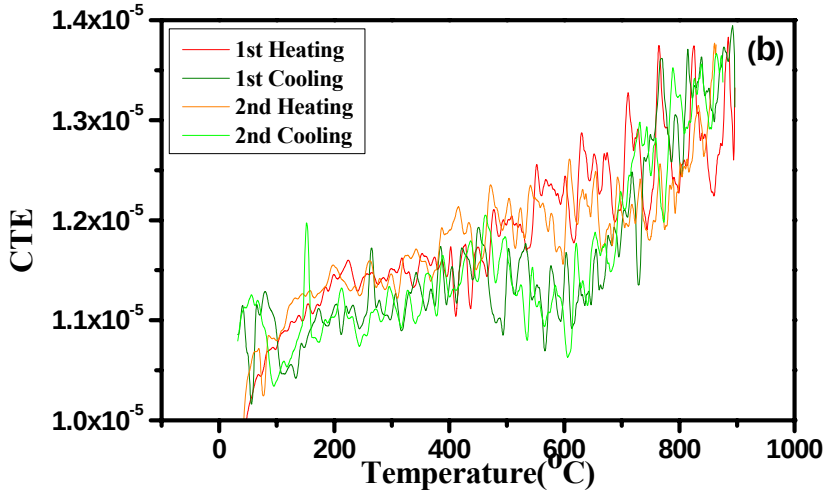

Figure 4-5 Magnified view of Fig- 4-4(b) - variation of CTE with temperature for GDC

4.1.3. Room and High Temperature Measurement of Elastic Moduli

This subsection deals with the resonant ultrasound spectroscopy of the YSZ, GDC and SCZ electrolyte materials that were used in the present study.

4.1.3.1. State of Art – Yttria Stabilized Zirconia (YSZ)

The variations of Young's and shear moduli with temperature for YSZ are shown in Fig. 4-6. It can be noted from the Fig. 4-6 that the variation of elastic moduli with temperature is non-linear. The room temperature elastic modulus is in well agreement with the reported results [76].

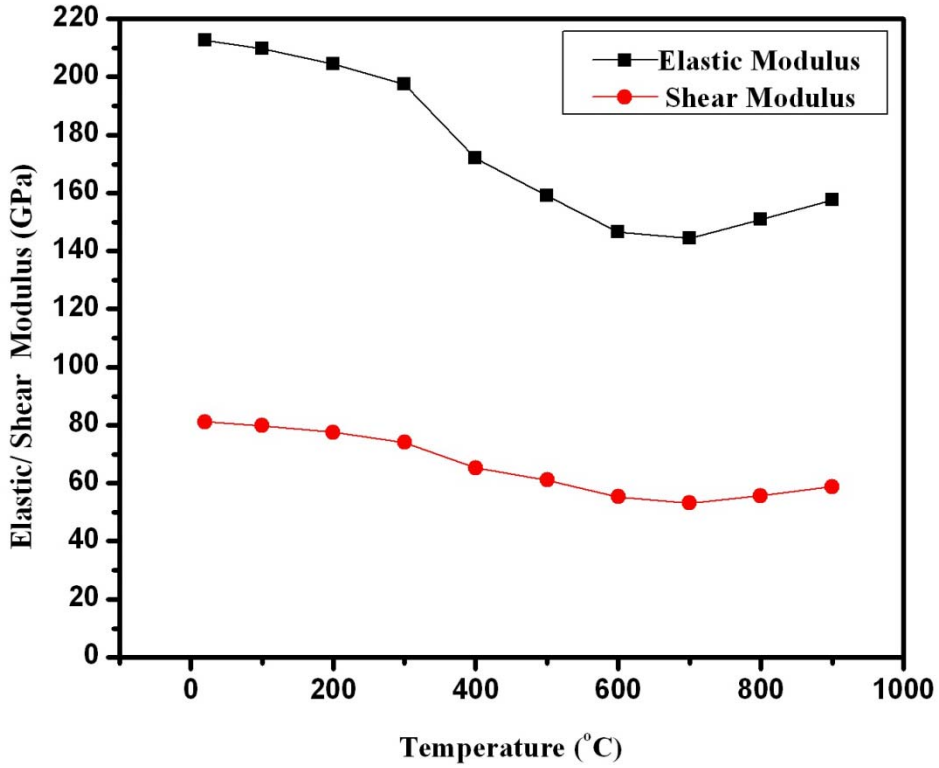

Figure 4-6 Variation of Young's and shear moduli with temperature for YSZ

In a temperature regime 200°C-400°C elastic modulus decreases and then increases above 600°C but at a much slower rate. This sharp decrease in elastic modulus in the temperature regime 250°C-600°C may be attributed to the internal friction associated with the relaxational damping of the oxygen vacancies. Relaxation damping is a widely observed phenomenon in oxide ion conductors (in this case YSZ) caused by short range order disorder transition between the lattice sites. This observation of the saddle point in elastic modulus vs. temperature plot in the above

mentioned temperature region is in very well accordance with the observation of composite peaks in reciprocal temperature vs. internal friction plot for 10mole%Y_2O_3 stabilized ZrO_2 that was reported elsewhere[77-79].The origination of the observed peaks has been suggested to caused by hoping of oxygen vacancy around neighboring Y ion and from relaxation of oxygen vacancies with in a cluster of two Y ions. The results obtained in the high temperature region are in well agreement with the reported ones in terms of the difference between the room temperature and high temperature values of elastic moduli [80,81].

4.1.3.2. Scandia Ceria Stabilized Zirconia (SCZ)

The results obtained for the variation of elastic and shear moduli with temperature for SCZ are presented in Fig. 4-7. The material used in present study (10.07mole% Sc_2O_3, 1.4 mole%TiO_2, 1.03%CeO_2 and 0.92mole% HfO_2) has been found to exhibit the similar behavior as its counterpart YSZ in terms of the appearance of saddle point and then increase in moduli after around 600^{o}C. The decrease in elastic moduli in the temperature regime 200^{o}C- 600^{o}C is (~70GPa) more than observed for YSZ (~50GPa) and this effect may be explained by the presence of various dopants/ additions to the host ZrO_2 namely Sc_2O_3, CeO_2, HfO_2 and TiO_2. The increased number of dopants might have caused increased interaction of highly mobile oxide ion and the doping ions and thus stronger attenuation in the material which has been reflected in the lowered elastic moduli in the 200^{o}C- 600^{o}C temperature regime.

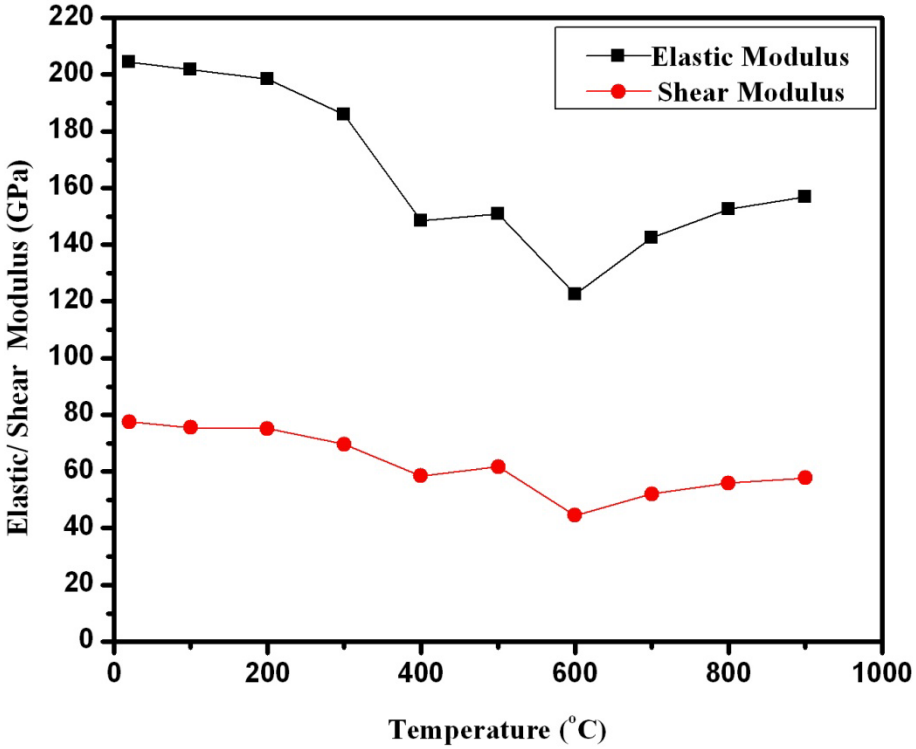

Figure 4-7 Variation of Young's and moduli with temperature for SCZ

4.1.3.3. Gadolinia Doped Ceria (GDC)

Variation of Young's moduli and shear moduli with temperature for GDC electrolyte material is shown in Fig. 4-8. It can be noted that there was also slightly non linear decrease in the Young's and shear modulus of Gadolinia doped ceria (GDC) with increasing temperature. The room temperature elastic modulus observed in the material (around 4% Porosity) used in present study (176GPa) is lower than the one reported in literature (212GPa) for fully dense material[76].

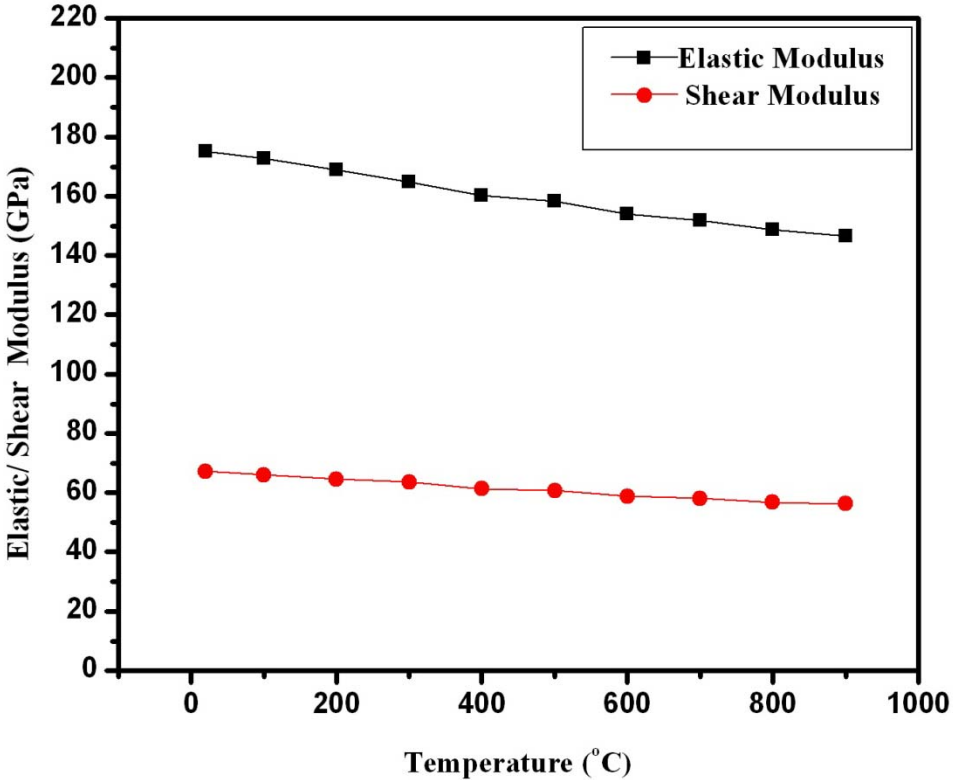

Figure 4-8 Variation of Young's and shear moduli with temperature for GDC

Also, the material used in present study exhibited a decrease from 176GPa at room temperature to 145 GPa at 900°C. This decrease in elastic modulus may be more than for pure CeO_2 because of the presence of larger bonds Gd^{+3}-O^{-2} in the crystal than in the otherwise un-doped crystal. However, as per our knowledge effect of increased temperature on the elastic modulus of pure ceria has not yet been reported. Also, increased drop in elastic modulus past the transition temperature (as explained in section 4.1.2.2) may be accounted for ease with which oxygen can leave the crystal resulting in increased oxygen vacancies. A marked drop in elastic modulus in CeO_2 and GDC with lowered oxygen partial pressure and thus the increased oxygen vacancies has been reported Duncan et al[82]. The drop in elastic modulus has been suggested to be caused by weakening of the bonds and thus of lowered binding energy of the system with increased concentration of oxygen vacancies[62,82].

4.2. Anode

In the present work two anodes have been studied (Table 3-1). Ni-YSZ is the state of the art anode being used for high temperature SOFC while Ni-SCZ has been developed as a potential anode for intermediate temperature SOFC. During the fabrication of a single cell, NiO-YSZ and YSZ (Ht-SOFC) or NiO-SCZ and SCZ electrolyte (IT-SOFC) are co-sintered at 1300^{o}C-1400^{o}C in air and air cooled at room temperature. During the very first thermal cycle, NiO reduces to Ni which is the electron conducting and catalytic phase of the anode. However, this transformation of a ceramic phase to metallic phase not only brings volume change but also results in pronounced change in thermo-mechanical properties of the reduced anode (as would be evident from the following results)[27]. This change in thermo-mechanical properties of unreduced and reduced anode is also the contributing factor for the observed thermal stresses in the multi-layered structure of (positive electrode- electrolyte- negative electrode) - PEN assembly of SOFC. In order to take these changes into the account while evaluating thermal stresses in the PEN assembly, it was in our interest to study the thermo-mechanical properties of both unreduced and reduced anodes. The fabrication details of each of these are provided in Table2-1.

4.2.1. Density and Porosity Measurement

The results of density and porosity measurement for unreduced and reduced anode samples are enlisted in Table 4-2. Relatively high porosities of the anode materials (as listed in Table 4-2) are required for an efficient anode since the high porosity provides easy flow of the fuel to the electrochemical active sites (triple phase boundaries-TPBs) for the effective oxidation of the fuel, as was mentioned in Chapter 2.

Table 4-2 Density and porosity of examined anode materials

Anode	Theoretical Density (gm/cm^3)	Archimedean Density (gm/cm^3)		Open Porosity		Closed Porosity	
		Avg	Std. Dev.	Avg.	Std. Dev.	Avg.	Std. Dev.
NiO-YSZ	6.3	4.41	0.64	27.12	1.04	1.02	0.15
Ni-YSZ*	7.1	3.95	0.28	40.39	0.39	4.95	0.28
NiO-SCZ	6.17	4.25	0.22	30.87	1.51	0.24	0.214
Ni-SCZ*	6.74	4.2	0.25	38.80	3.36	-1.11	0.88

*after reduction in 4%H_2+96% argon gas mixture at 800^{o}C for 4 h

4.2.2. Thermo-mechanical Analysis

The results of thermo-mechanical analysis of NiO-YSZ and NiO-SCZ anode materials before and after reduction in 4%H_2-96%Ar gas mixture are reported in this subsection. NiO-YSZ and NiO-SCZ samples were reduced in 4%H_2-96%Ar gas mixture at 800^{o}C for 4 hours. To ensure full reduction of NiO to Ni in the examined anode materials, the mass of the samples before and after reduction was monitored. From thus observed mass change, the percentage of the NiO that reduced to Ni was calculated and found to be above 99% for all examined samples.

4.2.2.1. State of Art Anode - Ni-YSZ

The results obtained by thermo-mechanical analysis of the reduced anode Ni-YSZ are provided in Fig. 4-9. These results have directly been incorporated from previously published work[80].

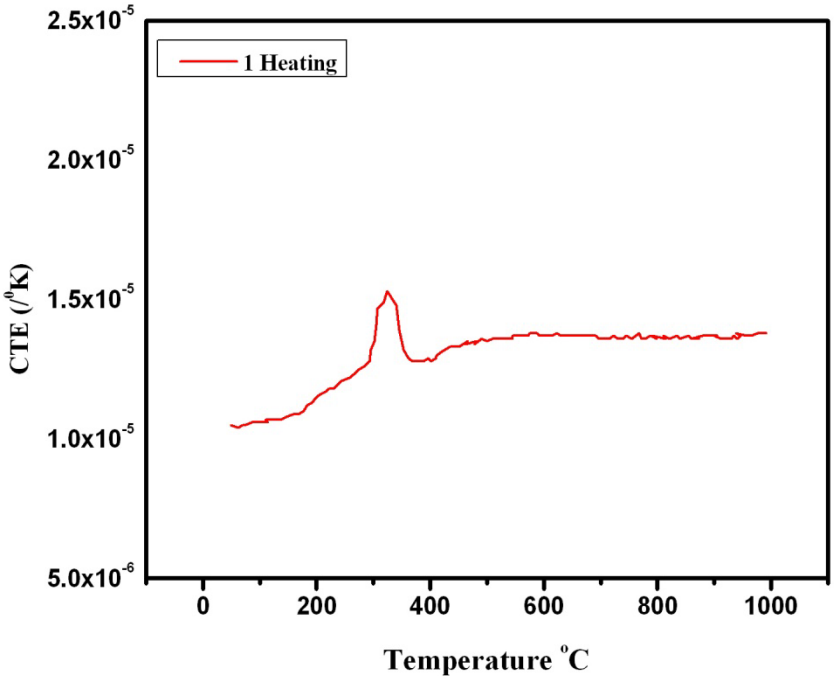

Figure 4-9 Instantaneous CTE vs. temperature plot for Ni-YSZ

An increase in CTE from 10.52 x10^{-6}/°C at 50°C to 13.81x10^{-6}/°C at 900°C was observed for Ni-YSZ. The observed CTE for the present material (~47 vol% Ni) are little higher than the reported by Mori et al for 40vol%Ni-YSZ[70] and the reasoning can be given the higher amount of metallic phase (which has higher CTE than YSZ ceramic phase) in the former case. In a study by Aruna et al it has further been confirmed that higher Ni Content in the cermet (Ni-YSZ) results in higher CTE[83]. However, the presence of an anomalous peak corresponding to 15.2x10^{-6}/°C at 323°C was also observed. This marked increase in CTE has been suggested to be in correlation with ferromagnetic to paramagnetic transition of Ni in the cermet- (Curie temperature of Ni around 350°C)[80,84]. Further increase in CTE with increasing temperature may be the consequence of contribution from thermal expansion of metal Ni and thermo-chemical expansion of YSZ as described in section 4.1.2.1.

4.2.2.2. Un-Reduced Anode- NiO-SCZ

The results obtained from the Thermo- mechanical analysis of 50 wt% Nickel Oxide (NiO) -50 wt% Scandia Ceria Stabilized Zirconia (SCZ) from room temperature to 900°C in air are shown in Fig. 4-10.

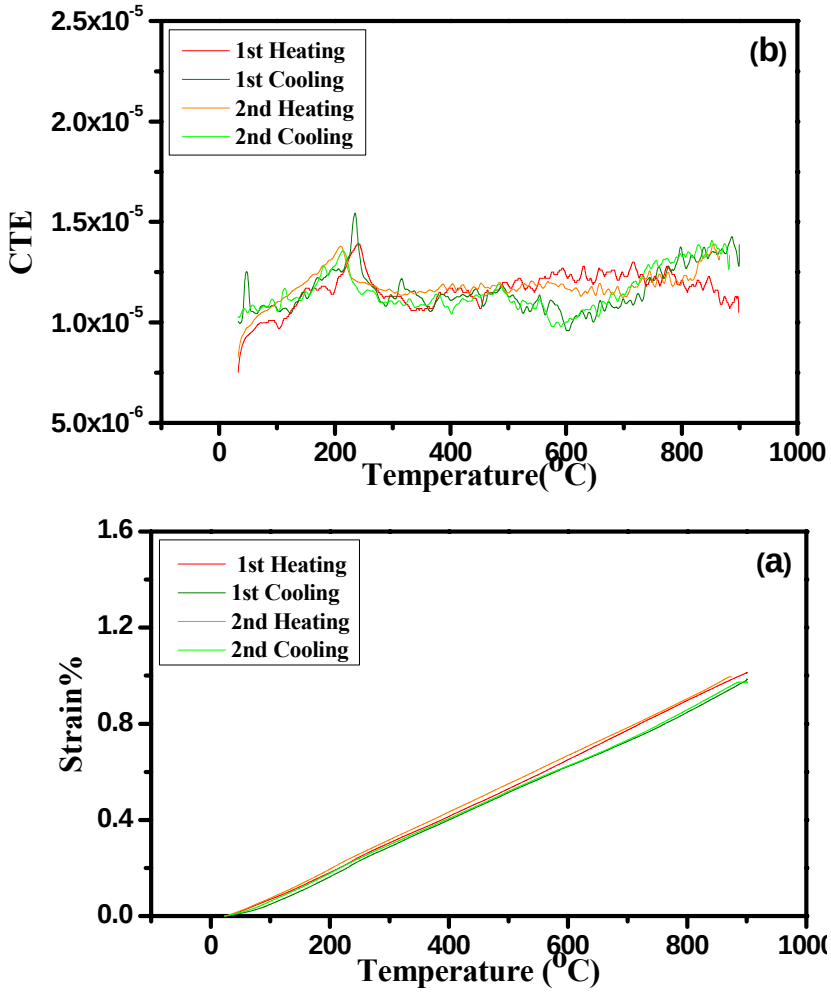

Figure 4-10 (a) Thermal expansion and (b) instantaneous CTE vs. temperature plot for NiO-SCZ

The variation of CTE from 8.365×10^{-6}/°C at 26°C to 13.8×10^{-6}/°C at 900°C was observed for NiO-SCZ. CTE of NiO-SCZ was found to be higher than that of SCZ (Section 4.1.2.1). The higher observed CTE on NiO-SCZ may be accounted for the presence of 50 wt% NiO which has

a higher CTE ($14x10^{-6}/^{o}C$) than SCZ[85]. The peak at 280°C in Temperature vs. CTE plot is attributed to an inherent anti-ferromagnetic to paramagnetic transition of NiO. During this transition the crystal structure changes from rhombohedral to cubic structure[70]. Further increase in CTE with increased temperature is attributed to the increased CTE of both of the constitutive phases NiO and SCZ.

4.2.2.3. Reduced Anode- Ni-SCZ

The variation of coefficient of thermal expansion with respect to temperature is shown in Fig. 4-11. The CTE of the material was found to increase from 9.5 $x10^{-6}/^{o}C$ at room temperature to $14.8x10^{-6}/^{o}C$ at 900°C which is slightly larger than in the case of unreduced NiO-SCZ anode. The observed large drop in CTE at around 350°C may also be attributed to ferromagnetic to paramagnetic transition of Ni in the cermet- i.e. Curie temperature of Ni around 350°C[80]. However, the different shape of the CTE peaks at Curie temperature for Ni-YSZ (Fig. 4-9) and Ni-SCZ (Fig. 4-10b) may be accounted for the difference in the number of data points that were averaged during smoothening and derivation process for these two materials. Also it can be noted that this cermet has exhibited slightly higher CTE at 900°C when compared to its counterpart being used for High temperature- SOFC, namely Ni-YSZ (section 4.2.2.1). This effect may be attributed to larger amounts of Ni in the Ni-SCZ than in examined Ni-YSZ cermet. Also, it can be noted that at 600°C- the proposed temperature for operation of IT-SOFC, this anode has lower CTE ($12.24x10^{-6}/^{o}C$) than Ni-YSZ ($13.76x10^{-6}/^{o}C$), making it an even more considerable anode for low temperature applications.

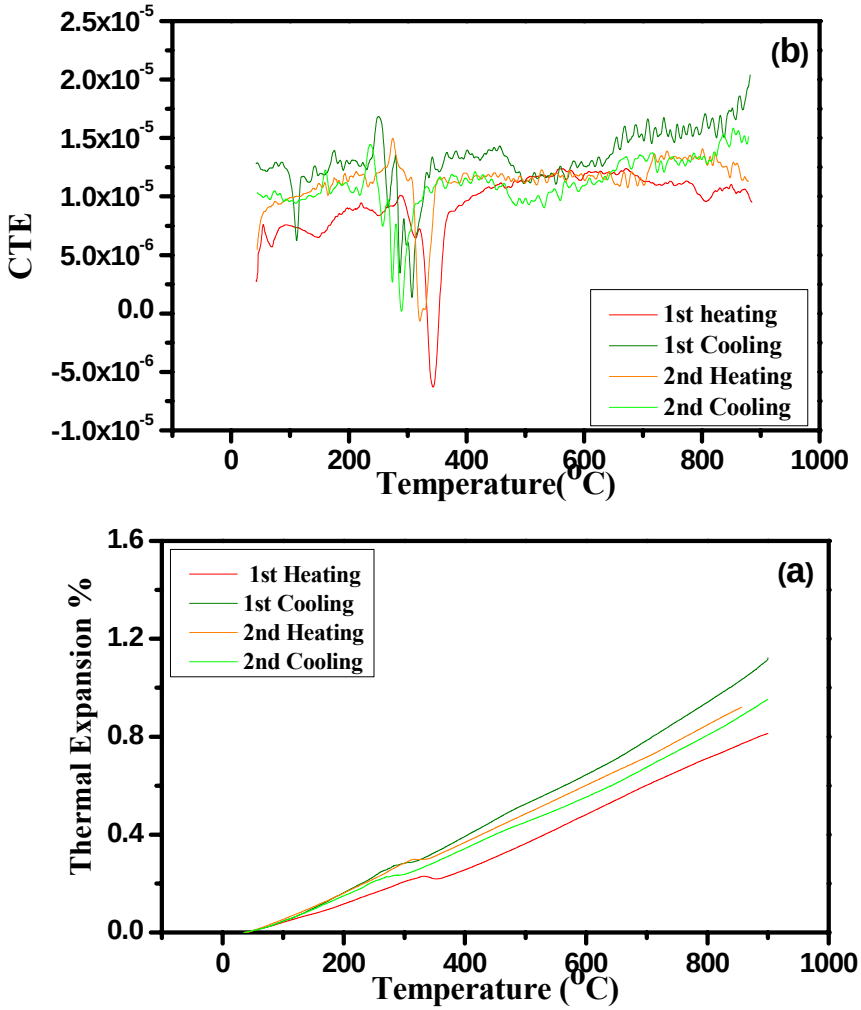

Figure 4-11 (a) Thermal expansion and (b) instantaneous CTE vs. temperature plot for Ni-SCZ

4.2.3. Room and High Temperature Measurement of Elastic Moduli

The results of resonant ultrasound spectroscopy of unreduced and reduced NiO-YSZ and NiO-SCZ anode are summarized and discussed in this section.

4.2.3.1. State of Art Anode- Ni-YSZ

The variation of Young's modulus and shear modulus with respect to temperature are shown in Fig. 4-12. The room temperature value of elastic and shear moduli are in well agreement with the reported values[86,87].

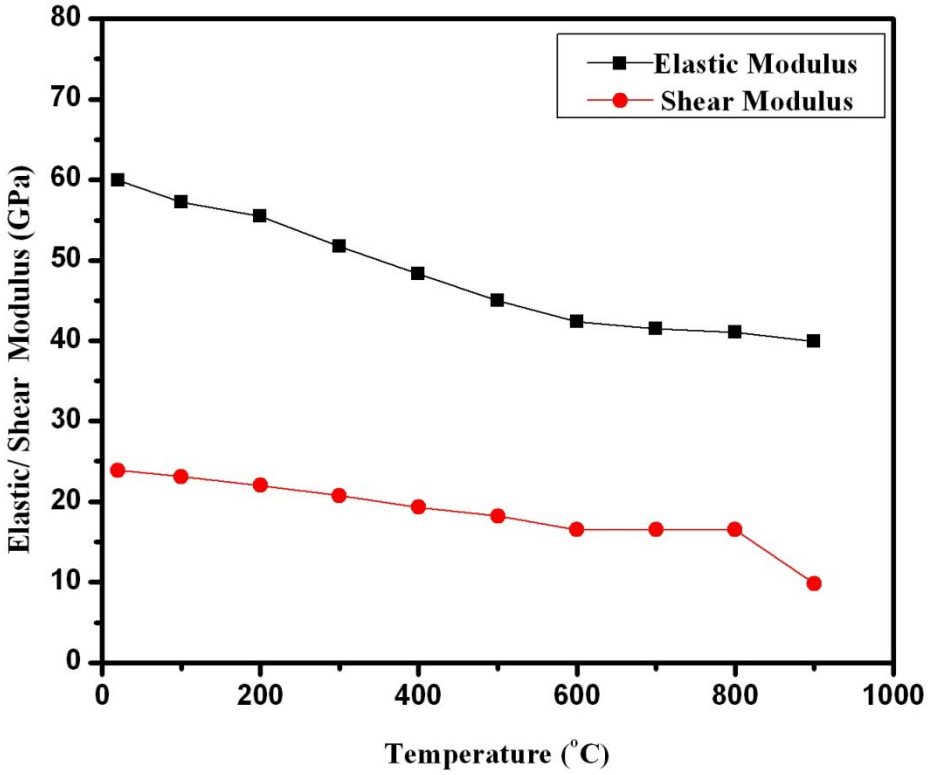

Figure 4-12 Variation of Young's and shear moduli with temperature for Ni-YSZ

It can be noted that there is a sharp decrease in elastic modulus from room temperature to 900°C. However, decrease in moduli with in the temperature range from 200°C to 600°C is slightly non-linear. This non-linear behavior can be attributed order-disorder transition of oxygen vacancies in YSZ, as was explained in section 4.1.3.2.

4.2.3.2. Un-Reduced Anode- NiO-SCZ

Variations of Young's and shear moduli with temperature for NiO-SCZ are presented in Fig. 4-13. As can be noted elastic moduli were almost constant from room temperature to 200°C and then they increase at 300°C which is followed by their continuous decrease up to 500°C. An increasing trend in elastic moduli was observed from 600°C to 900°C.

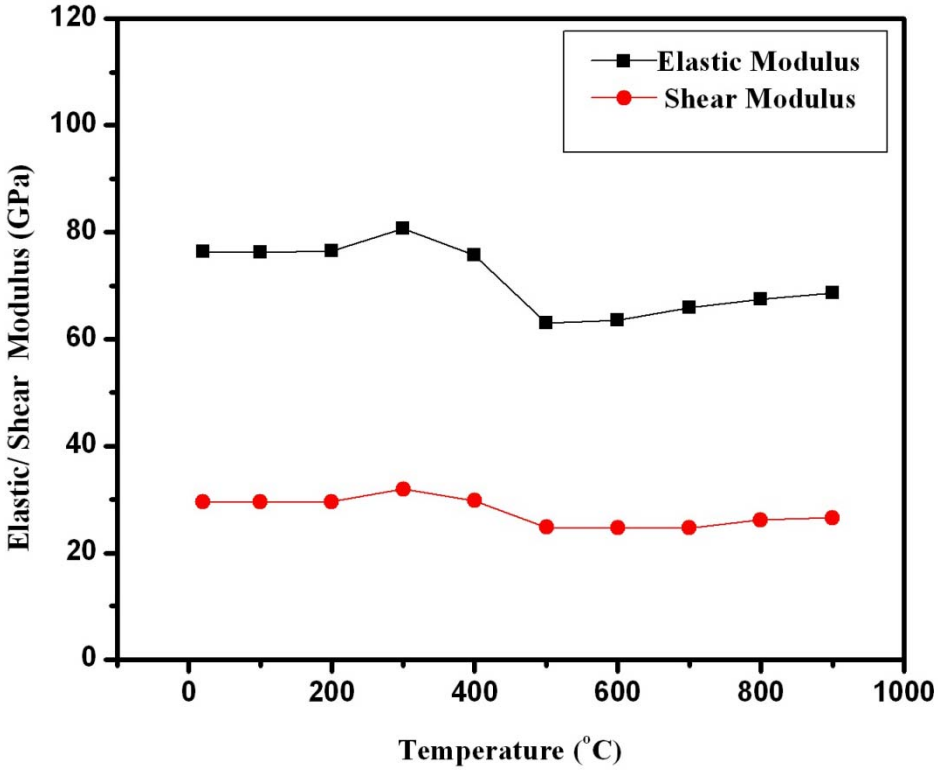

Figure 4-13 Variation of Young's and shear moduli with temperature for NiO-YSZ

Considering the behavior of individual constituents in the studied temperature range the increase in elastic moduli at 300°C can be attributed to anti-ferromagnetic to paramagnetic transition of NiO while that of decrease in temperature window 300°C-500°C can be attributed to order-

disorder transition of oxygen vacancies of SCZ. An increase observed above 600°C may again be considered as a contribution from SCZ.

4.2.3.3. Reduced Anode- Ni-SCZ

The variations of Young's and shear moduli with increasing temperature for Ni-SCZ are shown in Fig. 4-14.

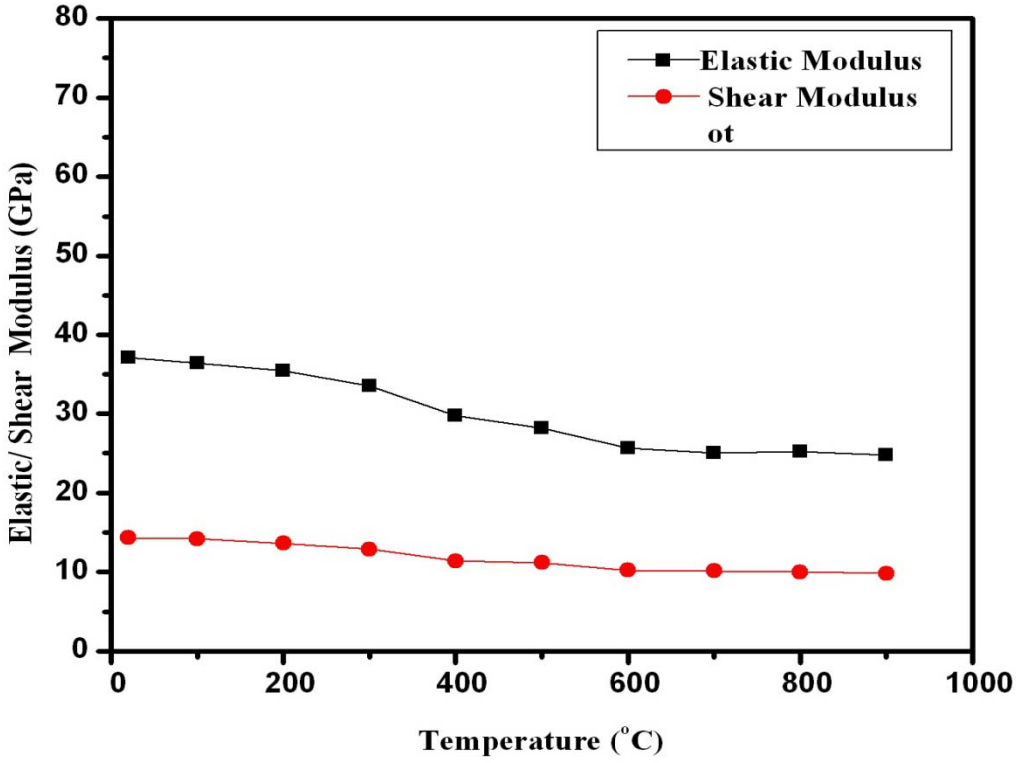

Figure 4-14 Variation of Young's and shear moduli with temperature for Ni-SCZ

As it can be noted below temperature of 200°C and in the 600°C-900°C temperature regime the changes in elastic moduli were not very significant. However, a rather sharp decrease in elastic moduli was observed in the temperature window 200°C-600°C for this cermet. In this case also a

significant contribution from oxygen vacancy relaxation in SCZ may be the reason for the observed behavior of this cermet. Also, it can be noted that room temperature elastic modulus of Ni-SCZ (fully reduced) is lower than the unreduced NiO-SCZ which is in well accordance with the reported results for the differences observed for NiO-YSZ and Ni-YSZ by Radovic et. al[59].

4.3. Cathode

Cathode materials studied in the present study include lanthanum manganite ($LaMnO_3$- LM), Lanthanum Strontium Manganite ($La_{0.7}Sr_{0.3}MnO_3$- LSM) and Lanthanum Strontium Cobalt Ferrite ($La_{0.6}Sr_{0.4}Fe_{0.8}Co_{0.2}O_3$- LSCF). LM is the very first cathode suggested for the operation for HT-SOFC while LSM is the improved version of LM in order to ensure the improved chemical compatibility with the adjacent electrolyte. LSCF has high electronic and ionic conductivity along with the superior catalytic activity at much lower operation temperature (600^oC) and thus is a potential cathode for intermediate temperature SOFC.

4.3.1. Density and porosity measurement

The density and porosity results of examined cathode materials are listed in the Table4-3. Considering the electrochemical function of a cathode in SOFC, the prime requirement is to ensure the maximum possible TPBs to facilitate oxidant reduction reaction. For this purpose, the ionic phase, electronic phase and gaseous phase must be in sufficient amount and in contact with each other. Thus it is general practice to ensure good amount of open pores in the material to allow the passage of oxidant and then reduction followed by the diffusion of oxide ions towards electrolyte.

Table 4-3 Density and porosity of examined cathode materials

	Theoretical Density, (g/cm^3)	Archimedean Density (gm/cm^3)		Open Porosity		Closed Porosity	
		Avg.	Std. Dev.	Avg.	Std. Dev.	Avg.	Std. Dev.
LM	6.59	6.24	0.37	1.1	1.47	4.17	4.18
LSM	6.36	5.07	1.23	17.06	23.52	3.12	4.07
LSFC	6.36	5.95	0.31	4.05	5.54	2.45	0.69

4.3.2. Thermo- mechanical Analysis

The response of above mentioned cathode materials when heated from room temperature to 900^{o}C at a heating rate of 5^{o}C/min in N_2 atmosphere is presented in the following subsection. In the present study the CTE observed for these materials are in some cases slightly higher than the reported in literature because of the partial reducing atmosphere (N_2) that was employed during testing. The sensitivity towards exposure to high temperature (900^{o}C) for long period (isothermal holding for 1 hr) is well exhibited in the hysteresis in heating and cooling cycles being caused by oxygen loss during isothermal hold.

4.3.2.1. Lanthanum Manganite (LM) cathode

The results obtained from the thermo-mechanical analysis of perovskite Lanthanum Manganite $LaMnO_3$ are shown in Fig.4-15. The variation of CTE with temperature exhibited a non linear increase from 5x10^{-6}/^{o}C at room temperature to 11.5x10^{-6}/^{o}C at 530^{o}C and then a decrease to 10x10^{-6}/^{o}C at 630^{o}C. Above 630^{o}C instantaneous CTE increases with temperature and approaches the values of 20x10^{-6}/^{o}C at 850^{o}C. This drop of CTE in the temperature range 530^{o}C-

630°C may be associated with the with orthorhombic ⇔ rhombohedral phase transition[88]. This transformation is attributed to oxidation of Mn^{+3} to Mn^{+4} and is very sensitive to the stoichiometry of the material. For an undoped stoichiometric $LaMnO_3$ this transition temperature has been reported to be 600°C. The CTE observed for LM in the present study is in well accordance with the values reported (20 $x10^{-6}$/°C by Kingery et al.)[89,90]. However it is much higher than reported by (Minh- 11 $x10^{-6}$/°C)[2], (Kendall – 11.5 $x10^{-6}$/°C)[14], (Wandekar 7.89 $x10^{-6}$/°C)[91] and (Montross- 11.20 $x10^{-6}$/°C)[92].

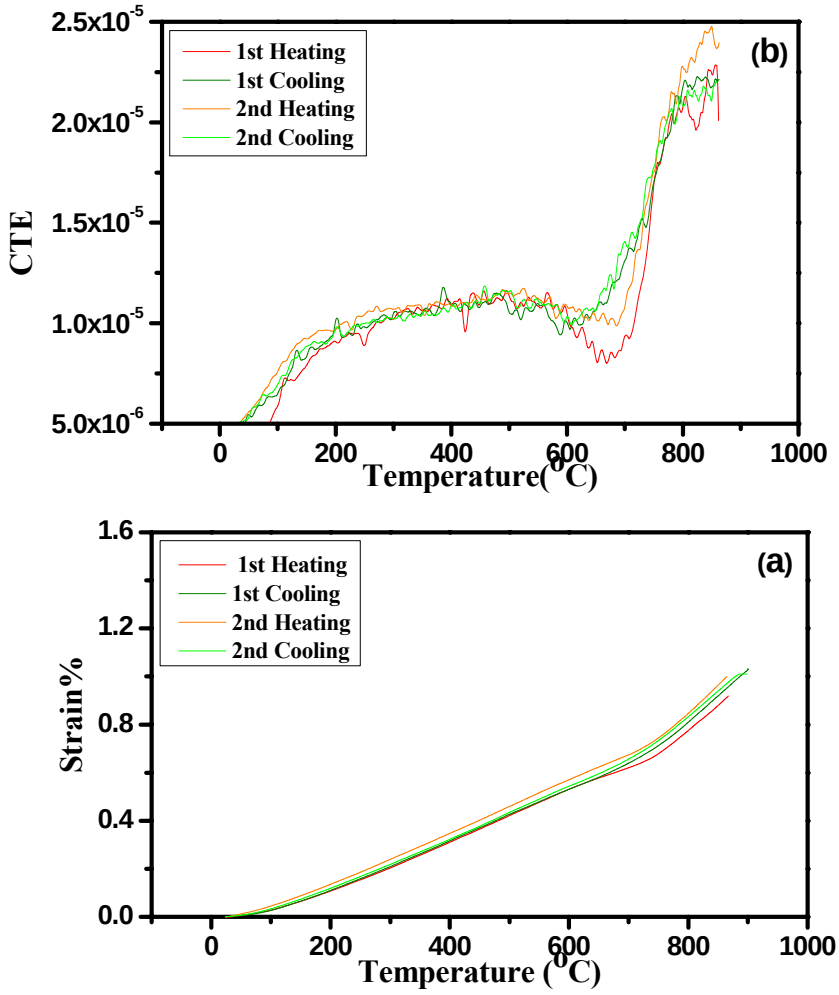

Figure 4-15 a) Thermal expansion and (b) instantaneous CTE vs. temperature plot for LM

4.3.2.2. Lanthanum Strontium Magnetite (LSM) Cathode

The results obtained from the Thermo- mechanical analysis of Lanthanum Strontium Manganite $(La_{0.7}Sr_{0.3})_{0.98}MnO_3$ are shown in Fig. 4-16. The CTE of this cathode material found to be varied from $11x10^{-6}/^oC$ at room temperature to $13x10^{-6}/^oC$ at 850^oC. These results are in well agreement with the reported value (Gauckler et. al. -12.3 $x10^{-6}/^oC$)[13] and (Mori et. al. $-12.5x10^{-6}/^oC$)[93]. These values are much closer to CTEs of examined electrolyte (YSZ section 4.1.2.1) and anode (Ni-YSZ section 4.2.2.1) materials than those of LM, confirming the significance of suitability of this cathode as the high temperature SOFC.

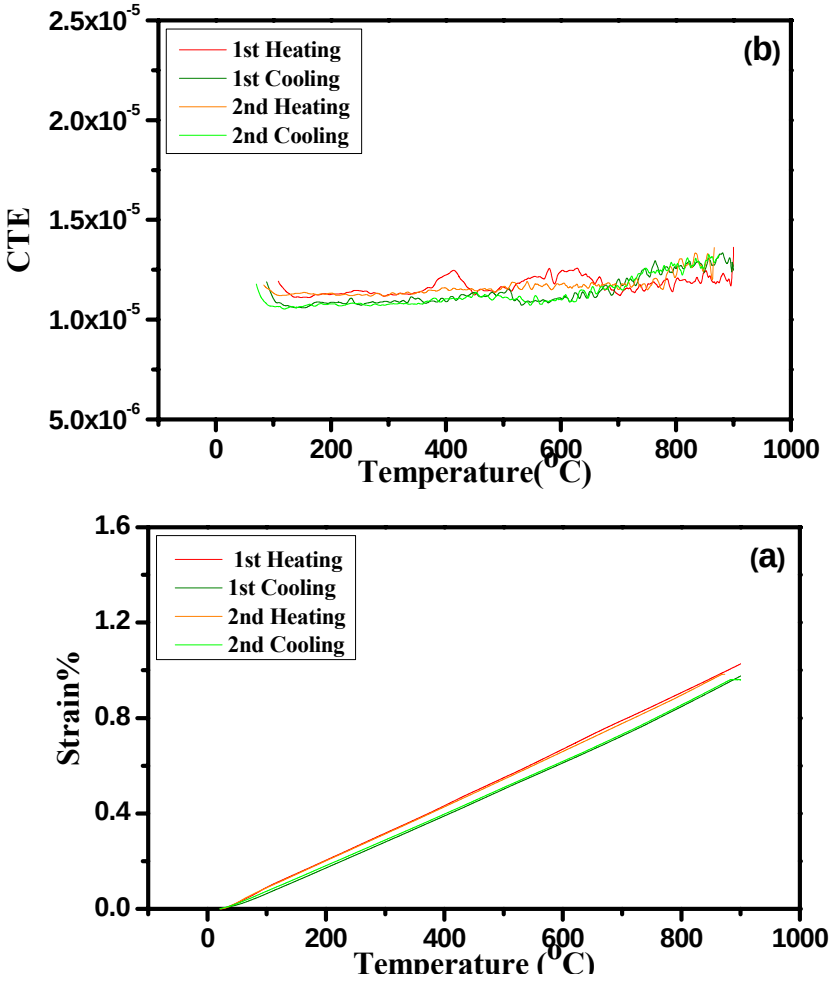

Figure 4-16 a) Thermal expansion and (b) instantaneous CTE vs. temperature plot for LSM

The change in the slope of CTE vs. temperature plot can be observed at around 500^{o}C Fig. 4-16(b)). The increase of CTE after 500^{o}C can be attributed to the incorporation of oxygen vacancies in the crystal. However, this increase is much smaller when compared to undoped stoichiometric $LaMnO_3$. The suppression of orthorhombic $\Leftrightarrow$ rhombohedral transition and its effect on CTE is attributed to substitution of La with lower valence cation – Sr^{+3}[14]. This substitution of Mn in $LaMnO_3$ with Sr not only increases the compatibility[14] with YSZ electrolyte by lowering the CTE at operation temperature but also optimizes the chemical and mechanical compatibility as well.

4.3.2.3 Lanthanum Strontium Cobalt Ferrite (LSCF) Cathode

The results obtained from the Thermo-mechanical analysis of $La_{0.6}Sr_{0.4}Co_{0.2}Fe_{0.8}O_3$ (LSCF) from room temperature to 900^{o}C in air are presented in Fig. 4-17. As can be noted from the CTE vs. temperature plot, a significant increase in the slope starts at around~650^{o}C. The CTE varied from 10x10^{-6}/^{o}C at room temperature to 15.5x10^{-6}/^{o}C at 650^{o}C while a steep rise in CTE was observed from 650^{o}C to 850^{o}C. This observed increase in CTE with temperature (15.5x10^{-6}/^{o}C at 650^{o}C and 20x10^{-6}/^{o}C at 800^{o}C) is higher than the reported values (15.5 x10^{-6}/^{o}C at 700^{o}C and 20 x10^{-6}/^{o}C at 1000^{o}C)[94] and (21.4 x10^{-6}/^{o}C at 1000^{o}C)[50]. Similarly, CTE of LSCF has been reported to be 13.5x10^{-6}/^{o}C for 25^{o}C-600^{o}C temperature range by Tai et al which is lower than the observed CTE 14.69x10^{-6}/^{o}C in the present case[95]. Thus observed higher CTE may be a consequence of employing N_2 as the environment. A steep rise in CTE with temperature above 600^{o}C similar to that observed in case of $LaMnO_3$ suggests some accompanied phase transition in the material or chemical expansion due to increase in oxygen vacancy concentration. However, as far as we know, there has not been any published study that would confirm the hypothesis that observed changes in CTE can be explained by phase transitions or increase in oxygen vacancy concentration.

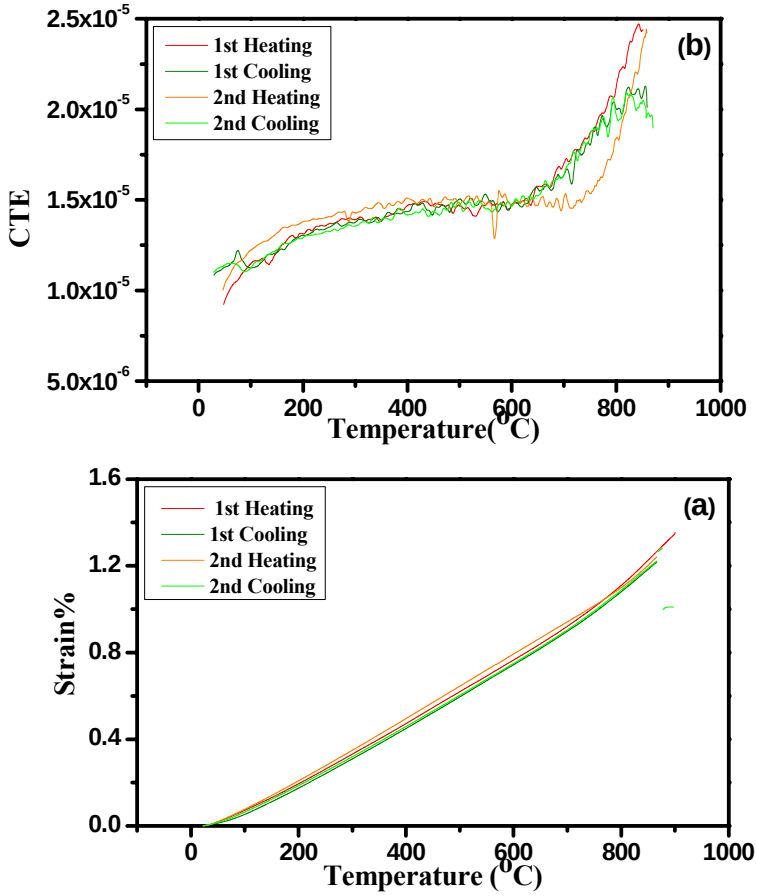

Figure 4-17 a) Thermal expansion and (b) instantaneous CTE vs. temperature plot for LSCF

4.3.3. Room and High Temperature Measurement of Elastic Moduli

This section deals with the results of resonant ultrasound spectroscopy of examined LM, LSM and LSCF cathode materials.

4.3.3.1 Lanthanum Manganite (LM) Cathode

Variation of Young's and shear modulus with respect to temperature is shown in Fig. 4-18 for Lanthanum Manganite (LM). A non linear decrease in Young's and shear modulus was observed with increased temperature. Similar non linear variation of elastic modulus has been reported by Troyanchuk et al in temperature range (27^{o}C-527^{o}C) and a transition in the temperature region 100^{o}C-400^{o}C has been reported depending on the non stoichiometry (variation of oxygen content)of the material used[96]. A closer observation of this variation suggests that the slightly non linear decrease in Young's and shear moduli was observed in 200- 600^{o}C and after that material has exhibited an increase in the Young's and shear moduli. Considering the former case, a non-linear decreasing trend in Young's and shear moduli with temperature may also attributed to the oxygen vacancy relaxation like in other oxide ceramics with cubic structures[97].

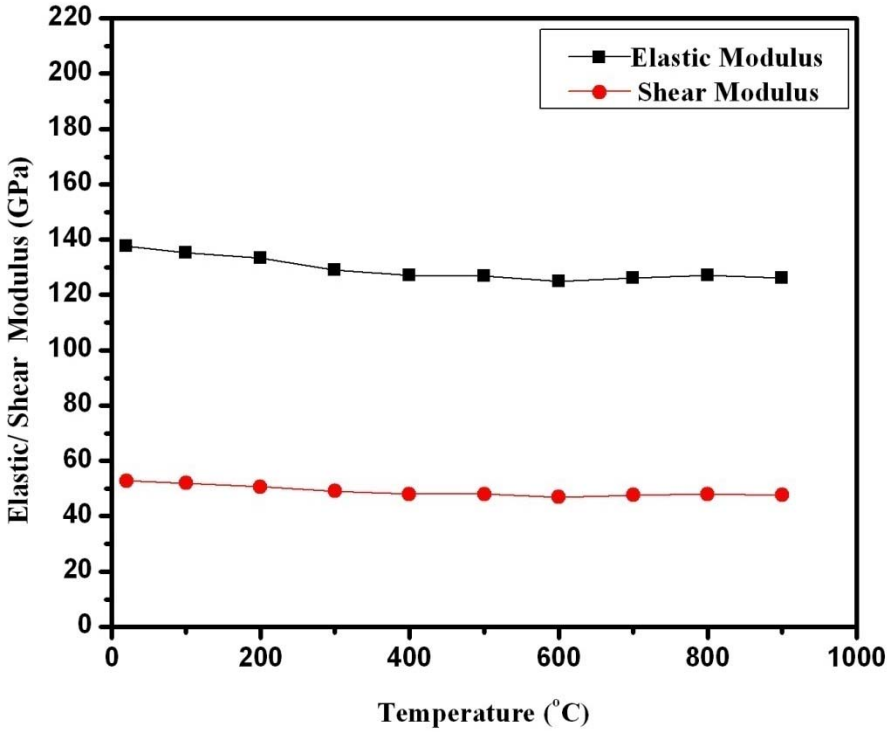

Figure 4-18 Variation of Young's and shear moduli with temperature for LM

4.3.3.2 Lanthanum Strontium Magnetite (LSM) Cathode

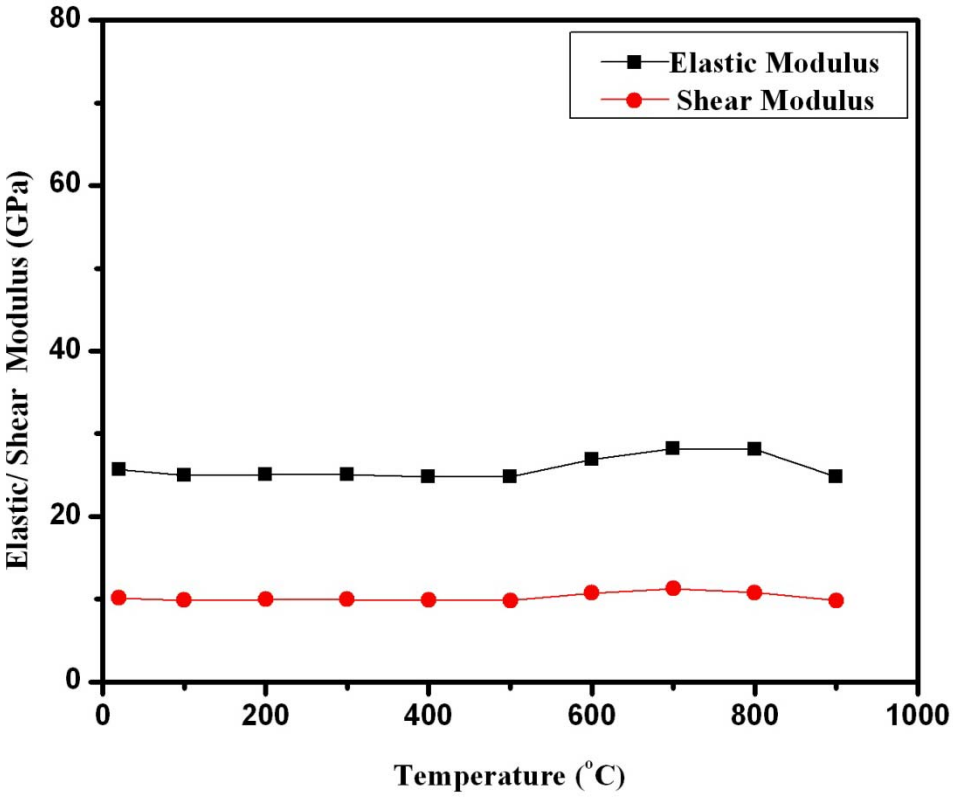

Figure 4-19 Variation of Young's and shear moduli with temperature for LSM

The variation of Young's /shear moduli with increasing temperature is shown in Fig. 4-19. The room temperature measurement of Young's modulus was observed to be 27GPa (for 33.5% porosity) which is in well accordance to the reported (41GPa for a sample of 29%open porosity) by Giraud et al[81]. It can be noted from the plot that the elastic modulus remained almost constant till 400°C and then dropped at 500°C which was further followed by an increase in elastic moduli till 900°C. Also, a closer observation suggests a drop in elastic moduli at around 100°C. This perovskite has been suggested to exhibit only one transition in 100°C-150°C temperature namely anti-ferromagnetic to paramagnetic at around 100°C[98]. This transition temperature is marked by

the observed increase in attenuation of the longitudinal and shear velocities. The increase in elastic moduli after 600°C may be attributed to increased concentration of Mn^{+4} ions and thus the higher binding energy in the crystal with increased temperature[99].

4.3.3.3 Lanthanum Strontium Cobalt Ferrite (LSCF) Cathode

The variations of Young's and shear moduli with temperature for LSCF are presented in Fig. 4-20. A closer observation of the plot suggests an increase in elastic/shear moduli with increasing temperature up to 300°C after that a decrease in moduli were observed until 700°C which was further followed by an increase above 700°C. The room temperature value of Young's modulus for LSCF obtained in this study is 83GPa which is lower than reported[100,101] and the reason may be different processing method employed and porosity of the samples.

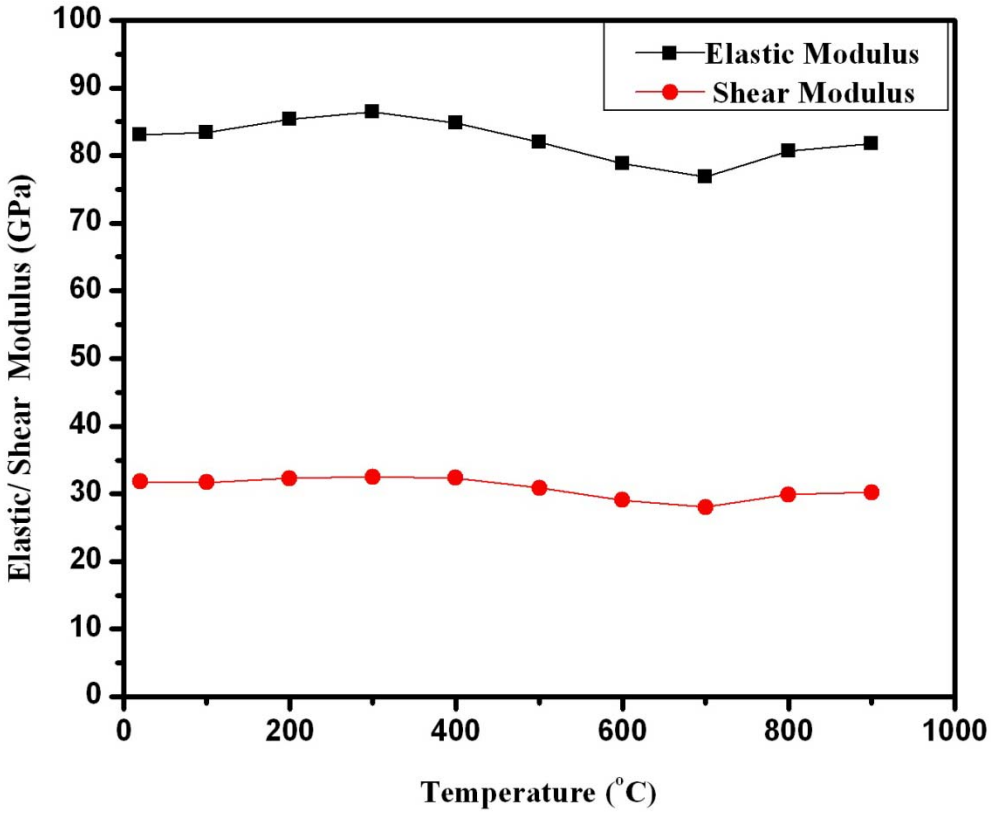

Figure 4-20 Variation of Young's and shear moduli with temperature for LSCF

4.4. Finite Element Analysis of Thermal Stresses

This section describes the results obtained from finite element analysis of the thermal stresses at various temperatures for the fully constrained positive electrode-electrolyte- negative electrode (PEN) assembly of a planar SOFC. A 100x00mm anode supported configuration of SOFC has been selected for the analysis of thermal stresses with anode, electrolyte and cathode having thickness of 1mm, 10μm and 30μm respectively. For high temperature SOFC (HT-SOFC), thermal stresses have been evaluated for Ni-YSZ as anode, YSZ as electrolyte and LSM as the cathode whereas intermediate temperature SOFC (IT-SOFC) has been simulated by considering Ni-SCZ, GDC and LSCF as the proposed anode, electrolyte and cathode respectively.

Thermal stresses have been determined at room temperature, 600^{o}C, 900^{o}C for HT-SOFC and at room temperature, 300^{o}C and 600^{o}C for IT-SOFC. For each of the temperature under consideration, normal stresses σ_x(Sigma X) , $\sigma_{y(}$SigmaY) and σ_z(SigmaZ) has been calculated, where σ_y is normal stress in the thickness direction, and σ_x and σ_z are mutually orthogonal normal stresses that are in the directions parallel to the edges of the SOFC plate. Anode, electrolyte and cathode layers have been bonded surface-to-surface and iso-strain condition has been imposed at the interface. The assembly has been considered in the fully constrained condition, i.e. displacement in x and z directions of the nodal points at the edges of the SOFC stack were fully constrained. This constrain is the worse scenario since the thermal stresses can not be relieved by expansion of any of the constitutive layer in x and z directions. For all the above mentioned materials for HT-SOFC and IT-SOFC, variations of elastic and shear moduli, Poisson's ratio, density, and Coefficient of thermal expansion (CTE) with respect to temperature (see Chapters 4.1, 4.2 and 4.3) have been taken into account while evaluating the stresses at studied temperatures. Considering the symmetry of the studied system, σ_x and σ_z have been found to have same magnitude and distribution over the thickness of the stack. Following subsection details the results obtained for the above mentioned imposed conditions on PEN assembly for HT-SOFC and IT-SOFC at different temperatures. For each of the SOFC system studied, results have been provided in terms of plots of σ_x, σ_y and σ_z evaluated at various temperatures in the center of the SOFC plate. The starting point is the cathode edge

(corresponding to 0.0 location in the plot), cathode/electrolyte (C/E) interface is marked by 0.03 point and the electrolyte/anode (E/A) interface is marked by 0.04 location. Stresses have been evaluated throughout the thickness of the assembly (1040μm). However, only region of interest (the interfaces C/E and E/A) are presented in the plots.

4.4.1. High Temperature Solid Oxide Fuel Cell

This subsection details the observation of for σ_x , σ_y and σ_z normal stresses in and across the constitutive cathode, electrolyte and anode layers of the PEN assembly of high temperature SOFC. For each of the normal stress, a plot detailing the distribution of stress at room temperature, 600°C and 900°C is presented which is further followed by the enlisting of the magnitude and nature of stresses across the layer.

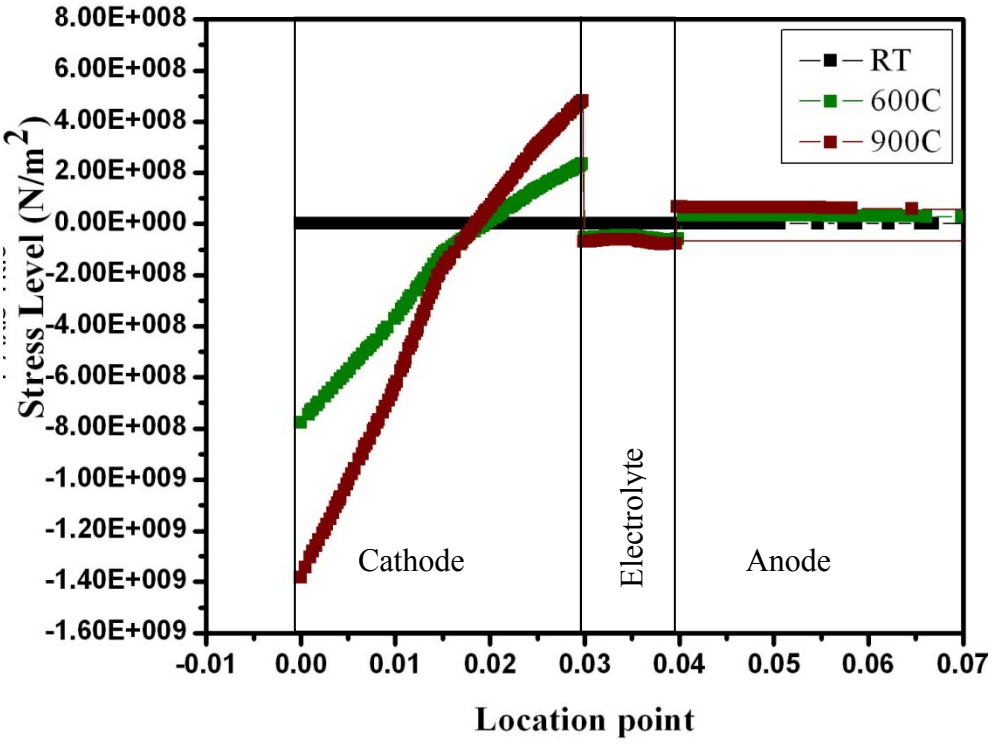

Figure 4-21 Variation of Sigma Z for high temperature SOFC

Variation of σ_z (or σ_x) in and across the constitutive layers of HT- SOFC is presented in Fig. 4-21 and the magnitude and nature of the stresses across the cathode/electrolyte and electrolyte anode interface are enlisted in the Table 4-4. As is evident from the Table 4-4, both of the adjacent layers of anode and cathode at C/E and E/A interfaces respectively, are subjected to high tensile stresses at the operating temperature (900^{o}C) of HT-SOFC while electrolyte is in state of compressive stress. Also it can be noted that stress level in the cathode layer adjacent to electrolyte is very high (500MPa) suggesting fracture strength of cathode layer to be the limiting factor for the sustainability of the assembly as a whole.

Table 4-4 Detailed presentation of Sigma Z stresses along the interfaces for HT- SOFC

σ_Z (Sigma Z) evaluated for HT- SOFC				
Temp.	Cathode/ Electrolyte interface		Electrolyte/ Anode interface	
	Cathode	Electrolyte	Electrolyte	Anode
600	233MPa (Tensile)	52 MPa (Comp.)	58 MPa (Comp.)	33 MPa(Tensile)
900	483MPa (Tensile)	70 MPa(Comp.)	75 MPa(Comp.)	67 MPa(Tensile)

Variation of σ_y in and across the constitutive layers of HT- SOFC is presented in Fig. 4-22 while magnitude and nature of the stresses across the cathode/electrolyte and electrolyte anode interface are enlisted in the Table 4-5. As is evident from the plot, all the three layers cathode (and layer adjacent to electrolyte), electrolyte and anode are predominately in the state of compressive stresses at both 600^{o}C and 900^{o}C temperatures. Tensile stresses only appear in the middle of the cathode layer, and their magnitude does not exceed 80MPa.

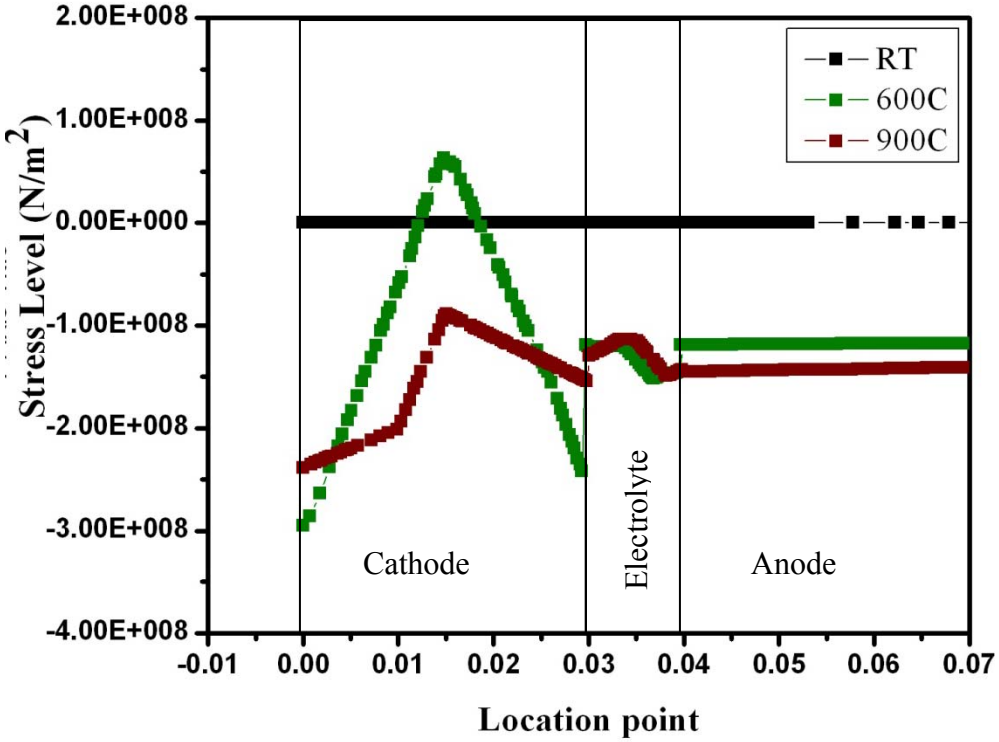

Figure 4-22 Variation of Sigma Y for high temperature SOFC

Table 4-5 Detailed presentation of Sigma Y stresses along the interfaces for HT-SOFC

σ_Y evaluated for HT- SOFC				
Temp.	Cathode/ Electrolyte interface		Electrolyte/ Anode interface	
	Cathode	Electrolyte	Electrolyte	Anode
600	242MPa (Comp.)	119MPa (Comp.)	146MPa (Comp.)	118MPa (Comp.)
900	154MPa (Comp.)	129MPa (Comp.)	144MPa (Comp.)	144MPa (Comp.)

4.4.2 Intermediate Temperature Solid Oxide Fuel Cell

This subsections details the thermal stress distribution in the anode, electrolyte and cathode layers of the PEN assembly as a function of thermo-mechanical properties of the constitutive layers of intermediate temperature SOFC, IT-SOFC. The PEN assembly of IT-SOFC was studied at room temperature, 300^{o}C and 600^{o}C temperature.

Variation of σ_z (or σ_x) in and across the constitutive layers of IT- SOFC is presented in Fig. 4-23 while magnitude and nature of the stresses across the cathode/electrolyte and electrolyte anode interface are enlisted in the Table 4-6. It can be noted that electrolyte is subjected to compressive stresses at both the interfaces while adjacent anode and cathode are in the tensile stress. Also, can be noted that the tensile stress to which IT- SOFC cathode is subjected to its suggested operating temperature is much lower (178 MPa) than in the case of HT- SOFC (500MPa). This analysis supports rather reliable operation of IT- SOFC when compared with HT- SOFC.

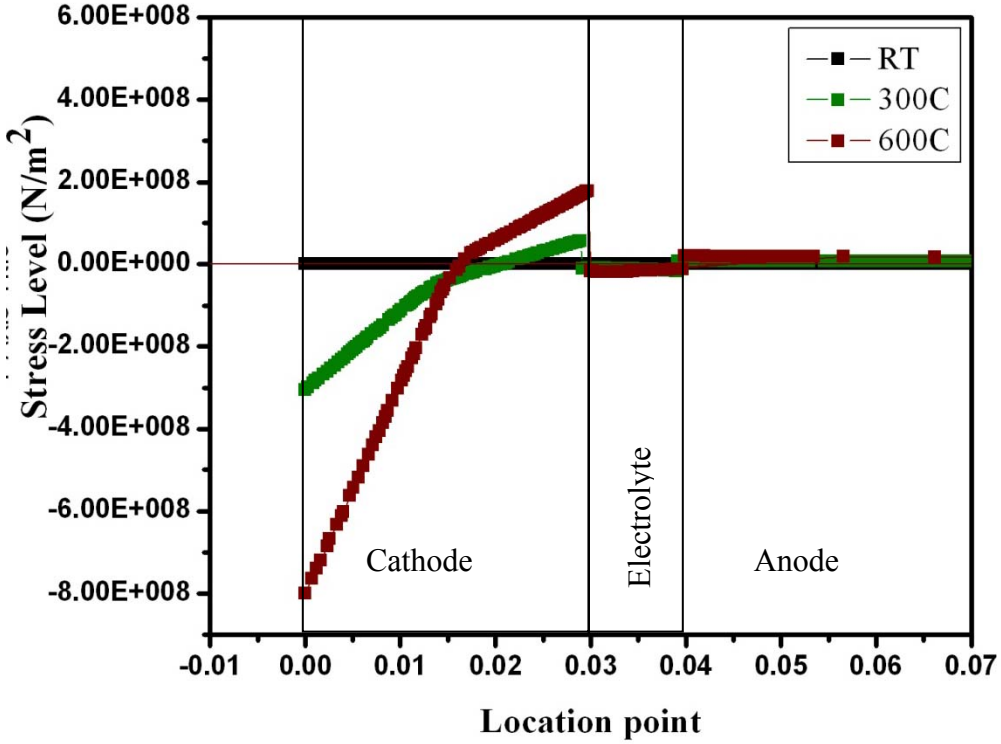

Figure 4-23 Variation of Sigma Z for intermediate temperature SOFC

Table 4-6 Detailed presentation of Sigma Z stresses along the interfaces for IT-SOFC

Sigma Z (σ_z) evaluated for IT- SOFC				
Temp.	Cathode/ Electrolyte interface		Electrolyte/ Anode interface	
	Cathode	Electrolyte	Electrolyte	Anode
300	56MPa(Tensile)	9.3MPa(Comp.)	11.3MPa(Comp.)	8.6MPa(Tensile)
600	180MPa(Tensile)	18.4MPa(Comp.)	12.4MPa(Comp.)	20MPa(Tensile)

The variation of σ_y in and across the cathode, electrolyte and anode layers is presented in Fig.4-24 while the nature and magnitude of the stresses across the cathode/ electrolyte and electrolyte/ anode interface is provided in Table 4-7. It can be noted here that the adjacent layers of the anode and cathode to the C/E or E/A interface are in compressive stress state ensuring the longetivity of the cell at the operating temperature. Tensile stresses only appear in the narrow area in the middle of cathode with the magnitude not exceeding 50 MPa at 600^{o}C.

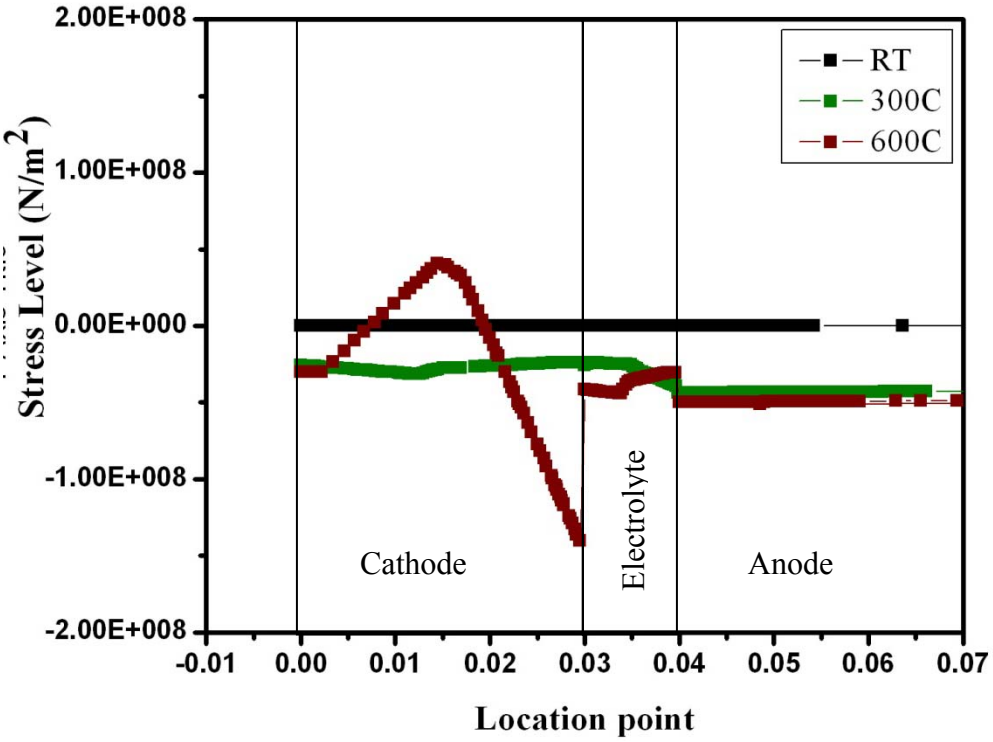

Figure 4-24 Variation of Sigma Y for intermediate temperature SOFC

Table 4-7 Detailed presentation of Sigma Y stresses along the interfaces for IT-SOFC

σ_y (Sigma Y) evaluated for IT- SOFC				
Temp.	Cathode/ Electrolyte interface		Electrolyte/ Anode interface	
	Cathode	Electrolyte	Electrolyte	Anode
300	25MPa(Comp.)	25MPa(Comp.)	44.3MPa(Comp.)	44.3MPa(Comp.)
600	140MPa(Comp.)	41MPa(Comp.)	28.7MPa(Comp.)	48.7MPa(Comp.)

From the above mentioned observations, it can be noted that the cathode layer at the interface with electrolyte is subjected to very high tensile stresses at the operating temperature of either of HT-SOFC or IT-SOFC. These stresses have arisen because of higher CTE of the cathode layer when compared with electrolyte and anode. In a work by Kanamura et al, effect of CTE of cathode on the developed thermal stresses have been studied and it has been reported that if by some means CTE of cathode could be brought down to equivalent to CTE of electrolyte, thermal stresses will be lowered significantly[90].

It is worth noting here that we have assumed the homogenous temperature distribution across the plane of the assembly while in practice there is wide distribution of temperature depending on the availability of fuel and oxidant at the point of concern[102]. Non-uniform temperature distribution will certainly in the plane of the SOFC cell will certainly results in different magnitude and distribution of the stresses. Also, thermal stresses have been determined considering the fully constrained layers. Fully constraint condition implies that the developed thermal stresses resulting from the mismatch of the thermo-mechanical properties of the constitutive layers at various temperatures can not be partially relieved by thermal expansion of the SOFC plate. In practice, anode and cathode are glass sealed. High operation temperature (above glass transition temperature Tg of the sealant) would result in softening of the glass sealant and may provide the stress relaxation in the SOFC stack as a whole[103].

Beside thermal stresses that generates in the SOFC components as a result of temperature gradients and mismatch in thermo-mechanical properties of constituent materials, residual stresses also play important role. In practice co-sintering of multi layered SOFC stack introduces

residual stresses and these stresses mitigate the effect of thermal stresses to certain extent. In a work by Fischer et al. residual compressive stresses in the electrolyte have been reported to be as high as ~500MPa which may lower down the resultant stress level to a much lower level[104].

5. CONCLUSIONS

In the present work, we have made an attempt to evaluate thermal stresses as a function of thermo-mechanical properties of different cathode, electrolyte and anode materials at various temperatures for high and intermediate temperature SOFC. The materials studied for HT-SOFC included YSZ as an electrolyte, Ni-YSZ as an anode, and LM and LSM as the cathodes while the materials for IT- SOFC included SCZ and GDC as electrolyte, NiO-SCZ as an anode and LSCF as the cathode. To study the effect of temperature on the thermal expansion behavior and on elastic constants, these materials were studied using thermo-mechanical analyzer (TMA) and resonant ultrasound spectroscope (RUS) in 25^{o}C-900^{o}C temperature regime. Thus obtained elastic and shear moduli, Poisson's ratio and average CTE were incorporated in the finite element modeling of stresses at various temperatures for HT-SOFC and IT-SOFC. This section provides the summary of the results obtained.

i. Thermo-mechanical analysis of the materials used in the present study illustrated that materials have exhibited a combination of thermal and chemical expansion in the studied temperature range in N_2 atmosphere. Also, the variation of CTE with respect to temperature was found to be non-linear and very sensitive to any phase transition in that temperature range. To name a few, the anomalies observed in the CTE vs. Temperature plot for NiO-SCZ or NiO-YSZ, Ni-YSZ, LM, have been correlated to Anti-ferromagnetic to paramagnetic transition of NiO, Ferromagnetic to paramagnetic transition of Ni (Curie temperature) and rhombohedral to cubic transition of LM. Also, for some materials whose composition is very sensitive to external environment (oxygen partial pressure) especially at high temperature, a sudden increase in CTE was observed due to a significant contribution from chemical expansion as well. This behavior was very well exhibited by GDC and LM and LSCF.

ii. Variations of elastic and shear moduli with temperature were studied using high precision dynamic technique- resonant ultrasound spectroscopy. A non-linear variation of elastic and shear moduli was exhibited with varied temperature in 25-900^{o}C temperature regime. Measurements were taken at an interval of 100^{o}C. Because elastic modulus is related to the shape of the free energy potential plot of the material under consideration, any structural

changes that were active in the studied temperature range, were very well reflected in the elastic and shear moduli vs. temperature plot. In case of electrolyte these changes were related to the relaxational damping of oxygen vacancies in a certain temperature region which occurs via order- disorder transition of the oxygen vacancies in and around dopants. In case of anodes, the points of inflection/change in the slope of elastic moduli vs. temperature were found to be in correlation to phase transitions in its constitutive phases (anti ferromagnetic to paramagnetic transition of NiO and that of relaxational damping of oxygen vacancies of SCZ or YSZ). Similarly, cathodes were also found to exhibit nonlinear variation of elastic constants with increased temperature. A decrease in elastic modulus with increasing temperature is favorable from the point of view of high temperature applications.

iii. Elastic and shear moduli, and CTE of the materials measured in this work were utilized in the evaluation of thermal stresses in PEN assembly as a function of temperature. We have considered the assembly to be fully constrained such that the[r]e is no operational stress relaxation mechanism. PEN assembly of HT SOFC was studied at room temperature (RT), 600^{o}C and 900^{o}C while that of IT-SOFC was studied at RT, 300 ^{o}C and 600^{o}C. A comparison of normal stresses $\sigma_{x,}$ σ_{y} and σ_{z} was studied along the thickness at the center point of the of the SOFC assembly. At the operation temperature of HT-SOFC (900^{o}C), the adjacent cathode and anode layers adjacent to electrolyte were found to be in the state of tensile stresses while that of electrolyte was in compressive state of stress. Of these two, cathode layer was under the 500MPa tensile stress suggesting the cathode/electrolyte interface to be the most sensitive one. At the operation temperature of IT- SOFC (600^{o}C) the cathode and anode layers adjacent to cathode/electrolyte and electrolyte/anode interface respectively were found to be in a state of tensile stress as well. However, this stress level is much lower (~175MPa at cathode and 22 MPa at anode) when compared to stress levels of HT-SOFC suggesting the cathode/electrolyte interface to be still vulnerable one but much more reliable than that of HT-SOFC. It is worth noting here, that we have not considered any contributions from the stress relaxation by softening of the glass sealant (when operating temperature is above it glass transition), residual stresses from co-

firing step of the fabrication process which certainly affect net stress level at the interface and thus operational reliability of SOFC.

6. RECOMMENDATIONS FOR FUTURE WORK

Based on the results of the experimental and computational work presented in this works, following recommendations for the future research on thermo-mechanical properties of materials for SOFC and their effect on the stresses in and SOFC components can be suggested:

i. In the present work, while studying the thermal expansion behavior of the materials, very unusual behavior exhibited by some of materials such as LM, LSCF and GDC above 600^{o}C was attributed to the partially reducing atmosphere employed (N_2 with a flow rate of 40ml/min). A verification of this hypothesis needs to be further evaluated by varying flow rates and or employing atmospheres with different oxygen partial pressures.

ii. In the present study while evaluating the thermal stresses across and in the different layers of the positive electrode - electrolyte - negative electrode (PEN) assembly, homogenous temperature has been assumed while in practice there is a wide distribution of temperature depending on the fuel and oxidant availability at the particular point on the SOFC, as it has been reported by[102,105,106]. Extension to the present work may include effect of in-homogenous temperature distribution across assembly.

iii. In the present case we have studied the worst scenario where in the thermal expansion of SOFC stack along the edges of the stack has been totally constrained and there is no margin for any of the constitutive layer to mitigate the effect of tensile thermals stresses by expansion. However, in practice glass sealants are used between SOFC stack and support frame. Due to softening of the glass at high temperature some of the thermal expansion and thus the thermal stresses in the layers can be accommodated. Thus, future work should also include the glass sealant in FEM model in order to obtain more accurate stress distribution.

iv. Also, the effect of residual stresses arising from fabrication of these layers has not been taken into account. These stresses have been reported to be significant. For example, the compressive stress in electrolyte can reach 500MPa[104,107]. These residual stresses, when superimposed to thermal stresses may lower down the magnitude of stresses in the SOFC stack and thus increase reliability of the SOFCs.

v. Finite element analysis of the thermal stresses at cathode/electrolyte and electrolyte/anode interfaces suggests the higher thermal (tensile) stresses to which cathode is subjected at the suggested operating temperature of 600oC for IT-SOFC and 900C for HT-SOFC. This can be attributed to high CTE of cathode material. Future work may also be dedicated to find some ways to lower down the CTE of the cathode by doping with some cations in order to minimize the thermal stresses.

REFERENCES

[1] Haile, S. M. Fuel cell materials and components *Acta Mater.* **51** (19), 5981-6000 (2003)

[2] Minh, N. Q. & Takahashi, T. *Science and Technology of Ceramic Fuel Cells*. (Elsevier Science, Amsterdam, The Netherlands, 1995)

[3] Carrette, L., Friedrich, K. A. & Shimming, U. Fuel cells: Fundamentals and applications. *Fuel Cells* **1** (1), 5-39 (2001)

[4] Fuel cells Handbook, EG&G Technical Services, Inc., under contract no. DE-AM26-99FT40575, available at http://www.netl.doe.gov/technologies/coalpower/fuelcells/seca/pubs/FCHandbook7.pdf, accessed on Jan.2008

[5] Larminie, J. & Dicks, A. *Fuel Cell Systems Explained*, Second ed. (John Wiley &Sons Ltd., West Sussex, England, 2003)

[6] O'Hayre, R., Cha, S. W., Colella, W. & Printz, F. B. *Fuel Cell Fundamentals*. (John Wiley & Sons, New York, US, 2006)

[7] Nice, K. & Strickland, J. How fuel cell works, Available at http://auto.howstuffworks.com/fuel-cell1.htm, (2006).

[8] Types of fuel cells, Available at http://www1.eere.energy.gov/hydrogenandfuelcells/fuelcells/fc_types.html#phosphoric, (2007).

[9] Brandon, N. P. & Thompsett, D. eds. *Fuel Cells Compendium*, 1st ed. (Elsevier Ltd, , Oxford, UK, 2005)

[10] Sammes, N. M. ed. *Fuel Cell Technology: Reaching Towards Commercialization*. (Springer -Verlag London Limited, London, 2006)

[11] Williams, K. R. *An Introduction to Fuel Cells*. (Elsevier Publishing Company, New York, USA, 1966)

[12] Kendall, K. Progress in solid oxide fuel cell materials. *Int. Mater. Rev.* **50** (5), 257-264 (2005)

[13] Gauckler, L. J., Beckel, D., Buergler, B. E., Jud, E., Muecke, U. P. *et al.* Solid oxide fuel cells: Systems and materials *Fuel Cell Research in Switzerland* **58**, 837-850 (2004)

[14] Singhal, S. C. & Kendall, K. eds. *High Temperature Solid Oxide Fuel Cells: Fundamentals, Design and Applications*. (Elsevier Advanced Technology, Oxford, U.K., 2003)

[15] Arachi, Y., Sakai, H., Yamamoto, O., Takeda, Y. & Imanishi, N. Electrical conductivity of the ZrO_2-Ln_2O_3 (Ln = lanthanides) system *Solid State Ionics* **121** (1-4), 133-139 (1999)

[16] Yamamoto, O. Solid oxide fuel cells: Fundamentals aspects and prospects. *Electrochim. Acta* **45** (15-16), 2423-2435 (2000)

[17] Uchida, H., Suzuki, H. & Watanabe, M. High-performance electrode for medium-temperature solid oxide fuel cells - effects of composition and microstructures on performance of ceria-based anodes *J. Electrochem. Soc.* **146** (2), 615-620 (1998)

[18] O.Yamamoto, Y. A., Takeda, Y., Imanshi, N., Mizutani, y., Kawai, M. *et al.* Electrical conductivity of stabilized zirconia with ytterbia and scandia. *Soild State Ionics* **79**, 137-142 (1995)

[19] Arachi, Y., Ashai, T., Yamamoto, O., Takeda, Y., Imanishi, N. *et al.* Electrical conductivity of ZrO_2- Sc_2O_3 doped with HfO_2, CeO_2, and Ga_2O_3. *J. Electrochem. Soc.* **148** (5), A520-A523 (2001)

[20] Y.Mizutani, M. Kawai, N. K., Nakamura, Y. & eds., O. Y. In *Electrochemical Society Proceedings-Pennington, NJ,97-40*, 1997

[21] Yahiro, H., Eguchi, Y., Eguchi, K. & Arai, H. Oxygen ion conductivity of the ceria samarium oxide with fluorite structure. *J. Appl. Electrochem.* **18** (4), 527-531 (1988)

[22] Godickemeier, M. & Gauckler, L. J. Engineering of solid oxide fuel cells with ceria-based electrolytes. *J. Electrochem. Soc.* **145** (2), 414-421 (1998)

[23] Brandon, N. P., Skinner, S. & Steele, B. C. H. Recent advances in materials research for fuel cells. *Annu. Rev. Mater. Sci.* **33**, 183-187 (2003)

[24] Weimhofer, J. & Weitkamp, H. D. Electronic conduction and conductivity of solid electrolytes based on lanthanum gallates. *Soild State Ionics* **597,** 154-155, (2002)

[25] Huang, H. Q., Wan, J. H. & Goodenough, J. B. Increasing power density of LSGM-based solid oxide fuel cells using new anode materials. *J. Electrochem. Soc.* **148** (7), A788-A794 (2001).

[26] Spacil, H. S. US patent no. 3558360. (1970)

[27] Steele, B. C. H. Materials for IT-SOFC stacks 35 years R & D: The inevitability of gradualness. *Solid State Ionics* **134** (1-2), 3-20 (2000)

[28] Kiratzis, N., Holtappels, P., Hatchwell, C. E., Mogensen, M. & Irvine, J. T. S. Preparation and characterization of Cu/yttria titania zirconia cermets for use as possible solid oxide fuel cell anodes. *Fuel Cells* **1**, 211-218 (2001)

[29] Tosga, A., Nikolopoulos, P., Kontogeorgakos, A., Teitz, F. & Naoumidis, A. In *Proceedings of Fifth International Symposium on Solid Oxide Fuel Cells (SOFC-V)*, Aachen, Germany, June, 1997 (unpublished)

[30] Koide, H., Someya, Y., Yoshida, T. & Maruyama, T. Properties of Ni/YSZ cermet as anode for SOFC. *Solid State Ionics* **132** (3-4), 253-260 (2000)

[31] Gubner, A., Landes, H., Metzger, J., Seeg, H. & Stubner, R. In *Proceedings of the Fifth International Symposium on Solid Oxide Fuel Cells (SOFC-V),* Aachen, Germany, 1997.

[32] Zhu, W. Z. & Deevi, S. C. Development of interconnect materials for solid oxide fuel cells. *Mater. Sci. Eng., A* **348** (1-2), 227-243 (2003)

[33] Zurcher, S. & Graule, T. Influence of dispersant structure on the rheological properties of highly-concentrated zirconia dispersions. *J. Eur. Ceram. Soc.* **25,** 863-873 (2005)

[34] Stochinol, G., Syskakis, E. & Naoumidis, A. Chemical compatibility between strontium -doped lanthanum manganite and yttria-stabilized zirconia. *J. Am. Ceram. Soc.* **78** (4), 929-932 (1995)

[35] Park, S. D., Vohs, J. M. & Gorte, R. J. Direct oxidation of hydrocarbons in a solid oxide fuel cell. *Nature* **404**, 265-267 (2000)

[36] Gorte, R. J., Kim, H. & Vohs, J. M. Novel SOFC anodes for the direct electrochemical oxidation of hydrocarbon. *J. Power Sources* **106** (1-2), 10-15 (2002)

[37] Verbraken, M. C., Boukamp, B. A., Blank, D. H. A., Holtapples, P. & Vogt, U. In *Proceedings of Electrochemical Society -9th International Symposium on Solid Oxide Fuel Cells*, Quebec PQ , Canada, 2005.

[38] Pudmich, G., Boukamp, B. A., Gonzalez-Cuenca, M., Jungen, W., Zipprich, W. *et al.* Chromite/titanate based perovskites for application as anodes in solid oxide fuel cells. *Solid State Ionics* **135** (1-4), 433-438 (2000)

[39] Vermoux, P., Guillodo, M., Fouletier, J. & Hammon, A. Alternative anode material for gradual methane reforming in solid oxide fuel cells. *Solid State Ionics* **135** (1-4), 425-431 (2000)

[40] Mogensen, M., Kindl, B. & Hansen, B. M. In *Proceedings of the Program and Abstracts of Fuel Cell Seminar,* Phoenix, AZ, Courtesy Associate Inc., Washington, DC 1990, 195 (1990)

[41] Steele, B. C. H. Appraisal of $Ce_{1-y}Gd_yO_{2-y/2}$ electrolytes for IT- SOFC operation at 500^{o}C. *Solid State Ionics* **129** (1-4), 95-110 (2000)

[42] Livermore, S. J. A., Cotton, J. W. & Ormerd, R. M. Internal fuel reforming in intermediate temperature CeO2- GdO2 based SOFCs. In *Proceedings of the Sixth International Symposium on Solid Oxide Fuel Cells (SOFC -VI)*-Honolulu- Hawaii, edited by S. C Singhal, M. Dokiya (17-22 October, 1999)

[43] Joerger, M. B. & Gaucker, l. J. In *Proceedings of Seventh International Symposium on Solid Oxide Fuel Cells (SOFC-VII)*, Tsukaba Ibarka, Japan 2001.

[44] Mogensen, M., Psimdahl, S., Jgrgensen, M. J. & Bagger, C. Composite electrodes in solid oxide fuel cells and similar solid state devices *J. Electrochem. Soc.* **5** (2), 141-152 (2000)

[45] Lau, S. K. & Singhal, S. C. Potential electrode/electrolyte interactions in solid oxide fuel cells. *Corrosion* **85** (1-9) (1985)

[46] Simner, S. P., Bonnett, J. G., Canfield, N. L., Meinhardt, K. D., Shelton, J. P. *et al.* Development of lanthanum ferrite SOFC cathodes. *J. Power Sources* **113** (1), 1-10 (2003)

[47] Tedmon, C. S., Spacil, H. S. & Mitoff, S. P. Cathode materials and performance in high-temperature zirconia electrolyte fuel cells *J. Electrochem. Soc.* **116** (9), 1170-1175 (1969)

[48] Horiuchi, M., Suganuma, S. & Watanabe, M. Electrochemical power generation directly from combustion flame of gases, liquids, and solids. *J. Electrochem. Soc.* **151** (9), A1402-A1405 (2004)

[49] Ralph, J. M., Rossignol, C. & Kumar, R. Cathode materials for reduced-temperature SOFCs *J. Electrochem. Soc.* **150** (11), A1518- A 1522 (2003)

[50] Petric, A., Huang, P. & Teitz, F. Evaluation of La-Sr-Co-Fe O_3 for cathodes and gas separation membranes. *Soild State Ionics* **135** (1-4), 719 (2000)

[51] Matsuzaki, Y. & Yasuda, I. Electrochemical properties of reduced-temperature SOFCs with mixed ionic–electronic conductors in electrodes and/or inter-layers. *Soild State Ionics* (Part A, Special Issue), **152,** 463-468 (2002)

[52] Dusastre, V. & Kilner, J. A. Optimization of composite cathodes for intermediate temperature sofc applications. *Soild State Ionics* **126** (1-2), 163 (1999)

[53] Singhal, S. C. Advances in solid oxide fuel cell technology. *Solid State Ionics* **135**, 305-313 (2000)

[54] Buchkremer, H. P., Dikemann, U., Haart, L. G. J. D., Kabs, H., Stover, D. *et al.* In *Proceedings of 3rd European SOFC Forum*, Lucerne, Switzerland, 1997.

[55] Malkow, T., Crone, U. V. D., Laptev, A. M., Koppitz, T., Breuer, U. *et al.* In *Proceedings of the Electrochmical Society,* Pennington, NJ, 1997.

[56] ASTM standard c20-00, "Standard test methods for apparent porosity, water absorption, apparent specific gravity, and bulk density of burned refractory brick and shapes by boiling water". *ASTM International* (2005)

[57] Migliori, A. & Sarrao, J. L. *Resonant Ultrasound Spectroscopy- Applications to Physics, Materials Measurements and Nondestructive Evaluation*. (John Wiley & Sons, Inc., 1997)

[58] Leisure, R. G. & Wills, F. A. Resonant ultrasound spectroscopy- review article. *J. Phys.: Condens. Matter* **9**, 6001-6029 (1997)

[59] Radovic, M. & Lara-Curzio, E. Elastic properties of nickel-based anodes for solid oxide fuel cells as a function of the fraction of reduced NiO. *J. Am. Ceram. Soc.* **87** (12), 2242-2246 (2004)

[60] Radovic, M., Curzio, E. L.-. & Riester, L. Comparison of different experimental techniques for determination of elastic properties of solids. *Mater. Sci. Eng., A* **368**, 56-70 (2004)

[61] TMA Q400 guide from TA Instruments. Available at http://www.tainstruments.com/product.aspx?id=198&n=1&siteid=11

[62] Duncan, K. L., Wang, Y., Bishop, S. R., Ebrahimi, F. & Wachsmana, E. D. The role of point defects in the physical properties of nonstoichiometric ceria. *J. Appl. Phys.* **101**, 044906-044901 to 044906-044906 (2007)

[63] Mogensen, M., Sammes, N. M. & Tompsett, G. A. Physical, chemical and electrochemical properties of pure and doped ceria. *Soild State Ionics* **129**, 63-94 (2000)

[64] Kim, D. J. *J. Am. Ceram. Soc.* **72**, 14-15 (1989)

[65] Fujishiro, H., Fukase, T. & Ikebe, M. Charge ordering and sound velocity anomaly in $La_{1-x}Sr_xMnO_3$ (x >= 0.5) *J. Phys. Soc. Jpn.* **67** (8), 2582-2585 (1998)

[66] Zhu, C. & Zheng, R. *Phys. Rev. B* **59**, 11169-11175 (1999)

[67] Du, Y., Sammes, N. M., Tompsett, G. A., Zhang, D., Swan, J. *et al.* Extruded tubular strontium and magnesium- doped lanthanum gallate gadolinium doped Ceria and yttria stabilized zirconia electrolytes. *J. Electrochem. Soc.* **150** (1), A74-A78 (2003)

[68] Sammes, N. M. & Du, Y. Fabrication and characterization of tubular solid oxide fuel cells. *Int. J. Appl. Ceram. Technol.* **4** (2), 89-102 (2007)

[69] Chen, H., Zhou, X. & Din, C. Investigation of the thermomechanical properties of a plasma-sprayed nanostructured zirconia coating. *J. Eur. Ceram. Soc.* **23**, 1449-1455 (2003)

[70] Mori, M., Yamamoto, T. & Itah, H. Thermal expansion of nickel zirconia anodes in solid oxide fuel cells during fabrication and operation. *J. Electrochem. Soc.* **145** (4), 1374-1381 (1998)

[71] Hayashi, H., Saitou, T., Naotaka Maruyama, H. I., Kawamura, K. & Mori, M. Thermal expansion coefficient of yttria stabilized zirconia for various yttria contents. *Solid State Ionics* **176**, 613-619 (2005)

[72] C.Haering, Roosen, A., Schichl, H. & Schnoller, M. Degradation of the electrical conductivity in stabilized zirconia system part ii: Scandia -stabilized zirconia. *Solid State Ionics* **176**, 261-268 (2005)

[73] Gorelov, V. P., Balakireva, V. B., Yaroslavtsev, I. Y., Kazantsev, V. A. & Vaganov, E. G. Conductivity and thermal expansion of the $Ce_{0.8}Gd_{0.2}O_{1.9}$ solid electrolyte in the oxidizing and reducing atmospheres. *Russ. J. Electrochem.* **43** (8), 888-893 (2007)

[74] Hayashi, H., Kanoh, M., Quan, C. J., Inaba, H., Wang, S. *et al.* Thermal expansion of Gd-doped ceria and reduced ceria. *Soild State Ionics* **132**, 227-233 (2000)

[75] Wang, S., Katsuki, M., Hashimoto, T. & Dokiya, M. Expansion behavior of $Ce_{1-y}Gd_yO_{2.0-0.5y-d}$ under various oxygen partial pressures evaluated by HT-XRD. *J. Electrochem. Soc.* **150** (7), A952-A958 (2003)

[76] Selcuk, A. & Atkinson, A. Elastic properties of ceramic oxides used in solid oxide fuel cells (sofc). *J. Eur. Ceram. Soc.* **17**, 1523-1532 (1997)

[77] Fang, Q. F., Liu, T., Li, C., Wang, X. P. & Zhang, G. G. Damping mechanisms in oxide materials and their potential applications. *Key Eng. Mater.* **319**, 167-172 (2006)

[78] Weller, M. & Schubert, H. Internal -friction, dielectric loss, and ionic-conductivity of tetragonal ZrO_2-3 percent Y_2O_3(Y-TZP). *J. Am. Ceram. Soc.* **69** (7), 573-577 (1986)

[79] Weller, M., Damson, B. & Lakki, A. Mechanical loss of cubic zirconia. *J. Alloys Compd.* **310**, 47-53 (2000)

[80] Radovic, M., Curzio, E. L.., Trezo, R. M., Wang, H. & Porter, W. D. In *30th Annual International Conference on Advanced Ceramics and Composites*, Cocoa Beach, Florida, 2006 (unpublished)

[81] Giraud, S. & Canel, J. Young's modulus of some SOFCs materials as a function of temperature. *J. Eur. Ceram. Soc.* **28**, 77-83 (2008)

[82] Duncan, K. L., Wang, Y., Bishop, S. R., Ebrahimi, F. & Wachsmanw, E. D. Role of point defects in the physical properties of fluorite oxides. *J. Am. Ceram. Soc.* **89** (10), 3162-3166 (2006)

[83] Aruna, S. T., Muthuraman, M. & Patil, K. C. Synthesis and properties of Ni-YSZ cermet: Anode material for solid oxide fuel cells. *Solid State Ionics* **111** (1-2), 45-51 (1998)

[84] Soffge, F., Steichele, E. & Stierstadt, K. Thermal expansion anomaly of nickel near curie point. *Phys. Status Solidi A* **42** (2), 621-627 (1977)

[85] Cox, P. A. *The Electronic Structure and Chemistry of Solids*. (Oxford University Press, Oxford, 1987)

[86] Radovic, M. & Lara-Curzio, E. Mechanical properties of tape cast nickel-based anode materials for solid oxide fuel cells before and after reduction in hydrogen. *Acta Mater.* **52**, 5747-5756 (2005)

[87] M. Radovic, Curzio, E. L.., Trejo, R., Armstrong, B. & Walls, C. In *The 28th Cocoa Beach Conference on Advanced Ceramics and Composite Ceramics*, 2005 (unpublished)

[88] Tofield, B. C. & Scott, W. R. Oxidative non-stoichiometry in perovskites, an experimental survey- defect structure of an structure of an oxidized lanthanum manganite by powder neutron- diffraction *J. Solid State Chem.* **10** (3), 183-194 (1974)

[89] Kingery, W. D., Bowen, H. K. & Uhlman, D. R. *Introduction to Ceramics*. (John Wiley & Sons, New York, 1976)

[90] Kanamura, Yoshioka, K., Zen-ichiro, S. & Takehara The calculation of temperature and thermal stress distributions in planar solid oxide fuel cell. *Chem. Soc. Jpn.* **65**, 309-313 (1992)

[91] Wandekar, R. V., Wani, B. N. & Bharadwaj, S. R. High temperature thermal expansion and electrical conductivity of $Ln_{0.95}MnO_{3+\delta}$ (ln = La, Nd or Gd). *J. Alloys Compd.* **433**, 84-90 (2007)

[92] Montross, C. S., Yokokawa, H. & Dokiya, M. Thermal stresses in planar solid oxide fuel cells due to thermal expansion differences. *Br. Ceram. Trans.* **101** (3), 85-93 (2002)

[93] Masashi Mori, Y. H., Sammes, N. M. & Tompsettb, G. A. Thermal-expansion behaviors and mechanisms for Ca- or Sr-doped lanthanum manganite perovskites under oxidizing atmospheres. *J. Electrochem. Soc.* **147** (4), 1295-1302 (2000)

[94] Kostogloudis, G. C. & Ftikos, C. Properties of A-site deficient $La_{0.6}Sr_{0.4}Co_{0.2}Fe_{0.8}O_{3-d}$ perovskite oxides. *Solid State Ionics* **126**, 143-151 (1999)

[95] Tai, L.-W., Nastrallah, M. M., Anderson, H. U., Sparlin, D. M. & Sehlin, S. R. *Solid State Ionics* **76**, 273-283 (1995)

[96] Troyanchuk, I. O., Mantytskaya, O. S., Chobot, A. N. & Szymczak, H. Transition from anti-ferromagnetic to ferromagnetic state of systems $LaMnO_{3+l}$ and $La_{1-x}Sr_x(Mn_{1-x/2}Nb_{x/2})O_3$. *J. Exp. Theor. Phys.* **95** (2), 300-307 (2002)

[97] Weller, M. in *Mechanical Spectroscopy Q^{-1} 2001 with Applications to Materials Science*, edited by Schaller, R., Fantozzi, G. & Gremaud, G. (Trans Tech Publications Limited, New York).

[98] Rajendran, V., Kumaran, S. M., Sivasubramanian, V., Jayakumar, T. & RaJ, B. Anomalies in elastic moduli and ultrasonic attenuation near ferromagnetic transition temperature in $La_{0.67}Sr_{0.33}MnO_3$ perovskite. *Phys. Solid State* **195** (2), 350-358 (2003)

[99] D'Souza, C. M. & Sammes, N. M. Mechanical properties of strontium doped lanthanum manganite. *J. Am. Ceram. Soc.* **83** (1), 47-52 (2000)

[100] Chou, Y.-S., Stevenson, J. W., Armstrong, T. R. & Pederson, L. R. Mechanical properties of $La_{1-x}Sr_xCo_{0.2}Fe_{0.8}O_3$ mixed-conducting perovskites made by the combustion synthesis technique. *J. Am. Ceram. Soc.* **83** (6), 1457-1464 (2000)

[101] Lein, H. L., Andersen, Ø. S., Vullum, P. E., Lara-Curzio, E., Holmestad, R. *et al.* Mechanical properties of mixed conducting $La_{0.5}Sr_{0.5}Fe_{1-x}Co_xO_{3-delta}$ (0 <= x <= 1) materials. *J. Solid State Electrochem.* **10**, 635-642 (2006)

[102] Recknagle, K. P., Willford, R. E., Chick, L. A., .Rector, D. R. & Khaleel, M. A. Three-dimensional thermo-fluid electrochemical modeling of planar SOFC stacks. *J. Power Sources* **113**, 109-144 (2003)

[103] Lin, C.-K., Chen, T.-T., Chyou, Y.-P. & Chiang, L.-K. Thermal stress analysis of a planar SOFC stack. *J. Power Sources* **164**, 238-251 (2007)

[104] Fischer, W., Malzebender, J., Blass, G. & Steinbrech, R. W. Residual stresses in planar solid oxide fuel cells. *J. Power Sources* **150**, 73-77 (2005)

[105] Neophytides, S. G. The reversed flow operation of a cross- flow solid oxide fuel cell monolith. *Chem. Eng. Sci.* **54**, 4603-4613 (1999)

[106] Iwata, M., Hikosaka, T., Morita, M., Iwanari, T., Ito, K. *et al.* Performance analysis of planar type unit SOFC considering current and temperatures distributions. *Solid State Ionics* **132**, 297-308 (2000)

[107] Batfalsky, P., Buchkremer, H. P., Froning, D., Meschke, F., H. Nabielek *et al.* In *Proceedings of the Third IFCC*, Nagoya. Japan, 1999 (unpublished)

VITA

Name: Manisha

Address: Scheme No.2, Lajpat Nagar, #363, Alwar, (Raj). 301001, India

Email Address: taneja.manisha@gmail.com

Education: B.E. Metallurgical Engineering, National Institute of Technology, Jaipur, India, 2002

M.S., Mechanical Engineering, Texas A&M University, 2008